LOW-COMPLEXITY FREQUENCY SYNCHRONIZATION FOR WIRELESS OFDM SYSTEMS

Yan Wu

LOW-COMPLEXITY FREQUENCY SYNCHRONIZATION FOR WIRELESS OFDM SYSTEMS

YAN WU

(*M. Eng, National University of Singapore*)

A THESIS SUBMITTED
FOR THE DEGREE OF DOCTOR OF PHILOSOPHY
DEPARTMENT OF ELECTRICAL & COMPUTER ENGINEERING
NATIONAL UNIVERSITY OF SINGAPORE
2009

Acknowledgements

First and foremost, I would like to express my sincere gratitude to my main supervisor Dr. Samir Attallah. I am grateful to him for introducing me to the NUS-TU/e joint PhD program, for his sustained guidance and encouragement in the past 5 years and for many exciting and enlightening technical discussions. I deeply appreciate his understanding of the difficulties I had trying to balance work and study as a part-time student during my study in Singapore. Besides being an excellent teacher, Samir is always a good friend. I enjoyed many casual discussions with him on work and life-related matters. I still remember our shared sympathy on the sending off of Zinedine Zidane in the 2006 world cup final. I am also truly grateful to my co-supervisor Prof. dr. ir. Jan Bergmans. His broad knowledge and deep technical insights have been a continuous source of inspiration. Jan has also shown me the importance of good scientific writing. I deeply appreciate his most valuable critique, suggestions and feedback to improve the quality of this thesis and my scientific writing in general. I also very much enjoyed many difficult yet intriguing challenges that he posed during our discussions. I also would like to thank him for providing me the opportunity to work fulltime in TU/e for my PhD.

I also want to thank a group of wonderful colleagues and friends in Institute for Infocomm Research (I^2R) in Singapore. They are Sumei, Patrick, Chin Keong, Woonhau, Peng Hui, Zhongding, Yuen Chau and many more. Working with you guys was a marvelous experience. Specially, I would like to thank Sumei for her support, guidance and understanding as a manager and for her valuable personal advices as a friend. In TU/e, I am also grateful to Prof. Peter Baltus for his expert knowledge in the RF front-end and to Prof. Jean Paul Linnartz for his help on the modeling of antenna mutual coupling and spatial correlation. I would like to acknowledge Yvonne Broers, Anja de Valk-Roulaux and Yvonne van Bokhoven for their kind assistance in administrative matters. I am very grateful to Sjoerd Ypma for meeting me at the railway station on a cold winter night on my first day in Eindhoven, and for providing me with so many useful information and tips on the life in the Netherlands. My appreciation goes to the whole SPS group for the pleasant atmosphere they created. I had great fun in the two cycling tours. I am lucky to have four great office mates, Hongming, Wim, Zhangpeng and Hamid. I am indebted to them for interesting discussions and many good jokes.

Many thanks go to prof.dr. C.C. Ko, prof.dr.ir. W.C. van Etten, dr. G. Leus, dr.ir. P.F.M. Smulders and prof.dr.ir. A.C.P.M. Backx for being in my doctorate committee and for their insightful comments and suggestions.

The love and support I get from my family are beyond what words can describe. I am deeply indebted to my grandma, my parents for their love from the first day I came to this world, and for their continuous encouragement, which has been a driving force throughout the years in my study, work and daily life. I would also like to thank my parents in law for their understanding and support. Last and definitely not the least, I would like to thank my wife Liu Ying. She has been most understanding and supportive for my study and work. I am heartily grateful for her love, for always being by my side and making me the happiest husband. I will never forget all the sacrifices she made to help me complete this thesis.

Contents

Summary

Low-Complexity Frequency Synchronization for Wireless OFDM Systems

The Orthogonal Frequency Division Multiplexing (OFDM) system provides an efficient and robust solution for communication over frequency-selective fading channels and has been adopted in many wireless communication standards. The multiple-input and multiple-out (MIMO) OFDM system further increases the data rates and robustness of the OFDM system by using multiple transmit and receive antennas. The multi-user MIMO-OFDM system is an extension of the MIMO-OFDM system to a multi-user context. It enables transmission and reception of information from multiple users at the same time and in the same frequency band. One drawback of all wireless OFDM systems is their sensitivities to frequency synchronization errors, in the form of carrier frequency offsets (CFO's). CFO causes inter-carrier interference, which significantly degrades the system performance. Accurate estimation and compensation of CFO is thus essential to ensure good performance of OFDM systems. To this end, many CFO estimation and compensation algorithms have been described in the literature for different wireless OFDM systems. These algorithms can be broadly divided into two categories, namely blind algorithms and training-based algorithms.

A key drawback of blind algorithms is their high computational complexity. In this thesis, we address this drawback by developing low-complexity blind CFO estimation algorithms exploiting null subcarriers in single-input single-output (SISO) OFDM systems. Null subcarriers are subcarriers at both ends of the allocated spectrum that are left empty and used as guard bands. To reduce the complexity of existing algorithms, we derive a closed-form CFO estimator by using a low-order Taylor series approximation of the original cost function. We also propose a successive algorithm to limit the performance degradation due to the Taylor series approximation. The null subcarrier placement that maximizes the signal to noise ratio (SNR) of the CFO estimation is also studied. We show that to maximize the SNR of CFO estimation, null subcarriers should be evenly spaced.

A key drawback of training-based algorithms is the training overhead from the transmission of training sequences, as it reduces the effective data throughput of the system. Compared to SISO-OFDM systems, the training overhead for MIMO-OFDM systems is even larger due to the use of multiple antennas. To address this drawback, in this thesis, we propose an efficient training sequence design for MIMO-OFDM systems using constant amplitude zero autocorrelation (CAZAC) sequences. We show that using the proposed training sequence, the CFO estimate can be obtained using low-complexity correlation operations and that the performance approaches the Cramer-Rao Bound (CRB). In the uplink of multi-user MIMO-OFDM systems, there are multiple CFO values between the base-station and different users. The maximum-likelihood CFO estimator is not practical here because its complexity grows exponentially with the number of users. To reduce this complexity, we propose a sub-optimal CFO estimation algorithm using CAZAC training sequences. Using the proposed algorithm, the CFO of each user can be estimated using simple correlation operations, while the computational complexity grows only linearly with the number of users. The performance approaches the single-user CRB for practical SNR values. We also find the CAZAC sequences that maximize the signal to interference ratio of the CFO estimation.

List of Figures

List of Tables

List of Abbreviations

3GPP:	3rd Generation Partnership Project
3GPP-LTE:	3rd Generation Partnership Project-Long Term Evolution
ADC:	Analog to Digital Converter
ASA:	Adaptive Simulated Annealing
AWGN:	Additive White Gaussian Noise
BER:	Bit Error Rate
BPSK:	Binary Phase Shift Keying
CAZAC:	Constant Amplitude Zero AutoCorrelation
CDMA:	Code Division Multiple Access
CRB:	Cramer-Rao Bound
CFO:	Carrier Frequency Offset
CP:	Cyclic Prefix
DAB:	Digital Audio Broadcasting
DFT:	Discrete Fourier Transform
DVB:	Digital Video Broadcasting
EM:	Electromagnetic
EMF:	Electromagnetic Fields
FDM:	Frequency Division Multiplexing
FIR:	Finite Impulse Response
FFT:	Fast Fourier Transform
GSM:	Global System for Mobile communications
ICI:	Inter-Carrier Interference
IDFT:	Inverse Discrete Fourier Transform
IEEE:	Institute of Electrical and Electronics Engineers

IFFT: Inverse Fast Fourier Transform
ISI: Inter-Symbol Interference
LAN: Local Area Network
LO: Local Oscillator
LOS: Line of Sight
MAI: Multiple Access Interference
Mbps: Megabits per second
ML: Maximum Likelihood
MSE: Mean Square Error
MIMO: Multiple Input Multiple Output
OFDM: Orthogonal Frequency Division Multiplexing
OFDMA: Orthogonal Frequency Division Multiple Access
PAS: Power Angular Spectrum
PAPR: Peak to Average Power Ratio
PDP: Power Delay Profile
ppm: parts per million
QAM: Quadrature Amplitude Modulation
QPSK: Quadrature Phase Shift Keying
RF: Radio Frequency
SER: Symbol Error Rate
SIR: Signal to Interference Ratio
SINR: Signal to Interference and Noise Ratio
SISO: Single Input Single Output
SNR: Signal to Noise Ratio
STF: Short Training Filed
WiMax: Worldwide Interoperability for Microwave Access
WLAN: Wireless Local Area Network

List of Symbols

$\angle$: angle of a complex number
ε: carrier frequency offset normalized with subcarrier spacing
$\hat{\varepsilon}$: estimate of the carrier frequency offset ε
γ: signal to noise ratio
λ: wavelength of the signal
ϕ: angular carrier frequency offset normalized with subcarrier spacing
$\hat{\phi}$: estimate of the angular carrier frequency offset ϕ
σ_s^2: variance of transmitted digital data symbols
σ_n^2: variance of the AWGN noise
c: speed of light
E_s: average energy of a digital data symbol
$\mathbf{E}$: diagonal carrier frequency offset matrix
f_c: carrier frequency of the signal
$\Im$: imaginary part of a complex number
$\mathbf{I}$: identity matrix
$\mathbf{I}_n$: identity matrix of size $n \times n$
N_0: power spectrum density of the AWGN noise
N_g: length of the cyclic prefix
$\Re$: real part of a complex number
$\mathbf{tr}$: trace of a matrix
$\mathbf{W}$: IDFT matrix
$\mathbf{w}_i^H$: i^{th} row of the DFT matrix

- *Symbols for single-input single-output (SISO) OFDM systems*:

d:	number of null subcarriers in an OFDM symbol
$\mathbf{H}$:	diagonal frequency-domain channel matrix
$\mathbf{H}^k$:	diagonal frequency-domain channel matrix for the k^{th} OFDM symbol
$\text{ICI}_{l_i}^k(\varepsilon)$:	inter-carrier interference on subcarrier l_i in the k^{th} OFDM symbol due to a carrier frequency offset of ε
K:	number of OFDM symbols used for carrier frequency offset estimation
$\mathbf{l}$:	vector containing the indices of all null subcarriers
N:	number of subcarriers in an OFDM symbol
P:	number of data subcarriers in an OFDM symbol
Q:	number of terms used in the Taylor series expansion
$\mathbf{r}$:	received time-domain OFDM symbol
$\mathbf{r}^{cp}$:	received time-domain OFDM symbol before removing cyclic prefix
$\mathbf{r}^k$:	k^{th} received time-domain OFDM symbol
$\mathbf{s}$:	transmitted frequency-domain OFDM symbol
$\mathbf{s}^k$:	k^{th} transmitted frequency-domain OFDM symbol
SNR_{CFO}:	SNR of carrier frequency offset estimation
$\mathbf{T}_k$:	carrier frequency offset compensation matrix for the k^{th} iteration
$\mathbf{x}$:	transmitted time-domain OFDM symbol
$\mathbf{x}^{cp}$:	transmitted time-domain OFDM symbol after appending cyclic prefix
$\mathbf{y}$:	frequency-domain received OFDM symbol
$y_{l_i}^k$:	frequency-domain received signal on subcarrier l_i in the k^{th} OFDM symbol

- *Symbols for multiple-input multiple-output (MIMO) OFDM systems*:

ϕ_d:	residual carrier frequency offset after compensation
$\rho_{m,n}$:	correlation coefficient between antennas m and n
$\mathbf{C}_{\text{tx}}$:	mutual coupling matrix of all transmit antennas
$\mathbf{C}_{\text{rx}}$:	mutual coupling matrix of all receive antennas
$\mathbf{H}$:	MIMO channel matrix in flat fading channels
$\mathbf{H}_{\text{iid}}$:	MIMO channel matrix in flat fading channel assuming all elements are identically and independently distributed

$\mathbf{H}(k)$: frequency-domain MIMO channel matrix on subcarrier k in a MIMO-OFDM system

$H_{i,j}(k)$: frequency-domain channel response on subcarrier k between the j^{th} transmit antenna and the i^{th} receive antenna

$\boldsymbol{\mathcal{H}}$: $(N \times n_t) \times n_r$ time-domain channel matrix containing the channel impulse responses for all transmit and receive antenna pairs

$\mathcal{H}$: $N \times n_r$ time-domain channel matrix simplified from $\boldsymbol{\mathcal{H}}$ assuming CAZAC training sequences

$\mathbf{h}_{i,j}$: $N \times 1$ vector consisting of the $L \times 1$ channel impulse response vector between the j^{th} transmit antenna and the i^{th} receive antenna and a $(N-L) \times 1$ zero vector

$\mathbf{h}_{i,j}^{\tau}$: vector obtained by circularly shifting $\mathbf{h}_{i,j}$ τ elements downwards

$h_{i,j}(k)$: k^{th} tap of the channel impulse response between the j^{th} transmit antenna and the i^{th} receive antenna

$\boldsymbol{\mathcal{I}}_L$: first L rows of an $N \times N$ identity matrix

$\bar{\boldsymbol{\mathcal{I}}}_L$: last $N-L$ rows of an $N \times N$ identity matrix

J_0: Bessel function of the first kind and order 0

L: number of multipath components in the impulse response of the channel

$\boldsymbol{\mathcal{N}}$: AWGN noise matrix for all the receive antennas

N: length of one period of the training sequence

n_t: number of transmit antennas

n_r: number of receive antennas

$\text{PAS}(\theta)$: power angular spectrum at an angle θ

$\boldsymbol{\mathcal{R}}$: Received signal matrix from all receive antennas

$\mathbf{R}_{\text{tx}}$: correlation matrix of all transmit antennas

$\mathbf{R}_{\text{rx}}$: correlation matrix of all receive antennas

$\mathbf{R}_{\text{r}}$: covariance matrix of the received signal

$\mathbf{S}_m$: an $N \times N$ circulunt matrix with the first column equal to the training sequence of the m^{th} transmit antenna

$\boldsymbol{\mathcal{S}}$: Matrix containing circulunt training matrices from all transmit antennas

Z_s: self impedance of the antenna

Z_m: mutual impedance between the antennas

Z_{load}: loading impedance of the antenna

Chapter 1

Introduction

In this chapter, we first provide an overview of the wireless communication system and the characteristics of the wireless communication channel. We then describe the Orthogonal Frequency Division Multiplexing (OFDM) system and show its numerous advantages that have made it one of the most widely adopted systems for wireless communications. We also briefly introduce the Multiple Input Multiple Output (MIMO) OFDM system and the multi-user MIMO-OFDM system, which uses OFDM technology in a multi-antenna and multi-user context to further increase the achievable data rates in wireless channels. The detrimental effect of frequency synchronization error in the form of carrier frequency offset (CFO) on the performance of OFDM systems is described next. We show that to guarantee good performance of OFDM systems, the CFO must be accurately estimated and compensated. We then present a literature review on the frequency synchronization, including CFO estimation and compensation, for different OFDM systems and high-

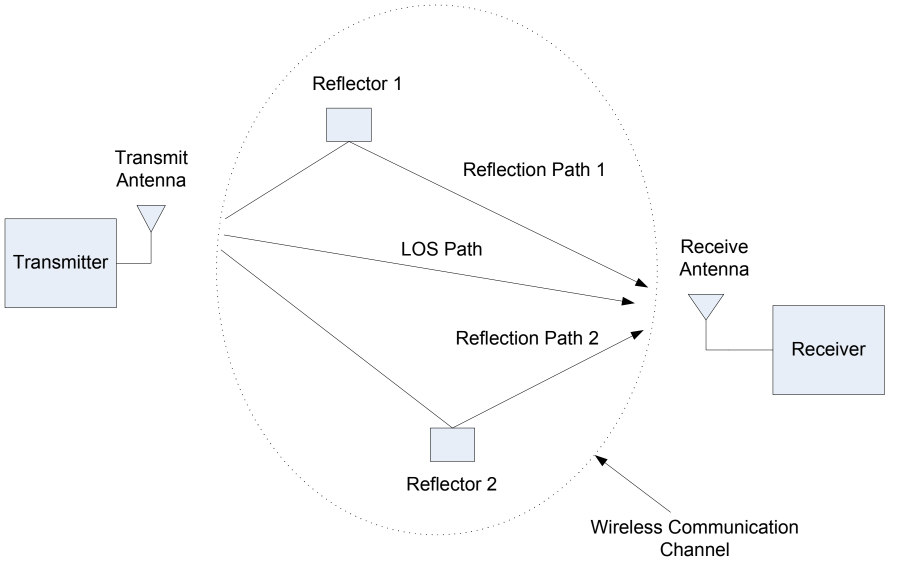

Fig. 1.1: Block diagram of a point to point wireless communication system.

light specific challenges, which motivate the research work in this thesis. This chapter concludes by a description of the outline of and contributions in the following chapters of this thesis.

1.1 Overview of Wireless Communication Systems

Figure 1.1 shows a brief block diagram of a point to point wireless communication system. The system consists of a transmitter with a transmit antenna, a receiver with a receive antenna and the wireless communication channel in between. For digital wireless communication systems, the transmitter takes the information that the user wants to transmit, encodes it, modulates the encoded signal to an allocated frequency band, and transmits it via the transmit antenna in the form of electromagnetic (EM) waves to the wireless communication channel. The wireless communication channel is the media where the transmitted EM waves from the transmit antenna propagate to the receive antenna. The functionalities of the receiver include gathering the EM waves using the receive antenna and processing them to produce an estimate of the transmitted information. One important parameter in wireless communications is the spectrum allocated for transmission. This determines the frequency band in which the wireless communication is allowed to take place, and also the bandwidth of the communication system.

The wireless communication channel is characterized by multi-path propagation. Besides the direct line of sight (LOS) propagation path, the transmitted signal reaches the receiver also via large numbers of reflection paths with different propagation delays. These reflections are caused by the terrain and obstacles in the propagation environments such as buildings, vehicles, pedestrians and walls *etc.* Figure 1.1 illustrate a simple example of multipath propagations in wireless communication channels for three paths. In this case, the transmitted signal from the transmit antenna reaches the receive antenna through both the LOS path and the reflection path 1 and 2 from reflector 1 and 2. Due to the different delays of these propagations paths, the receive antenna will receive multiple versions of the transmitted signal at slightly different times. In this case, the overall channel can be modeled as the summation of different channel components from different propagation paths [1] [2]. The maximum delay spread of the channel is defined as the difference between the maximum and the minimum delays among different propagation paths. As each path component has randomly distributed amplitude and phase over time, the amplitude and phase of the overall channel may experience rapid fluctuations over a short period of time. This type of channel is called fading channel.

In digital communications, the digital information is mapped to analog waveforms suitable for transmission over a communication channel using a digital modulator [3]. Normally, the digital modulator takes blocks of k binary bits and maps them to one of $M = 2^k$ deterministic analog waveforms. Each block of k binary bits is called a digital data symbol, while the duration of the analog waveform corresponds to a digital data symbol is called the symbol duration. When the bandwidth of the system is small, the symbol duration is usually much larger than the maximum delay spread of the channel. In this case, the gain (including both the amplitude and phase) of the overall fading channel can be modeled as a scalar random variable in the time domain. In the frequency domain, this type of channel has a constant (flat) frequency response over the transmission band and hence, is also called flat fading channel. When the bandwidth of the system is large, the symbol duration is smaller than the maximum delay spread of the channel. In this case, the channel can be viewed as a finite impulse response (FIR) filter with multiple nonzero taps and each tap is modeled as a random variable. In the frequency domain, the channel responses at different frequencies in the transmission band are different. This type of fading channel is called frequency selective fading channel. In the time domain, the frequency selective fading channel causes inter-symbol interference (ISI) in the received signal, which can significantly degrade the system performance.

In the past few decades, wireless communication technology has evolved enormously, from expensive and exclusive professional (e.g. military) equipment to today's omnipresent low-cost consumer systems such as Global System for Mobile communications (GSM), Bluetooth, and wireless local area networks (WLAN). We also see a trend in wireless technology from supporting only voice and low-rate data services towards supporting high-rate multimedia applications. For example, as shown in Figure 1.2, in well under a decade, WLAN technology has evolved from the first IEEE 802.11b system supporting a peak data rate of 11 Mb/s [4] to the state-of-the-art IEEE 802.11n system supporting a peak data rate of 600 Mb/s [5]. Moreover, in the IEEE 802.11 VHT (very high throughput) standard, which is expected to be finalized in 2012, the peak data rate will go beyond 1 Gb/s [6]. This trend is further confirmed by the Edholm's law [7], which states that data rates of wireless systems evolve exponentially over time, in lockstep with Moore's law [8] for the evolution of digital IC technology. To support such high data rates in the order of Mb/s or Gb/s, the bandwidth of the system is normally in the order of tens of MHz or a few GHz. These high data rate communication systems are also referred to as broadband communication systems in contrast with narrow band communication systems with bandwidth in the kHz order. For broadband communication systems, channels are usually frequency selective fading channels and they introduce ISI into the received signal. One method to mitigate the detrimental effect of ISI is to use adaptive equalization techniques [9] [10]. However, at data rates in the order of Mbps, adaptive equalization requires high-cost and sophisticated hardware [11].

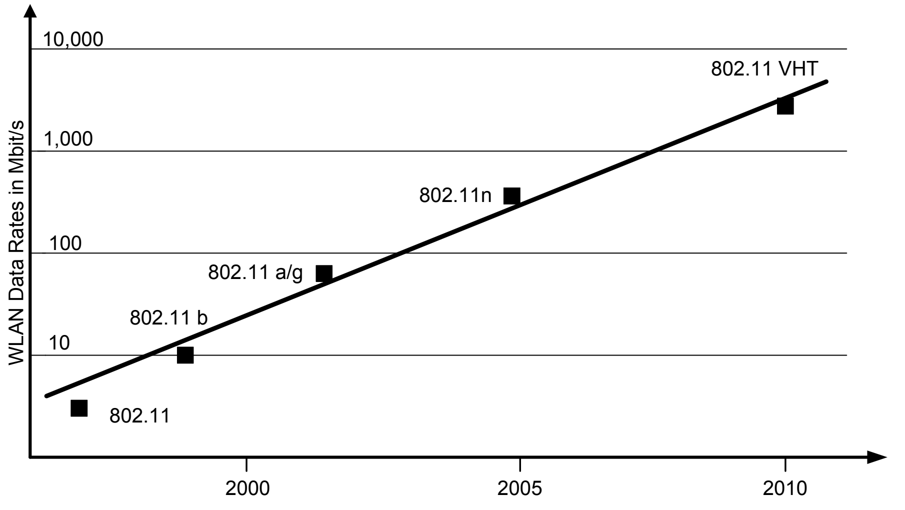

Fig. 1.2: Demand for data rate in WLAN systems.

1.2 Overview of OFDM Systems

As wireless communication evolves towards broadband systems to support high data rate applications, we need a technology that can efficiently handle frequency-selective fading. The Orthogonal Frequency Division Multiplexing (OFDM) system is widely used in this context. The pioneering work on OFDM was first started in the 60's in [12] and [13]. The key idea of OFDM is to divide the whole transmission band into a number of parallel subchannels (also called subcarriers) so that each subchannel is a flat fading channel [14] [15]. In this case, channel equalization can be performed in all subchannels in parallel using simple one-tap equalizers, which have very small computational complexity.

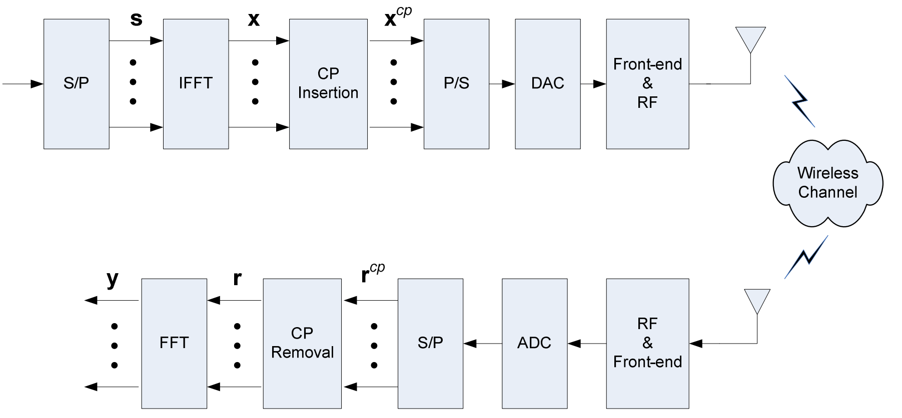

Fig. 1.3: Block diagram of an OFDM system.

1.2.1 Basic Principles of OFDM

A block diagram of an OFDM system is depicted in Figure 1.3. Here, for simplicity and clearness of illustration, we leave out the channel coding block. The incoming digital data are first passed to a serial to parallel converter (S/P) and converted to blocks of N data symbols. Each block is called a frequency-domain OFDM symbol and N is the number of subchannels (subcarriers). Let us use $\mathbf{s} = [s_0, s_1, \cdots, s_{N-1}]^T$, where superscript T denotes vector transpose, to denote one frequency domain OFDM symbol. The modulation in OFDM is performed using the inverse discrete Fourier Transform (IDFT) as follows

$$\mathbf{x} = \mathbf{W}\mathbf{s}, \tag{1.1}$$

where $\mathbf{W}$ denotes the $N \times N$ IDFT matrix, with the (m, n)th element given by

$$W_{m,n} = \frac{1}{\sqrt{N}} \exp\left(j2\pi \frac{mn}{N}\right).$$

In practice, the IDFT is normally performed using a more computationally efficient method, the inverse fast Fourier Transform (IFFT). We call elements of $\mathbf{x}$ samples. After modulation, the last N_g samples of $\mathbf{x}$ are appended in front of $\mathbf{x}$, such that $\mathbf{x}^{cp} = [x_{N-N_g}, x_{N-Ng+1}, \cdots x_{N-1}, x_0, x_1, \cdots, x_{N-1}]^T$ is cyclic. These N_g samples are called cyclic prefix (CP) and $\mathbf{x}^{cp}$ is called a time domain OFDM symbol. The process of CP insertion can be written in an equivalent matrix form as $\mathbf{x}^{cp} = \mathbf{A}^{cp}\mathbf{x}$, where $\mathbf{A}^{cp} = [\mathbf{I}_N(N-N_g : N-1, :); \mathbf{I}_N]$. Here, $\mathbf{I}_N$ denotes the identity matrix of size $N \times N$ and we use the MATLAB notation $\mathbf{I}_N(N - N_g : N - 1, :)$ to denote the last N_g rows of $\mathbf{I}_N$. After CP insertion, the time-domain OFDM symbol $\mathbf{x}^{cp}$ is passed to a parallel to serial converter (P/S). The output is converted to an analog signal using a digital to analog converter (DAC), modulated and amplified through the front-end and radio frequency (RF) block and transmitted via the antenna to the wireless channel.

At the receiver, the received RF signal at the receive antenna is first demodulated through the receiver RF and front-end block. The resulting analog signal is then converted to digital form using the analog to digital converter (ADC) and then the serial digital signal is converted to time-domain symbols $\mathbf{r}^{cp}$ of size $N + N_g$ through the serial to parallel converter (S/P). Considering the transmission of only the current OFDM symbol $\mathbf{x}^{cp}$, the k^{th} sample of $\mathbf{r}^{cp}$ can be written as

$$r_k^{cp} = \sum_{i=0}^{L-1} h_{k-i} x_i^{cp} + n_k, \tag{1.2}$$

where h_k is the k^{th} tap of the impulse response of the multi-path channel $\mathbf{h} = [h_0, \cdots, h_{L-1}]^T$, x_i^{cp} is the ith element of $\mathbf{x}^{cp}$ and n_k is the additive white Gaussian noise (AWGN). Here we use L to denote the maximum length of the channel impulse response. To make sure there is no ISI, the length of the CP should satisfy $N_g \geq L$. Using matrix notation, the received signal in (1.2) can be written equivalently as

$$\mathbf{r}^{cp} = \mathbf{H}_t \mathbf{x}^{cp} + \mathbf{n}, \tag{1.3}$$

where $\mathbf{H}_t$ is a $(N + N_g) \times (N + N_g)$ lower triangular Toeplitz matrix with the first column given by $[h_0, h_1, \cdots, h_{L-1}, 0, \cdots, 0]^T$ as shown below

$$\mathbf{H}_t = \begin{bmatrix} h_0 & 0 & \cdots & 0 & \cdots & 0 & 0 \\ h_1 & h_0 & \cdots & 0 & \cdots & 0 & 0 \\ \vdots & \vdots & \ddots & \vdots & \ddots & \vdots & \vdots \\ h_{L-1} & h_{L-2} & \cdots & h_0 & \cdots & 0 & 0 \\ \vdots & \vdots & \ddots & \vdots & \ddots & \vdots & \vdots \\ 0 & 0 & \cdots & 0 & \cdots & h_0 & 0 \\ 0 & 0 & \cdots & 0 & \cdots & h_1 & h_0 \end{bmatrix}.$$

At the receiver, the first N_g samples of $\mathbf{r}^{cp}$ due to the cyclic prefix are removed, which is indicated by the CP removal block in Figure 1.3. Again this can be written in matrix form as $\mathbf{r} = \mathbf{D}^{cp}\mathbf{r}^{cp}$, where $\mathbf{D}^{cp} = [\mathbf{0}_{N \times N_g}, \mathbf{I}_N]$ with $\mathbf{0}_{N \times N_g}$ denotes a matrix of size $N \times N_g$ whose elements are all 0. Hence, we have the received time-domain signal after CP removal given by

$$\begin{aligned} \mathbf{r} &= \mathbf{D}^{cp}\mathbf{H}_t\mathbf{A}^{cp}\mathbf{W}\mathbf{s} + \mathbf{n} \\ &= \mathbf{H}_c\mathbf{W}\mathbf{s} + \mathbf{n}, \end{aligned} \tag{1.4}$$

where $\mathbf{H}_c = \mathbf{D}^{cp}\mathbf{H}_t\mathbf{A}^{cp}$. Notice that the effects of CP insertion, channel convolution and CP removal are combined into a single matrix $\mathbf{H}_c$. It can be easily shown that $\mathbf{H}_c$ is an $N \times N$ circulant matrix given by

$$\mathbf{H}_c = \begin{bmatrix} h_0 & 0 & \cdots & 0 & \cdots & h_2 & h_1 \\ h_1 & h_0 & \cdots & 0 & \cdots & h_3 & h_2 \\ \vdots & \vdots & \ddots & \vdots & \ddots & \vdots & \vdots \\ h_{L-1} & h_{L-2} & \cdots & h_0 & \cdots & 0 & 0 \\ \vdots & \vdots & \ddots & \vdots & \ddots & \vdots & \vdots \\ 0 & 0 & \cdots & 0 & \cdots & h_0 & 0 \\ 0 & 0 & \cdots & 0 & \cdots & h_1 & h_0 \end{bmatrix}.$$

Next the time-domain signal $\mathbf{r}$ is transformed to the frequency domain using an N-point FFT. The frequency-domain received signal can be written as

$$\mathbf{y} = \mathbf{W}^H\mathbf{r} = \mathbf{W}^H\mathbf{H}_c\mathbf{W}\mathbf{s} + \mathbf{W}^H\mathbf{n},$$

where $\mathbf{W}^H$ is an $N \times N$ DFT matrix and superscript ^{H} denotes matrix Hermitian. Since $\mathbf{H}_c$ is a circulant matrix, it can be diagonalized by the IDFT matrix as follows

$$\mathbf{H}_c = \mathbf{W}\mathbf{H}\mathbf{W}^H,$$

where $\mathbf{H}$ is a diagonal matrix given by $\mathbf{H} = \mathrm{diag}(\mathbf{W}^H\mathbf{h}_c)$ and $\mathbf{h}_c$ is the first column of $\mathbf{H}_c$. In other words, the diagonal elements of $\mathbf{H}$ are the DFT of the channel impulse response $\mathbf{h}$ and can be interpreted as the channel frequency responses on N subchannels (subcarriers). Using this property, we can re-write the frequency domain received signal as

$$\begin{aligned}\mathbf{y} &= \mathbf{W}^H\mathbf{H}_c\mathbf{W}\mathbf{s} + \mathbf{W}^H\mathbf{n} = \mathbf{W}^H\left(\mathbf{W}\mathbf{H}\mathbf{W}^H\right)\mathbf{W}\mathbf{s} + \mathbf{W}^H\mathbf{n} \\ &= \mathbf{H}\mathbf{s} + \mathbf{n}',\end{aligned} \tag{1.5}$$

where $\mathbf{n}'$ is the frequency domain noise term, which is also Gaussian distributed with zero mean and has the same variance as $\mathbf{n}$. Because $\mathbf{H}$ is a diagonal matrix, we see that different subcarriers are perfectly decoupled after the FFT operation and the frequency selective fading channel can be equalized using a simple one-tap equalizer on each subcarrier individually.

By way of illustration, the amplitude spectra of subcarriers 6 to 10 for an OFDM system with $N = 16$ are sketched in Figure 1.4. We can see that the spectra of different subcarriers are overlapping. At the center of each subcarrier, the signals from the other subcarriers are 0. This means that in OFDM systems, different subcarriers are orthogonal at the center of each subcarrier, although their spectra are overlapping.

From above, we can see that in OFDM systems, the frequency selective fading channel is divided into a number of flat fading subchannels. As a result, complicated time-domain equalization of the frequency selective fading channel can be performed equivalently in the frequency domain using a simple one-tap equalizer on each subchannel. Hence, OFDM provides a more efficient method to handle frequency selective fading compared to single-carrier systems with time-domain equalizer.

By combining OFDM with error control coding, the coded OFDM system is

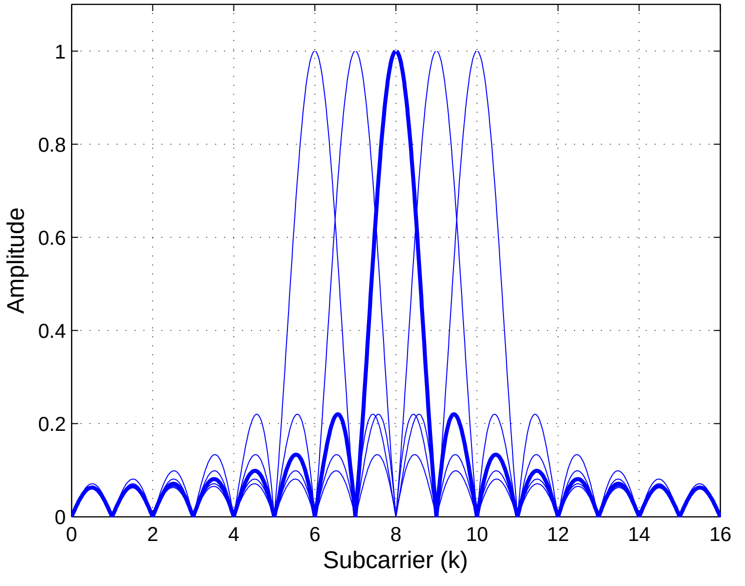

Fig. 1.4: Amplitude spectra of subcarriers 6 to 10 for an OFDM system with 16 subcarriers.

also more robust to narrow-band interferences [16]. This is because narrow-band interferences only affects a small number of subcarriers and causes detection errors on these subcarriers. These detection errors can usually be corrected by error control coding. Due to these advantages, OFDM has been adopted in many modern wireless communication standards such as IEEE 802.11a/g WLAN [17] [18], IEEE 802.16e Broadband Wireless Access (also known as WiMAX) [19], Digital Audio Broadcasting (DAB) [20] and Digital Video Broadcasting (DVB) [21].

However, OFDM also has some disadvantages. Firstly, because the modulation is performed using IDFT, the peak to average power ratio (PAPR) of time-domain OFDM signals is higher compared to single-carrier systems. This puts high requirements on the dynamic range of the RF amplifiers and introduces extra clipping noise in the system [22] [23]. Another disadvantage of the OFDM system is that it is more sensitive to frequency synchronization errors compared to single-carrier systems. This topic will be discussed in more detail in Section 1.3.

1.2.2 MIMO-OFDM and Multi-user MIMO-OFDM systems

In wireless communications, the term multiple input multiple output (MIMO) refers to systems using multiple transmit and multiple receive antennas. Since the discovery in [24] and [25] that the capacity of wireless channels is linearly proportional to the minimum of the number of transmit and receive antennas, MIMO has become one of the hottest topics in wireless communications. In academia, thousands of research papers were published addressing capacity limits, transmission schemes, and receiver signal processing and algorithm design. In industry, MIMO has been included in various industrial standards, including WiMAX (IEEE 802.16e) [19], high-throughput WLAN (IEEE 802.11n) [5] and 3rd Generation Partnership Project (3GPP) [26].

Compared to the single input single output (SISO) system, the use of multiple antennas enables the MIMO system to exploit the extra spatial dimension. One of the many benefits of having this extra spatial dimension can be illustrated using the following example. For a SISO system with a deterministic channel h, the received signal can be written as $r = hs + n$, where s is the transmitted symbol with symbol energy E_s and n is the zero mean AWGN noise with power spectrum density N_0. The well-known Shannon capacity in bits per second per Hertz (bps/Hz) for this channel can be written as

$$C = \log_2\left(1 + \frac{E_s}{N_0}|h|^2\right) \quad \text{bps/Hz}. \tag{1.6}$$

For a MIMO system with n_t transmit and n_r receive antennas, the channel is an $n_r \times n_t$ matrix and the received signal vector from n_r receive antennas can be written as

$$\begin{aligned}
\begin{bmatrix} r_1 \\ \vdots \\ r_{n_r} \end{bmatrix} &= \begin{bmatrix} H_{1,1} & \cdots & H_{1,n_t} \\ \vdots & \ddots & \vdots \\ H_{n_r,1} & \cdots & H_{n_r,n_t} \end{bmatrix} \begin{bmatrix} s_1 \\ \vdots \\ s_{n_t} \end{bmatrix} + \begin{bmatrix} n_1 \\ \vdots \\ n_{n_r} \end{bmatrix} \\
\mathbf{r} &= \mathbf{Hs} + \mathbf{n},
\end{aligned} \tag{1.7}$$

where r_i is the received signal from the ith receive antenna, and $H_{i,j}$ is the channel response between the jth transmit antenna and ith receive antenna. The $n_t \times 1$ transmitted signal vector is denoted $\mathbf{s}$ with covariance matrix $\mathrm{E}(\mathbf{ss}^H) = E_s/n_t\mathbf{I}_{n_t}$, where $\mathrm{E}(\bullet)$ denotes statistical expectation and $\mathbf{I}_{n_t}$ denotes identity matrix with size $n_t \times n_t$. The noise $\mathbf{n}$ is an $n_r \times 1$ vector with covariance matrix given by $\mathrm{E}(\mathbf{nn}^H) = N_0\mathbf{I}_{n_r}$. The capacity of this MIMO channel can be calculated as [27]

$$\begin{aligned}
C &= \log_2\left[\det\left(\mathbf{I}_{n_r} + \frac{E_s}{n_t N_0}\mathbf{HH}^H\right)\right] \\
&= \log_2\left[\det\left(\mathbf{I}_{n_r} + \frac{E_s}{n_t N_0}\boldsymbol{\Lambda}\right)\right] \\
&= \sum_{k=1}^{R_{\mathbf{H}}}\left(1 + \frac{E_s}{n_t N_0}\lambda_k\right) \quad \text{bps/Hz},
\end{aligned} \tag{1.8}$$

where det(•) denotes the determinant of a matrix, $\mathbf{\Lambda}$ is an $n_r \times n_r$ diagonal matrix with elements equal to the eigenvalues of $\mathbf{HH}^H$. In the last line of (1.8), $R_\mathbf{H}$ is the rank of the channel matrix $\mathbf{H}$ and λ_k is the k^{th} eigenvalue of $\mathbf{HH}^H$. In wireless environments with many scatterers and reflectors, such as the indoor environment, the rank of the channel matrix $R_\mathbf{H} \approx \min(n_t, n_r)$. Comparing (1.8) with (1.6), it can be seen that in MIMO systems, multiple ($R_\mathbf{H}$) parallel SISO channels are created in the spatial domain. This significantly increases the capacity of the wireless fading channel.

MIMO systems have the following key benefits compared to SISO systems [28]:

- Array gain: The signal to noise ratio (SNR) of the received signal can be enhanced by coherently combining the desired signals at the transmit and receive antenna arrays. This can be done either using receive beamforming techniques at the receiver, or using transmit beamforming techniques at the transmitter.
- Diversity gain: In wireless channels, the received signal level fluctuates due to channel fading. By having multiple antennas, we are able to receive multiple independent copies of the same transmitted signal. In this way, the probability of all these copies experiencing deep fades is significantly smaller compared to SISO systems, where only one copy of the transmitted signal is available. Therefore, the system is more robust to fading and this gain in performance is called diversity gain. The diversity in MIMO systems can be exploited at the transmitter using space-time coding techniques [29] [30], or at the receiver using diversity combining techniques [31].
- Spatial multiplexing gain: As shown in the example above (1.8), multiple

antennas at the transmitter and the receiver create multiple parallel SISO transmission channels in the spatial domain. This makes it possible to multiplex different data streams on different transmit antennas and achieve a higher data rate using the same bandwidth.

- Interference mitigation: In a multi-user environment, interference from other users using the same frequency band can severely degrade the performance of the desired user. This interference can be mitigated using signal processing techniques in the spatial dimension provided by MIMO systems. For example, using beamforming techniques, the receiver can create beam patterns with main lobes pointing to the desired user and with nulls pointing to the interfering users.

Notice that the received signal model for a MIMO system in (1.7) is for flat fading channels. In frequency selective fading channels, the channel impulse response between each transmit and receive antennas becomes a vector. Moreover, the multiplication of $\mathbf{H}$ and $\mathbf{s}$ in (1.7) becomes the convolution of the channel impulse response with the transmitted signal. Conventional time domain equalization in MIMO systems is more complicated compared to SISO systems as there are now $n_t \times n_r$ channels to equalize. In SISO systems, OFDM can transform the frequency-selective fading channel into a numbers of flat fading subchannels. This makes the combination of MIMO and OFDM, i.e. the MIMO-OFDM system, an excellent solution for employing MIMO in frequency selective fading channels [32] [33] [34]. A block diagram of a MIMO-OFDM system with n_t data streams, n_t transmit antennas and n_r receive antennas is shown in Figure 1.5. We can see that at the transmitter, for each data stream, there is one SISO OFDM transmitter chain similar to that in Figure

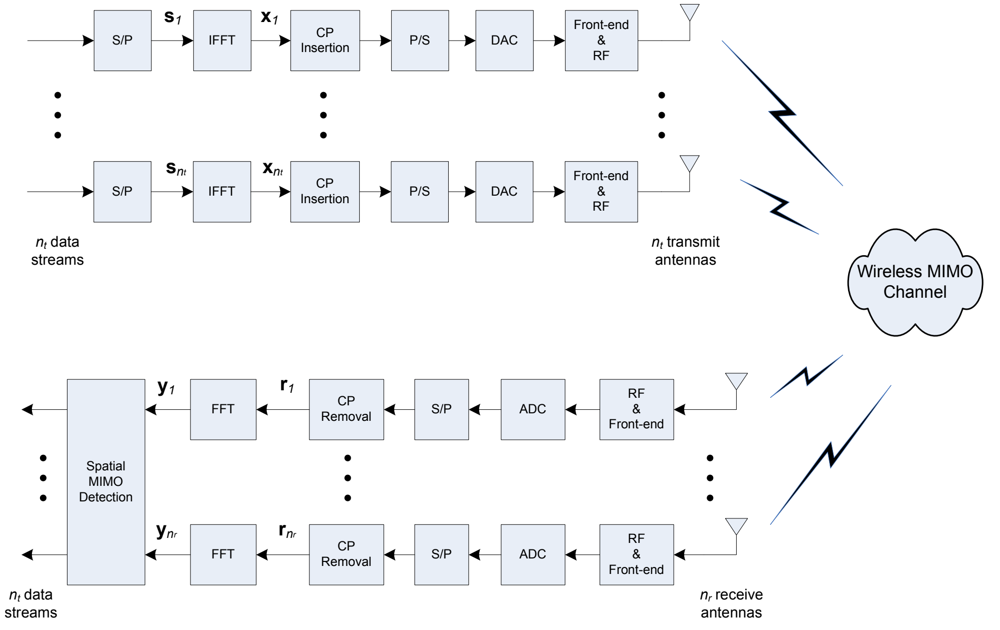

Fig. 1.5: A block diagram of a MIMO-OFDM system.

1.3. At the receiver, the signals from different receive antennas are processed in a parallel fashion similar to a SISO OFDM receiver to get the frequency domain received signals $\mathbf{y}_1$ to $\mathbf{y}_{n_r}$. On the k^{th} subcarrier, the received signal for a MIMO-OFDM system can be written as

$$\begin{bmatrix} y_1(k) \\ \vdots \\ y_{n_r}(k) \end{bmatrix} = \begin{bmatrix} H_{1,1}(k) & \cdots & H_{1,n_t}(k) \\ \vdots & \ddots & \vdots \\ H_{n_r,1}(k) & \cdots & H_{n_r,n_t}(k) \end{bmatrix} \begin{bmatrix} s_1(k) \\ \vdots \\ s_{n_t}(k) \end{bmatrix} + \begin{bmatrix} n_1(k) \\ \vdots \\ n_{n_r}(k) \end{bmatrix}. \quad (1.9)$$

We can see that on each subcarrier in a MIMO-OFDM system, the signal model is equivalent to a flat fading MIMO system. Therefore, the received signal from different receive antennas can be processed subcarrier wise in the spatial MIMO detection block as shown in Figure 1.5.

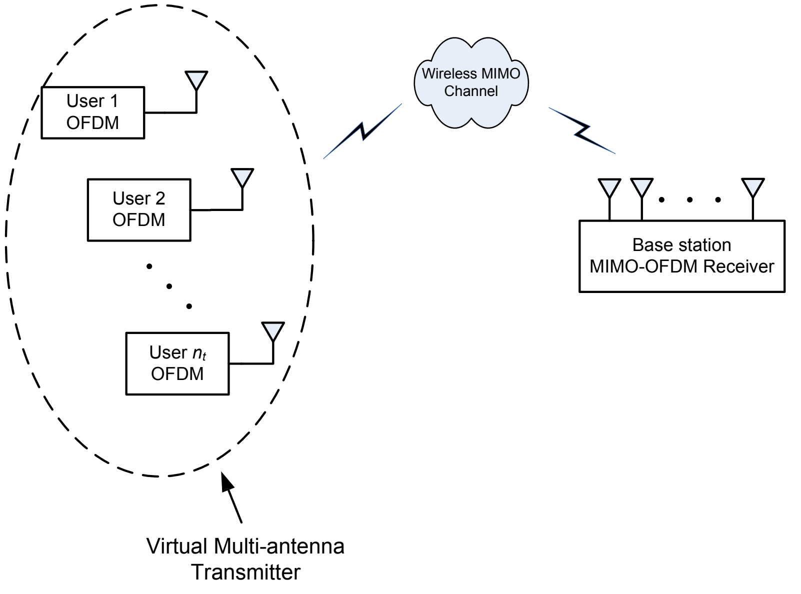

Fig. 1.6: Illustration of a multi-user MIMO-OFDM system.

The multi-user MIMO-OFDM system is an extension of the MIMO-OFDM system to the multi-user context. An illustration of the multi-user MIMO-OFDM system is shown in Figure 1.6. Here multiple users, each with one or more transmit antennas, transmit simultaneously using OFDM in the same frequency band. For clearness of illustration, in Figure 1.6, we only illustrate the case where each user has one transmit antenna. The receiver is a base station with multiple receive antennas. It uses MIMO-OFDM spatial processing techniques to separate the signals from different users. If we view the signals from different users as signals from different transmit antennas of a virtual multi-antenna transmitter, then the whole system can be viewed as an MIMO-OFDM system. This system is also known as the virtual MIMO-OFDM system [35].

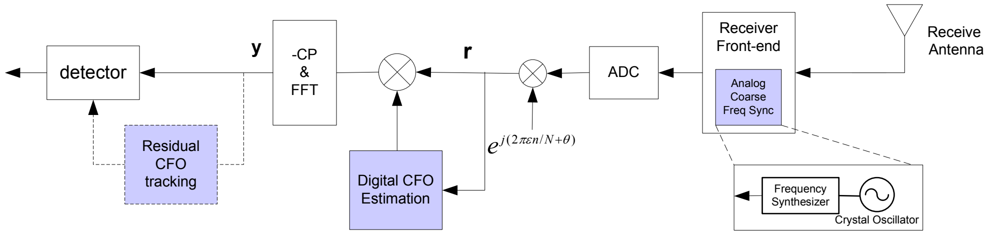

Fig. 1.7: An OFDM receiver with frequency synchronization.

1.3 Effects of Frequency Synchronization Errors in OFDM Systems

In the previous section, we presented an overview of OFDM and MIMO-OFDM systems. We highlighted the advantages of OFDM and MIMO-OFDM and also mentioned that sensitivity to frequency synchronization errors in the form of carrier frequency offset (CFO), is a key disadvantage of OFDM systems. In this section, we present a more detailed study on the effects of CFO on the performance of OFDM systems. As the name suggests, CFO is an offset between the carrier frequency of the transmitted signal and the carrier frequency used at the receiver for demodulation. In wireless communications, CFO comes mainly from two sources:

- The mismatch between oscillating frequencies of the transmitter and the receiver local oscillators (LO);
- The Doppler effect of the channel due to relative movement between the transmitter and the receiver.

In this thesis, we focus on the CFO caused by the mismatch between the transmitter and receiver local oscillators. At the receiver, the effect of CFO is mitigated through frequency synchronization. Figure 1.7 shows an OFDM receiver with frequency synchronization implemented in both the analog and the digital domains. The received signal from the receive antenna is first passed to the receiver front-end. Here, to ensure that the local oscillator at the receiver front-end is operating with sufficient accuracy, its reference frequency is continuously adjusted by the analog coarse frequency synchronization unit [36], which consists of a crystal oscillator and a frequency synthesizer. To get an idea on the accuracy required of the analog coarse synchronization, we look at the IEEE 802.11g standard [18] for wireless LAN systems. In the IEEE 802.11g standard, the specifications for the worst-case frequency errors for both transmitter and receiver LOs (crystal oscillator and frequency synthesizer) are ± 20 ppm (parts per million). This leads to a worst-case CFO of 96 kHz (40 ppm) for center frequency of 2.4 GHz after analog coarse frequency synchronization. For WLAN applications, the maximum duration of a data packet is in the order of ms and the variation of the LO output frequency within this short time duration is negligible. Therefore, the digital domain CFO after analog frequency synchronization can be considered a constant value and estimated once per data packet. After the analog to digital converter, we denote the digital domain CFO normalized with respect to the subcarrier spacing of the OFDM system as ε. This CFO introduces a time dependent phase rotation $e^{j(2\pi\varepsilon n/N)}$ to the received digital time-domain signal, where n is the time index, and N is the number of subcarriers. Together with a constant phase offset θ due to the channel and the analog processing, this introduces a phase rotation of $e^{j(2\pi\varepsilon n/N+\theta)}$ as shown in Figure 1.7. In this way, we can write the received time-domain signal in the m^{th} OFDM symbol interval in the following form [37]

$$\mathbf{r}^m = \mathbf{E}\mathbf{W}\mathbf{H}^m\mathbf{s}^m e^{j(2\pi\varepsilon(m-1)(1+N_g/N)+\theta)} + \mathbf{n}^m. \tag{1.10}$$

The CFO matrix $\mathbf{E} = \mathrm{diag}(1, e^{j2\pi\varepsilon/N}, \cdots, e^{j2\pi(N-1)\varepsilon/N})$ is a diagonal matrix containing the CFO value ε, and N is the number of subcarriers. Matrix $\mathbf{W}$ is the $N \times N$ IDFT matrix, $\mathbf{H}^m$ is a diagonal matrix containing the channel frequency response for different subcarriers, $\mathbf{s}^m$ is the transmitted signal for the m^{th} OFDM symbol and $\mathbf{n}^m$ is the AWGN noise vector. Here we split the phase rotation caused by the CFO into the CFO matrix $\mathbf{E}$ and a phase offset $e^{j2\pi\varepsilon(m-1)(1+N_g/N)}$ for OFDM symbol m.

Notice from (1.10) that the effects of the CFO ε and the constant phase offset θ are represented in the following three terms:

1. a constant phase offset $e^{j\theta}$,
2. a CFO matrix $\mathbf{E}$,
3. a CFO and OFDM symbol index (m) dependent phase offset $e^{j(2\pi\varepsilon(m-1)(1+N_g/N))}$.

The constant phase offset $e^{j\theta}$ is a common scalar multiplied with all the received signals. This gives the same phase offset of $e^{j\theta}$ on all the frequency domain received signals. In this way, it can be considered as part of the frequency domain channel and can be estimated together with the frequency domain channel and compensated using one-tap equalizers. However, the CFO (ε) has to be estimated and compensated in the time domain. This is because, as we are going to show later, in OFDM systems, CFO introduces inter-carrier interference (ICI) in the frequency-domain received signals. For IEEE 802.11g systems, the worst-case digital domain CFO of 96 kHz corresponds to $\varepsilon = 0.31$. The power of ICI due to this CFO is much larger than that of the AWGN noise. This makes CFO estimation in the frequency domain much more complicated compared to that in the time domain as the signal to interference ratio in the frequency domain is very low due to the large ICI. In Figure 1.7, the time-domain CFO estimation is performed in the digital CFO estimation block. The effect of the CFO is compensated from the received signal using the estimate. The compensated signal is passed through the -CP(CP removal) & FFT block and is transformed to the frequency domain. The frequency-domain signal is then passed to the detector. Now let us use an example to show how the digital domain CFO estimation is done for a practical system. Figure 1.8 shows the packet structure of a wireless LAN data packet for IEEE 802.11g systems [18]. Each packet is made up of the following components:

- a preamble, consisting of a short and a long preamble, which contains training symbols known to the receiver for timing synchronization, CFO and channel estimation;
- a signal field, which contains parameters values for the packet, such as packet length N_p, code rate and modulation used in the packet;
- the data: which contains N_p OFDM symbols of useful data from the transmitter. In each OFDM symbol, there are four subcarriers at subcarriers -21, -7, 7 and 21 that contain pilot symbols known to the receiver. These four subcarriers are called pilot subcarriers.

In this system, the digital domain CFO estimation is only performed at the beginning of the packet using both short and long preambles. This estimation must achieve sufficient accuracy such that ICI due to the residual CFO $\Delta\varepsilon$, i.e. the difference between the actual ε and its estimate, is significantly smaller than the AWGN noise. The constant phase offset $e^{j\theta}$ is estimated as part of the channel using the long preamble. Although the ICI due to $\Delta\varepsilon$ is insignificant, the residual CFO still causes a OFDM symbol index (m) dependent phase offset $e^{j(2\pi\Delta\varepsilon(m-1)(1+N_g/N))}$. Different from the constant phase offset $e^{j\theta}$, this phase offset cannot be estimated using channel estimation, because the channel is only estimated at the beginning of the packet using the long preamble, and can become significant when the number of OFDM symbols in a packet is large. This phase offset is estimated and compensated in the frequency domain in the residual CFO tracking block as shown in Figure 1.7 using the four pilot subcarriers in each OFDM symbol. Notice that this phase offset estimation is done after the initial CFO estimation and compensation using the preambles, because without the initial CFO estimation and compensation, the ICI from the CFO will become too large for the phase offset estimation to work properly. As this block is only necessary for packet-based OFDM systems, where CFO and channel estimations are performed at the beginning of the packet, we use dotted lines in Figure 1.7 to indicate that it is optional. The research work in this thesis concerns the time domain estimation of the CFO ε.

As shown in Figure 1.4, in OFDM systems, orthogonality between different subcarriers is maintained only when sampling occurs at the correct frequency, i.e. in the center of each subchannel. Figure 1.9 illustrates what happens when there is a positive CFO ε. Firstly, the amplitude of the desired signal is attenuated. Secondly, the orthogonality between different subcarriers is destroyed and on the desired subcarrier, there exists non-zero ICI from all the

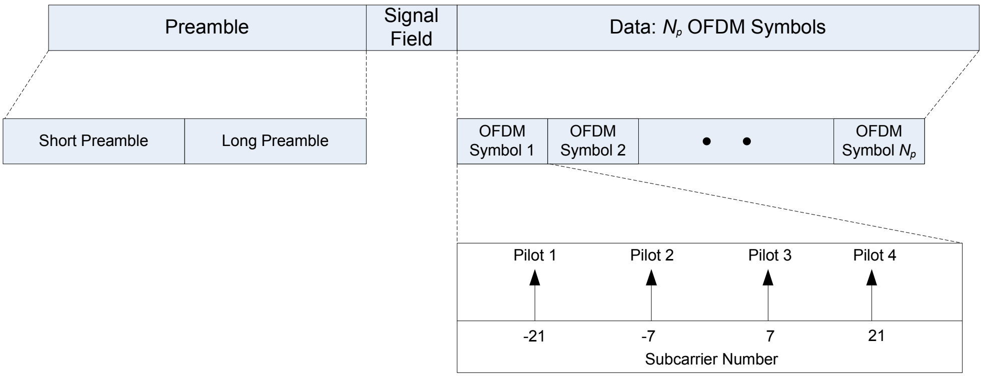

Fig. 1.8: The packet structure of a IEEE 802.11g data packet.

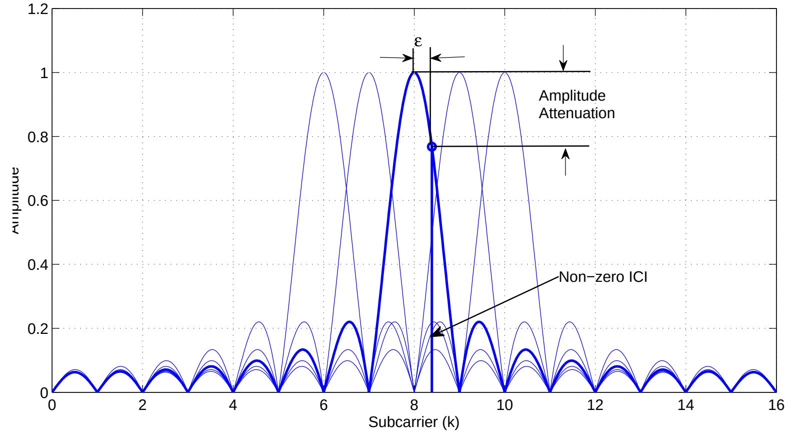

Fig. 1.9: Effects of CFO in OFDM systems

other subcarriers. From (1.10), we can re-write each element of $\mathbf{r}$ in summation form as

$$r_k = \frac{1}{\sqrt{N}} \sum_{l=0}^{N-1} H_l s_l \exp\left(j2\pi \frac{(l+\varepsilon)k}{N}\right) + n_k, \tag{1.11}$$

where H_l and s_l are the channel response and transmitted signal on the lth subcarrier respectively. Here we omit the constant phase offset $e^{j\theta}$ because it can be considered as part of the channel response. Moreover, as the length of the CP is larger than the length of the channel impulse response, there is no ISI between different OFDM symbols. Hence, the OFDM symbol index m in (1.10) is not important for the analysis and is also dropped. Taking the FFT of the received signal $\mathbf{r}$, we get the received signal on the lth subcarrier as

$$\begin{aligned} y_l &= \frac{1}{\sqrt{N}} \sum_{k=0}^{N-1} r_k \exp\left(-\frac{j2\pi kl}{N}\right) \\ &= \frac{1}{N} \sum_{k=0}^{N-1} \sum_{i=0}^{N-1} H_i s_i \exp\left(-\frac{j2\pi k}{N}(l-i-\varepsilon)\right) + n_l' \\ &= \sum_{i=0}^{N-1} H_i s_i \exp\left[j\pi(i-l+\varepsilon)\left(1-\frac{1}{N}\right)\right] \frac{\sin\left(\pi(i-l+\varepsilon)\right))}{N\sin\left(\frac{\pi(i-l+\varepsilon)}{N}\right)} + n_l' \\ &= \left\{\frac{\sin(\pi\varepsilon)}{N\sin\left(\frac{\pi\varepsilon}{N}\right)} \exp(j\pi\varepsilon(1-1/N))\right\} H_l s_l + I_l + n_l', \end{aligned} \tag{1.12}$$

where I_l is the inter-carrier interference from all the other subcarriers on subcarrier l given by

$$I_l = \sum_{k=0,k\neq l}^{N-1} H_k s_k \exp\left[j\pi(k-l+\varepsilon)\left(1-\frac{1}{N}\right)\right] \frac{\sin\left(\pi(k-l+\varepsilon)\right)}{N\sin\left(\frac{\pi(k-l+\varepsilon)}{N}\right)}, \tag{1.13}$$

and n_l' is the AWGN noise in the frequency domain with variance σ_n^2. Equation (1.12) gives the mathematical description of the two detrimental effects of the CFO in OFDM systems. Firstly the amplitude of the desired signal is attenuated to $\frac{\sin(\pi\varepsilon)}{N\sin\left(\frac{\pi\varepsilon}{N}\right)} < 1$. Secondly, besides AWGN noise n_l', there is an additional ICI term I_l. In this case, the signal to interference and noise ratio

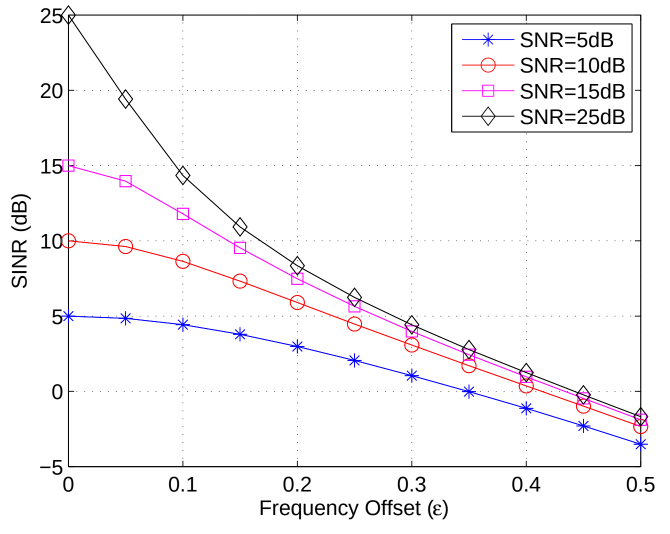

Fig. 1.10: SINR of the received signal in OFDM systems for different CFO values.

(SINR) of the received signal on subcarrier l is given by

$$\mathrm{SINR}_l = \frac{\mathrm{E}(|H_l|^2)\mathrm{E}(|s_l|^2)\frac{\sin^2(\pi\varepsilon)}{N^2\sin^2\left(\frac{\pi\varepsilon}{N}\right)}}{\mathrm{E}(|I_l|^2)+\sigma_n^2}. \tag{1.14}$$

In Figure 1.10, we plot the SINR given in (1.14) for an OFDM system with 64 subcarriers for different CFO values and for 4 signal to AWGN noise ratios ($\mathrm{E}[|H|^2|s|^2]/\sigma_n^2$) of 5, 10, 15 and 25 dB. From the figure, we can see that the SINR degrades significantly as the CFO value increases. As the ICI power is independent of the AWGN noise power, the ICI causes more degradation in high SNR cases compared to low SNR cases. From Figure 1.10, the worst-case CFO of $\varepsilon = 0.31$ in IEEE 802.11g WLAN systems causes a degradation of about 21 dB for SNR of 25 dB. In the same vein, CFO also causes significant performance degradation for MIMO-OFDM and multi-user

MIMO-OFDM systems. Therefore, to guarantee good performance of OFDM systems, CFO must be accurately estimated and compensated.

1.4 Status and Challenges in CFO estimation for OFDM systems

In this section, we present a brief literature review on CFO estimation algorithms for OFDM systems. We also identify challenges in the CFO estimation for SISO, MIMO and multi-user MIMO OFDM systems and motivate the research work carried out in this thesis.

1.4.1 CFO estimation for SISO-OFDM systems

The CFO estimation algorithms for SISO-OFDM systems can be broadly divided into two categories:

1. Training-based CFO estimation algorithms;
2. Blind CFO estimation algorithms.

1.4.1.1 Training based CFO estimation algorithms

In training-based CFO estimation algorithms, specially designed training signals (including preambles and/or pilot subcarriers) known to the receiver are inserted into the data symbols to assist the receiver in estimating the CFO.

Two well-known training-based CFO estimation algorithms for SISO-OFDM systems were proposed by P. Moose [38] and by T.M. Schmidl & D.C. Cox [39].

In Moose's algorithm, two repeated OFDM symbols are transmitted as training symbols. As the second OFDM symbol is identical to the first one, the last N_g samples of the first OFDM symbol have the same effect as the cyclic prefix for the second OFDM symbol. Hence, it is not necessary to append a CP to the second OFDM symbol. The assumption in this algorithm is that the starting point of an OFDM symbol is known. In this case, using similar notations as in (1.10), the time domain received signals in these two OFDM symbol intervals can be written as

$$\mathbf{r} = \begin{bmatrix} \mathbf{EWHs} \\ e^{j2\pi\varepsilon}\mathbf{EWHs} \end{bmatrix} + \mathbf{n}, \tag{1.15}$$

where $\mathbf{r}$ is a $2N \times 1$ vector containing received signal for two OFDM symbols. Here we assume a slowly time-varying channel such that the channel within the two OFDM symbol intervals can be considered the same. Taking the FFT of the received signals, we get the frequency-domain signals in the two OFDM symbol intervals given by

$$\mathbf{y} = \begin{bmatrix} \mathbf{W}^H\mathbf{EWHs} \\ e^{j2\pi\varepsilon}\mathbf{W}^H\mathbf{EWHs} \end{bmatrix} + \mathbf{n}', \tag{1.16}$$

where $\mathbf{n}'$ is the frequency domain noise vector, which has the same statistical properties as $\mathbf{n}$. In the noiseless condition, the difference between the first and the second N elements of $\mathbf{y}$ is a constant phase shift of $e^{j2\pi\varepsilon}$ due to the CFO. It is shown in [38] that the maximum likelihood (ML) estimate of the CFO ε is given by

$$\hat{\varepsilon} = \frac{1}{2\pi}\tan^{-1}\left\{\frac{\sum_{l=0}^{N-1}\Im[y_{l+N}y_l^*]}{\sum_{l=0}^{N-1}\Re[y_{l+N}y_l^*]}\right\}, \tag{1.17}$$

where $\Im(\bullet)$ and $\Re(\bullet)$ denote the imaginary and the real parts of a complex number respectively and superscript * denotes complex conjugation. It is shown in [38] that this estimate is conditionally unbiased for small CFO values. The mean square error (MSE) of this estimator is given by

$$\mathrm{MSE}(\hat{\varepsilon}) = \frac{1}{(2\pi)^2 N\gamma}, \tag{1.18}$$

where

$$\gamma = \frac{\mathbf{tr}\left(\mathbf{H}\mathbf{H}^H\right)}{N}\frac{\sigma_s^2}{\sigma_n^2}$$

is the SNR of the received signal. Here we use $\mathbf{tr}(\bullet)$ to denote the trace of a matrix, and σ_s^2 and σ_n^2 are the power of the transmitted signal and noise respectively. The acquisition range of this algorithm is limited in ± 0.5 subcarrier spacing. This is smaller than the worst-case CFO of 0.64 in IEEE 802.11a wireless LAN systems operating in the 5 GHz band. It is suggested in [38] that the acquisition range can be increased by using shorter repeated frequency domain training symbols. Decreasing the length of the training symbol by a factor of n will increase the acquisition range n times. On the other hand, from (1.18), we can see that reducing the length of training symbol degrades the MSE of the CFO estimation. The length of the training symbol also needs to be kept longer than the channel delay spread so as not to cause any distortion when estimating the CFO.

One limitation of Moose's algorithm is that it requires knowledge of the starting point of an OFDM symbol. In [39], Schmidl & Cox proposed an algorithm that can estimate timing and frequency offset using the same time-domain training sequence. In their method, the time-domain OFDM symbol used for training consists of two identical halves, i.e. $x_k = x_{k+N/2}$ for $k = 0, \cdots, N/2-1$. At the receiver, it can be easily shown that $r_{k+N/2} = e^{j\pi\varepsilon} r_k$ for $k = 0, \cdots, N/2 - 1$. Here $k = 0$ corresponds to the index of the first time-domain sample after the CP. Hence, the received signal also consists of two identical halves, except for a phase difference $e^{j\pi\varepsilon}$ that is caused by the CFO. To determine the start of the OFDM symbol, in [39], a timing metric is calculated as

$$M_k = \frac{\left|\sum_{m=0}^{N/2-1} r_{k+m}^* r_{k+m+N/2}\right|^2}{\sum_{m=0}^{N/2-1} \left|r_{k+m+N/2}\right|^2}. \tag{1.19}$$

We can see that the numerator of $M(k)$ in (1.19) is an autocorrelation function of the received signal in a window of size $N/2$, while the denominator in (1.19) is a normalization constant equal to the power of the second-half of the training symbol.

Figure 1.11 shows an example of the timing metric M_k for an OFDM system with 512 subcarriers and cyclic prefix equal to 64. The channel is an AWGN channel with SNR of 20 dB and the CFO $\varepsilon = 0.6$. Here we put the start of the OFDM symbol as the 0 timing point. We can see that the timing metric function reaches a plateau of length equal to the length of the cyclic prefix. For multi-path fading channel, the length of the plateau is equal to the length

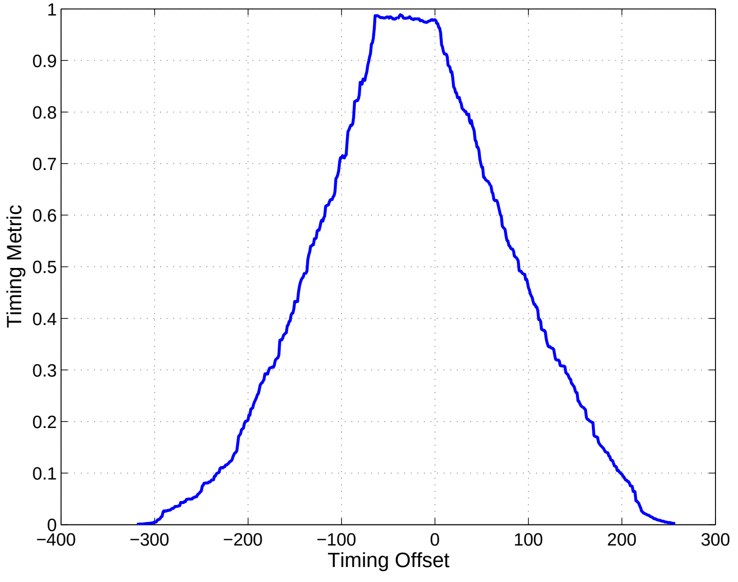

Fig. 1.11: An example of timing metric using the autocorrelation method (AWGN Channel SNR=20dB).

of the cyclic prefix minus the length of the channel impulse response. The starting point of the OFDM symbol can be taken at any point on the plateau and there will be no inter-symbol interference (ISI) [39]. Once the timing point k is determined, it is shown in [39] that the ML estimate of the CFO can be obtained as

$$\begin{aligned} \hat{\varepsilon} &= \frac{1}{\pi}\angle\left(\sum_{m=0}^{N/2-1} r^*_{k+m} r_{k+m+N/2}\right) \\ &= \frac{1}{\pi}\tan^{-1}\left[\frac{\Im\left(\sum_{m=0}^{N/2-1} r^*_{k+m} r_{k+m+N/2}\right)}{\Re\left(\sum_{m=0}^{N/2-1} r^*_{k+m} r_{k+m+N/2}\right)}\right], \end{aligned} \tag{1.20}$$

where $\angle(\bullet)$ denotes the angle of a complex number. The CFO estimator in (1.20) has an acquisition range of ± 1 subcarrier spacing and the MSE of the

CFO estimation is given by [39]

$$\mathrm{MSE}(\hat{\varepsilon}) = \frac{2}{\pi^2 N\gamma}, \tag{1.21}$$

which has a similar expression as the frequency domain method in (1.18).

Both methods in [38] and [39] use periodic training sequences in either the frequency or the time domain to estimate the CFO in OFDM systems. In both methods, the ML CFO estimate can be obtained using simple correlation operations as shown in (1.17) and (1.20). Compared to the frequency domain method in [38], the time domain method in [39] has two advantages. Firstly, timing synchronization can be obtained using the same training sequence. Secondly, frequency synchronization is performed in the time domain, thus it saves the complexity of FFT operations required in the frequency domain methods. As a result, time-domain periodic training sequences have been adopted in various wireless standards as the training sequence for timing and CFO estimation [17] [18] [5]. In [40], the authors extended the CFO estimation using periodic sequences to the case where the number of periods is larger than 2. A more practical treatment on CFO and timing estimation in OFDM systems was given in [41]. The acquisition range of CFO values and method to resolve the ambiguity in CFO estimation were addressed in [42]. In [43] and [44], the CFO and timing estimation algorithms were studied specifically in the context of IEEE 802.11 training sequences. The Cramer-Rao bounds (CRB) for CFO estimation using a general and a periodic training sequence in frequency selective fading channels were derived in [45].

In summary, the use of periodic training sequences for CFO estimation in SISO-OFDM systems has been extensively studied in both theoretical and practical aspects. Moreover, the computational complexity required for CFO estimation in SISO-OFDM systems is already very small. Therefore, in this thesis, we will not further study the training-based CFO estimation in SISO-OFDM systems. However, training-based CFO estimation algorithms have some limitations. The training sequence used for CFO estimation is an extra overhead for transmission and it reduces the effective data throughput of the system. For a typical application like IEEE 802.11a/g WLAN, the total overhead used for CFO estimation and residual CFO tracking, including both the short preamble and the pilots, is about 10% of the total data throughput. The WLAN system is designed for low mobility applications, in which the CFO can be assumed to be constant within a packet. In the case of mobile systems, the CFO becomes time varying due to the Doppler effect of the channel [46]. This requires more frequent transmission of training sequences, which further reduces the data throughput. To avoid this problem, in this thesis, we study another class of CFO estimation algorithms, namely blind algorithms, for SISO-OFDM systems. Blind algorithms do not require training sequences and hence have no training overhead. The disadvantage is that their computational complexity is normally higher than that of training-based algorithms. This means that in practice, the implementation of blind algorithms requires more silicon area and it leads to higher power consumption. A detailed overview on blind CFO estimation algorithms for SISO-OFDM systems is given in Section 1.4.1.2.

For MIMO-OFDM and multi-user MIMO-OFDM systems, the computational complexity for blind algorithms becomes too high for practical implementations. Therefore, in Chapter 4 and Chapter 5, we will come back to training-based algorithms. We will study low complexity CFO estimation algorithms for MIMO-OFDM and multi-user MIMO-OFDM systems using periodic training sequences.

1.4.1.2 Blind CFO estimation algorithms

Blind CFO estimation algorithms are a class of algorithms where the CFO is estimated using the statistical properties of the received signal only, without explicit knowledge of the transmitted signal. Therefore, it does not require training sequences. In SISO-OFDM systems, blind CFO estimation algorithms usually make use of some special properties of OFDM symbols such as the cyclic prefix in the time domain and guard null subcarriers in the frequency domain.

In [47], the authors proposed a CFO estimation algorithm making use of the time-domain cyclic prefix in OFDM systems. For an AWGN channel, the received time-domain OFDM signal has the following property

$$\mathrm{E}\{r_k^* r_{k+N}\} = \sigma_s^2 \exp(j2\pi\varepsilon) + \sigma_n^2, \tag{1.22}$$

if k is in the part of the OFDM symbol that corresponds to the cyclic prefix. Based on this property, the authors showed that a maximum-likelihood CFO estimator is given by

$$\hat{\varepsilon} = \frac{1}{2\pi}\angle\left(\sum_{k=t}^{t+N_g-1} r_k^* r_{k+N}\right), \tag{1.23}$$

where t is the start of the cyclic prefix portion of the received signal. From (1.23), we can see that CFO estimation only requires the computation of the autocorrelation of the received signal. Therefore, the computational complexity is low. However, there are a few drawbacks of this method. Firstly, if the channel is dispersive, the number of terms in (1.23) is equal to the difference of CP length and the length of the channel impulse response. In this case, the MSE of the CFO estimation is degraded compared to that in flat fading channels. Secondly the acquisition range of this method is limited to ± 0.5 subcarrier spacing.

Another popular blind CFO estimation method was proposed by Liu and Tureli in [37]. This method makes use of the frequency-domain characteristics of OFDM systems. Figure 1.12 shows the spectrum of a practical OFDM system with N subcarriers. In this system, there are d_1 and d_2 subcarriers at two ends of the allocated spectrum that are left empty and used as guard bands to avoid aliasing to the adjacent channels [17]. We will refer to the non-data-carrying subcarriers as null subcarriers and we call the data-carrying subcarriers data subcarriers. In the absence of noise and ICI, the received signal on the null subcarriers should be 0. Based on this observation, Liu and Tureli proposed a blind CFO estimation algorithm based on the minimization of the received signal power on null subcarriers [37]. It was shown

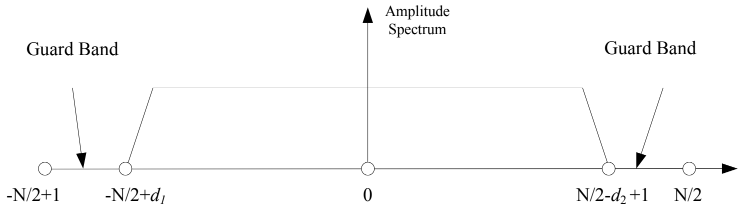

Fig. 1.12: Typical spectrum of an OFDM system with guard bands (null subcarriers).

in [48] that this CFO estimation method is optimal in the ML sense. Because it makes use of the frequency-domain characteristics of OFDM systems, its performance is not affected by the length of the channel impulse response. Moreover, compared to the method in [47], it is more robust against timing errors. A disadvantage of the algorithm is its computational complexity. This is because the cost function in the minimization problem in [37] is a polynomial with the complex variable of order $2(N-1)$. For a typical application, like wireless LAN, $N = 64$ [17]. Hence, the order of the cost function becomes 126, and the computational complexity required to find the minimum is very high. Therefore, it is important to find methods to reduce the computational complexity of the blind algorithm in [37] to make it implementable in practice. Moreover, it is also important that the reduction in complexity does not lead to big performance degradations. Finding such a solution is a technical challenge that requires both mathematical analysis and practical considerations. This challenge is addressed in Chapter 2 and Chapter 3 of this thesis.

1.4.2 CFO estimation for MIMO-OFDM systems

For MIMO-OFDM systems, all the transmit antennas are driven by the one local oscillator (LO) while all the receive antennas are driven by another LO. Therefore, the CFO between the transmitter and receiver LO's is still a single parameter to estimate. In this sense, the CFO estimation is very similar to that in SISO-OFDM systems. The difference here is that we have multiple received signals from multiple receive antennas. The CFO estimation concerns how to optimally combine these signals to extract the CFO estimate. To this end, there have been many papers in the literature addressing the CFO estimation in the MIMO context. In [49], the CFO estimation was performed in two steps. Firstly, the fractional CFO, up to ± 0.5, was estimated and compensated in the time domain using cyclic prefix. Secondly the integer part of the frequency offset was estimated in the frequency domain by cross correlating the received frequency domain signal with the training sequence. In [50], the CFO in MIMO-OFDM systems was estimated using periodical training sequences in a similar fashion as for the SISO-OFDM systems. The training sequence design for CFO estimation was addressed in [51].

Compared to SISO-OFDM systems, the training in MIMO-OFDM systems requires significantly more overhead. For example, the channel estimation for a MIMO-OFDM system with n_t transmit and n_r receive antennas requires estimation of $n_r \times n_t$ channel coefficients for each subcarrier. In the literature, this normally requires training sequences of at least n_t OFDM symbols [5] [52]. On top of this, additional overhead is required for timing and CFO estimations. Therefore, it is important and remains a challenging problem to develop low-overhead training schemes that enable joint estimation of CFO and channel. In addition, for practical implementation, these schemes should also require low computational complexity. One efficient training scheme for low-complexity joint CFO and channel estimation is proposed in Chapter 4 of the thesis.

In the theoretical study of MIMO-OFDM systems, different antennas are assumed to be independent and there is no interaction between signals from different antennas. In practice, as MIMO antennas are placed close to each other, the channel responses among different transmit and receive antennas are actually correlated [53] [54] [55]. This correlation is related to the propagation environment. Besides spatial correlation, closely placed antennas also experience mutual coupling among the antennas. The mutual coupling is due to the interactions of electro-magnetic (EM) fields at different antennas [56] [57]. It changes the amount of spatial correlation related to the propagation environment [58] [59]. The mutual coupling also changes the signal power at different antennas. Therefore, it is of great practical importance to study the effects of spatial correlation and antenna coupling and their impacts on the CFO estimation in MIMO systems. Such a study is provided in Chapter 4 of the thesis.

1.4.3 CFO estimation for Multi-user MIMO-OFDM systems

In the uplink of a multi-user MIMO-OFDM system, different users transmit simultaneously to the base station. In this case, different users use LO signals from their own LO's while the receiver uses an LO signal generated by the receiver LO. Therefore, CFO exists between the base station LO and the LO's from different users. The base station receiver needs to estimate these multiple CFO values from multiple users. In [60] and [61], algorithms were proposed to estimate multiple CFO values for MIMO systems in flat fading channels. In [62], a semi-blind algorithm was proposed to estimate the CFO and channel for the uplink of multi-user MIMO-OFDM systems in frequency selective fading channels. The joint CFO and channel estimation for multi-user MIMO-OFDM systems was studied in [63]. Training sequences that minimize the asymptotic Cramer-Rao Bound were also designed in [63]. The computational complexity is the main problem in the CFO estimation for multi-user MIMO-OFDM systems. Most of the existing algorithms in the literature have computational complexity that increases exponentially with the number of users. This makes practical implementation of such algorithms difficult. Therefore, development of low complexity CFO estimation algorithms in the multi-user context is of great practical importance. We will propose a low-complexity algorithm to estimate these multiple CFO values in Chapter 5.

1.5 Outline and Contributions of the Thesis

In this section, we outline the contents of each chapter in the rest of the thesis. We also highlight the contributions in each chapter. As the title of the thesis suggests, we focus on low-complexity frequency synchronization techniques for different wireless OFDM systems. This thesis can be divided into three parts covering different types of wireless OFDM systems. In Chapter 2 and Chapter 3, we study low-complexity blind CFO estimation in SISO-OFDM systems. In

Chapter 4, we move to MIMO-OFDM systems, while in Chapter 5, the CFO estimation in multi-user MIMO-OFDM systems is studied.

In Chapter 2, we study low-complexity blind CFO estimation algorithms for SISO-OFDM systems using null subcarriers. Compared to the existing low-complexity method using Taylor series approximation, we propose a new factorization method for the cost function such that the Taylor series approximation is more accurate, and thereby the CFO estimate. Moreover, for small CFO values, we also derive a closed-form solution for the CFO estimate. The contributions in this chapter also include a new successive CFO estimation and compensation algorithm that reduces the performance degradation due to Taylor series approximation errors in the cost function.

In Chapter 2, we found that the performance of CFO estimation is closely related to the placement of the null subcarriers. In Chapter 3, we present an analytical study on this relationship. We show mathematically that the SNR of the CFO estimation is a function of the null subcarrier placement. We then formulate the optimization problem for null subcarrier placement as an SNR maximization problem. Optimal null subcarrier placement is obtained analytically when the number of subcarriers is divisible by the number of null subcarriers. For the other cases, a near-optimal placement is developed. We further demonstrate that the SNR-optimal null subcarrier placement also minimizes the theoretical MSE (i.e. the linear approximation of the MSE in the high SNR region) of the CFO estimation. For practical OFDM systems, it is necessary to have fixed-position null subcarriers as guard band. With this constraint, we propose a method to optimally place a few null subcarriers in the data band and the algorithm improves the performance of CFO estimation significantly.

In Chapter 4, we study the CFO estimation in MIMO-OFDM systems. We develop a training scheme that uses the same constant amplitude zero autocorrelation (CAZAC) training sequence for joint CFO and channel estimation. We demonstrate that the training overhead can be significantly reduced using the developed training scheme and that the computational complexity is low. We show that the MSE of the CFO estimation approaches the Cramer Rao bound (CRB) at practical SNR values. We also present a mathematical analysis on the effect of CFO estimation errors (residual CFO) on the performance of channel estimation. A study on practical problems in MIMO-OFDM systems such as spatial correlation, antenna coupling and their impacts on CFO estimation is also presented in Chapter 4.

The CFO estimation for multi-user MIMO-OFDM systems is studied in Chapter 5. We first derive the ML CFO estimator and show that the computational complexity grows exponentially with the number of users. To reduce this complexity, we develop a sub-optimal CFO estimation algorithm using constant amplitude zero autocorrelation (CAZAC) sequences, the complexity of which grows only linearly with the number of users. The multiple CFO values in the uplink cause interference in the CFO estimation of different users using the proposed low-complexity algorithm.. To mitigate this interference, we propose a method to find the CAZAC sequence that maximize the signal-to-interference ratio for different classes of CAZAC sequences.

The concluding remarks of this thesis in given in Chapter 6 together with suggestions for possible future work.

1.6 List of Publications by the Author

The research work carried out in this thesis has resulted in the following publications.

1.6.1 Journals

1. S. Attallah, Y. Wu, and J.W.M. Bergmans, "Low complexity blind estimation of residual carrier offset in OFDM-based wireless LAN systems", *IET Communications*, vol. 1, no. 4, pp. 604-611, Aug. 2007.
   Chapter 2
2. Y. Wu, S. Attallah, and J.W.M. Bergmans, "On the optimality of the null subcarrier placement for blind carrier offset estimation in OFDM systems", *IEEE Trans. Veh. Technol.*, vol. 58, no. 4, pp. 2109-2115, May 2009.
   Chapter 3
3. Y. Wu, J.W.M. Bergmans, and S. Attallah, "Carrier frequency offset estimation for multi-user MIMO OFDM uplink using CAZAC sequences: performance and sequence optimization", *submitted to IEEE Trans. Signal Process.* .
   Chapter 5

1.6.2 Conference Proceedings

1. Y. Wu, S. Attallah, and J.W.M. Bergmans, "Blind iterative carrier offset estimation for OFDM systems", in *Proc. IEEE International Symposium on Signal Processing and its Applications*, vol. 1, pp. 123-126, Aug. 2005.
   Chapter 2
2. Y. Wu, S. Attallah, and J.W.M. Bergmans, "On the SNR-optimal null subcarrier placement for blind carrier offset estimation in OFDM systems", in *Proc. IEEE Global Telecommunications Conference*, Nov. 2006.
   Chapter 3
3. S. Attallah, Y. Wu, and J.W.M. Bergmans, "Low complexity blind residual carrier offset estimation in OFDM-based wireless LAN systems", in *Proc. IEEE Wireless Communications and Networking Conference*, pp. 1970-1975, Mar. 2007.
   Chapter 2
4. Y. Wu, S. Attallah, and J.W.M. Bergmans, "Efficient training sequence for joint carrier frequency offset and channel estimation for MIMO-OFDM systems", in *Proc. IEEE International Conference on Communications*, pp. 2604-2609, Jun. 2007
   Chapter 4
5. Y. Wu, J.P. Linnartz, J.W.M. Bergmans, and S. Attallah, "Effects of antenna mutual coupling on the performance of MIMO systems", in *Proc. 29th Symposium on Information Theory in the Benelux*, pp. 207- 214, May 2008.
   Chapter 4
6. Y. Wu, S. Attallah, and J.W.M. Bergmans, "Carrier Frequency offset esti-

mation for multi-user MIMO OFDM uplink using CAZAC sequences", *Accepted IEEE Wireless Communications and Networking Conference*, Apr. 2009.

Chapter 5

Chapter 2

Low-Complexity Blind CFO Estimation for OFDM Systems

2.1 Introduction

The presence of carrier frequency offset (CFO) in an orthogonal frequency division multiplexing (OFDM) system leads to a loss of orthogonality between subcarriers. This introduces inter-subcarrier interference (ICI) and degrades the system performance significantly. Therefore, to guarantee good performance of OFDM systems, the CFO must be accurately estimated and compensated. Compared to training-based CFO estimation algorithms, blind CFO estimation algorithms have the advantage that no extra training symbols are required. In the literature, Liu and Tureli [37] proposed a blind CFO estimation algorithm exploiting null subcarriers. These are subcarriers at both ends of the spectrum that are left empty and used as guard bands. The algorithm in [37] estimates the CFO through minimizing the received signal power on these null subcarriers. However, a drawback of the algorithm is its high computational complexity. To reduce this complexity, a low-complexity algorithm was proposed in [64], which uses Taylor series approximation of the original cost function. To improve the accuracy of this approximation, we propose a new factorization method for the cost function that helps to reduce the number of terms of the Taylor series. By limiting this number to 2 (first-order approximation), we also derive a closed-form solution for the CFO estimate. Comparison with the original algorithm in [37] shows a significant reduction in computation complexity using the new method. Moreover, the performance of the new method is very close to that of the algorithm in [37] for small CFO values. However, the low-order (first and second order) Taylor series approximation can lead to some performance degradation. This degradation is more obvious in the medium to high SNR region, where an error floor appears. To mitigate this degradation, we further develop a successive CFO estimation and compensation algorithm. In each iteration of the proposed successive algorithm, the residual CFO from the previous iteration is estimated and compensated from the received signal. A convergence monitoring mechanism is introduced which ensures the convergence of the successive algorithm. We further propose a decision-directed CFO estimation algorithm where the performance of CFO estimation can be further improved at a slightly higher computational cost.

The rest of this chapter is organized as follows. In Section 2.2, we review the null subcarrier based blind CFO estimation algorithm in [37] and the low-complexity algorithm in [64]. The proposed new factorization method to improve the Taylor series approximation is presented in Section 2.3. In 2.4, we present the successive CFO estimation and compensation algorithm and its decision-directed extension is developed in Section 2.5. The simulation results are presented in Section 2.6 and concluding remarks are given in Section 2.7.

2.2 Previous Methods

For an OFDM system with N subcarriers and P data subcarriers, after removing the cyclic prefix, the received time-domain OFDM signal in the k^{th} OFDM symbol interval can be written as

$$\mathbf{r}^k = \mathbf{E}\mathbf{W}_P\mathbf{H}^k\mathbf{s}^k e^{j\phi_0(k-1)(N+N_g)} + \mathbf{n}^k \tag{2.1}$$

where $\mathbf{E} = \text{diag}(1, e^{j\phi_0}, \cdots, e^{j(N-1)\phi_0})$ is the diagonal CFO matrix and ϕ_0 is the actual angular CFO given by $\phi_0 = 2\pi\varepsilon_0/N$. Here we use angular CFO ϕ_0 to simplify notification so that in later derivations, we need not deal with the constant factor $2\pi/N$ to the original CFO ε. The difference between (2.1) and (1.10) is that $\mathbf{s}$ is a $P \times 1$ vector containing the transmitted signal on the P data subcarriers. Correspondingly, $\mathbf{H}$ is a $P \times P$ diagonal matrix containing the channel responses on the P data subcarriers and $\mathbf{W}_P$ is a $N \times P$ submatrix that is obtained from the $N \times N$ IDFT matrix $\mathbf{W}$ by extracting the P columns that correspond to the data subcarriers. Let us define $\mathbf{l} = [l_1, l_2, \cdots l_d]$ as the null subcarrier indices and $d = N - P$ as the number of null subcarriers.

In [37], Liu and Tureli showed that a CFO estimate can be obtained from the minimization of a cost function $\mathcal{J}(z)$ given by

$$\mathcal{J}(z) = \sum_{k=1}^{K} \sum_{i=1}^{d} \left\| \mathbf{w}_{l_i}^{H} \mathbf{Z}^{-1} \mathbf{r}^{k} \right\|^{2}, \tag{2.2}$$

where K is the total number of OFDM symbols used for CFO estimation, $\mathbf{w}_{l_i}^H$ is row l_i of the DFT matrix and $\mathbf{Z} = \mathrm{diag}\Big(1, z, z^2, \cdots, z^{(N-1)}\Big)$ with $z = e^{j\phi}$. Here ϕ is the trial value for the actual CFO ϕ_0. Using (2.2), it can be shown that $z = e^{j\phi_0}$ is a zero of $\mathcal{J}(z)$ in the absence of noise.

This algorithm is shown to have a good performance as compared to Cramer-Rao bound (CRB) [37] and its acquisition range for CFO is much larger than that of the blind CFO estimation algorithm using the cyclic prefix [47]. It is shown in [37] that the CFO estimate that minimizes the cost function in (2.2) can be attained by using either a MUSIC-like search algorithm or a rooting method [65]. The practical aspects of this blind CFO estimation algorithm and its experimental implementations are further studied in [66]. The identifiability of CFO using this algorithm is studied in [48] and [67]. A major disadvantage of this algorithm is its high computational complexity. The cost function $\mathcal{J}(z)$ represents a polynomial of order $2(N-1)$ in the complex variable z. For a typical application, like wireless LAN (IEEE 802.11a standard), $N = 64$. Hence, the order of $\mathcal{J}(z)$ becomes 126, and the computational complexity required to find its roots is very high. To reduce this complexity, an ESPRIT-like method is proposed in [68]. However, the computational complexity is still very high as a subspace computation is required.

In [64], a method is proposed to reduce the computational complexity of the method in [37]. This algorithm exploits the fact that the inverse diagonal matrix $\mathbf{Z}^{-1}$ in (2.2) can be re-written as follows

$$\begin{aligned}\mathbf{Z}^{-1} &= \operatorname{diag}\left(1,\ e^{-j\phi},\ e^{-j2\phi},\cdots,\ e^{-j(N-1)\phi}\right) \\ &= e^{-j\phi(N-1)/2}\operatorname{diag}\left(e^{j\phi\frac{(N-1)}{2}},\ e^{j\phi\frac{(N-3)}{2}},\cdots,e^{j\phi\frac{(1-N)}{2}}\right).\end{aligned} \tag{2.3}$$

Taking into account the fact that the residual CFO after analog coarse frequency synchronization tends to be very small in practice, using Taylor series expansion of an exponential function, we have

$$\mathbf{Z}^{-1} \approx e^{-j\phi(N-1)/2} \times \sum_{n=0}^{Q} \frac{(j\phi)^n}{2^n n!}\mathbf{D}^n \tag{2.4}$$

where $\mathbf{D} = \operatorname{diag}((N-1),\ (N-3),\cdots,(1-N))$ and Q is a suitable integer ($Q \ll N$) such that the error due to the series truncation in (2.4) is negligible [64]. The assumption of small residual CFO in the digital domain is justified, on the one hand, by the use of a coarse synchronization at the analog part of the receiver [36] [69] and, on the other hand, by the precision of currently available crystal oscillators [70]. In IEEE 802.11a WLAN standard [17], the precision of the carrier frequency at both the transmitter and the receiver is ± 20 ppm maximum. This leads to a worst case CFO value of ± 0.64 subcarrier spacing or $\phi_0 = 0.063$ at a carrier frequency of $f_c = 5$ GHz. Furthermore, the accuracy of the LO's has been further improved in recent years. In the comparison criterion document of the IEEE 802.11n high-throughput wireless LAN working group [71], the CFO value between the transmitter and receiver

LO's has been strengthened to 13.675 ppm which corresponds to normalized CFO value of $\phi_0 = 0.023$ at $f_c = 5$ GHz. All these facts show that the assumption of $|\phi| \ll 1$ is valid in practice. Now using (2.4) in (2.2) and letting $a_{i,n}(k) = \mathbf{w}_{l_i}^H \mathbf{D}^n \mathbf{r}^k$, we get the approximated cost function given by

$$\mathcal{J}_{2Q}(\phi) = \sum_{l=0}^{2Q} c_l \phi^l \tag{2.5}$$

where the polynomial coefficients c_l are given by

$$c_l = \left(\frac{j}{2}\right)^l \sum_{m=0}^{l} \frac{(-1)^m}{(l-m)!m!} \sum_{i=1}^{d} \sum_{k=1}^{K} a_{i,l-m}(k) a_{i,m}^*(k) \tag{2.6}$$

with $a_{i,l}(k) = 0$ for $l > Q$. The new cost function (2.5) is a polynomial of the real variable ϕ of degree $2Q$. In addition, it has been proven in [64] that all the polynomial coefficients are real-valued. The minimization of (2.5) can be carried out by setting the derivative to 0 and using some standard rooting methods to search for the CFO estimate. Since $Q \ll N$, the computational complexity required to find the root of (2.5) is significantly lower than that for the original problem. Moreover, as both ϕ and the polynomial coefficients are real, the rooting methods require only real arithmetic operations. This on its own provides large computational savings.

2.3 Proposed New Factorization Method

The factorization in (2.3) is aimed at increasing the denominators of the Taylor series terms in (2.4) by a factor of 2^n so that a good approximation to $\mathbf{Z}^{-1}$ can be achieved with a limited number of terms. Next, we will propose another factorization method which allows us to increase this number to $(2^n)^2 = 4^n$ and more if needed. Based on (2.3), we can write

$$\mathbf{Z}^{-1} = e^{-j\phi(N-1)/2}(\mathbf{E}_1 + \mathbf{E}_2), \tag{2.7}$$

where

$$\begin{aligned}
\mathbf{E}_1 &= \operatorname{diag}\left(e^{j\phi\frac{(N-1)}{2}}, \mathbf{e}^{j\phi\frac{(N-3)}{2}}, \cdots, e^{j\phi\frac{1}{2}},\ 0, \cdots, 0\right) \\
&= e^{j\phi(N-1)/4}\operatorname{diag}\left(e^{j\phi\frac{(N-1)}{4}}, \cdots, e^{j\phi\frac{(3-N)}{4}},\ 0, \cdots, 0\right), \\
\mathbf{E}_2 &= \operatorname{diag}\left(0, \cdots, 0, e^{-j\phi\frac{1}{2}} \cdots, e^{j\phi\frac{(1-N)}{2}}\right) \\
&= e^{j\phi(1-N)/4}\operatorname{diag}\left(0, \cdots, 0, e^{j\phi\frac{(N-3)}{4}}, \cdots, e^{j\phi\frac{(1-N)}{4}}\right).
\end{aligned} \tag{2.8}$$

Now, using Taylor series expansion in (2.8), we obtain

$$\begin{aligned}
\mathbf{E}_1 &= \sum_{m=0}^{+\infty} \frac{(j\phi)^m}{4^m m!}(N-1)^m \sum_{n=0}^{+\infty} \frac{(j\phi)^n}{4^n n!}\mathbf{D}_1^n \\
&= \sum_{m=0}^{+\infty}\sum_{n=0}^{+\infty} \frac{(j\phi)^{n+m}}{4^{n+m} n! m!}(N-1)^m \mathbf{D}_1^n,
\end{aligned} \tag{2.9}$$

where

$$\mathbf{D}_1^n = \mathrm{diag}((N-1)^n,\ (N-5)^n, \cdots (3-N)^n,\ 0, \cdots, 0). \tag{2.10}$$

Similarly, we can show that

$$\mathbf{E}_2 = \sum_{m=0}^{+\infty}\sum_{n=0}^{+\infty}(-1)^m \frac{(j\phi)^{n+m}}{4^{n+m}n!m!}(N-1)^m \mathbf{D}_2^n, \tag{2.11}$$

where

$$\mathbf{D}_2^n = \mathrm{diag}(0, \cdots, 0,\ (N-3)^n,\ (N-7)^n, \cdots (1-N)^n). \tag{2.12}$$

Substituting (2.9) and (2.11) into (2.7) leads to

$$\mathbf{Z}^{-1} = e^{j\phi(N-1)/2}\sum_{m=0}^{+\infty}\sum_{n=0}^{+\infty}\frac{(j\phi)^{n+m}}{4^{n+m}n!m!}(N-1)^m \left[\mathbf{D}_1^n + (-1)^m \mathbf{D}_2^n\right]. \tag{2.13}$$

If the Taylor series of each exponential is truncated to a suitable number of Q terms, then equation (2.13) can be approximated by the following matrix polynomial

$$\mathbf{Z}^{-1} \approx e^{j\phi(N-1)/2}\sum_{q=0}^{2Q}\mathbf{C}_q \phi^q, \tag{2.14}$$

where

$$\mathbf{C}_q = \left(\frac{j}{4}\right)^q \sum_{m=0}^{q}\frac{(N-1)^m}{m!(q-m)!}\left[\mathbf{D}_1^{(q-m)} + (-1)^m \mathbf{D}_2^{(q-m)}\right]. \tag{2.15}$$

Note that $\mathbf{C}_q$ is a non-zero matrix for $q = 0, 1, \cdots 2Q$ and it is equal to the zero-matrix for $q > 2Q$. To simplify the calculations, let us define the scalar $b_{i,q}(k)$ as follows

$$b_{i,q}(k) = \mathbf{w}_{l_i}^H \mathbf{C}_q \mathbf{r}^k. \tag{2.16}$$

Now, let us substitute (2.14) into the cost function (2.2). This leads to the new approximate cost function

$$\begin{aligned} \mathcal{J}(z = e^{j\phi}) \quad \approx \mathcal{J}_{4Q}(\phi) \quad &= \sum_{r=0}^{2Q} \sum_{l=0}^{2Q} \phi^{l+r} \sum_{i=1}^{d} \sum_{k=1}^{K} b_{i,l}(k) b_{i,r}^*(k) \\ &= \sum_{q=0}^{4Q} d_q \phi^q, \end{aligned} \tag{2.17}$$

where the polynomial coefficients are given by

$$d_q = \sum_{s=0}^{q} \sum_{i=1}^{d} \sum_{k=1}^{K} b_{i,q-s}(k) b_{i,s}^*(k). \tag{2.18}$$

We can notice that $b_{i,l}(k) = 0$ for $l > 2Q$ as $\mathbf{C}_l$ is a zero matrix for $l > 2Q$. Moreover, it is straightforward to show that $d_q = d_q^*$. Hence, all the coefficients of the polynomial are real-valued.

In practice, the residual CFO can be so small that only a very limited number of terms is needed for the Taylor series approximation. In this case, we can compute directly the CFO through a simple formula as follows. For $Q = 1$, the cost function polynomial is of degree four and its derivative with respect to ϕ is a cubic polynomial whose zeroes or roots can be computed directly using Cardano's formula [72]. To this end, we should first rewrite the derivative of the cost function as follows:

$$\frac{1}{4d_4}\frac{\partial \mathcal{J}_{4Q}(\phi)}{\partial \phi} = \phi^3 + u\phi^2 + v\phi + r = 0, \tag{2.19}$$

where

$$u = \frac{3d_3}{4d_4}, \quad v = \frac{d_2}{2d_4}, \quad r = \frac{d_1}{4d_4}. \tag{2.20}$$

Now, let us compute

$$\begin{aligned} a &= (3v - u^2)/3, & b &= (2u^3 - 9uv + 27r)/27, \\ S &= \left(-\frac{b}{2} + \sqrt{\frac{b^2}{4} + \frac{a^3}{27}}\right)^{1/3}, & T &= \left(-\frac{b}{2} - \sqrt{\frac{b^2}{4} + \frac{a^3}{27}}\right)^{1/3}. \end{aligned} \tag{2.21}$$

Finally, the three roots are given by [72]

$$\begin{aligned} \tilde{\phi}_1 &= (S+T) - \frac{u}{3}, \\ \tilde{\phi}_2 &= -\frac{1}{2}(S+T) + j\frac{\sqrt{3}}{2}(S-T) - \frac{u}{3}, \\ \tilde{\phi}_3 &= -\frac{1}{2}(S+T) - j\frac{\sqrt{3}}{2}(S-T) - \frac{u}{3}. \end{aligned} \tag{2.22}$$

Once the three roots are determined, we substitute them in (2.17) and choose the one that leads to the minimum of $\mathcal{J}_4(\phi)$ as the CFO estimate. As we are looking for a real solution, we should test only the real roots for the minimum. The complex-valued roots need not be tested. It is worthwhile to mention that for a cubic polynomial with real coefficients as in our case, at least one of the roots will always be real [73]. The summary of this algorithm is given in Table 2.1.

Initialization
Start with the received signal vector $\mathbf{r}^0$*, and set* $Q = 1$.
Algorithm:
1) Compute the coefficients d_q *of the cost function polynomial* $\mathcal{J}_4(\phi)$ *using (2.18) for* $q = 0, 1, 2, 3, 4$.
2) Compute the coefficients u*,* v *and* r *of* $\frac{1}{4d_4}\frac{\partial \mathcal{J}_4(\phi)}{\partial \phi}$ *using (2.20).*
3) Compute the three roots $\tilde{\phi}_1$*,* $\tilde{\phi}_2$ *and* $\tilde{\phi}_3$ *using (2.22) and discard the complex roots. At least one root should be real as explained in the text.*
4) If more than one root is real, then compute $\mathcal{J}_4(\phi)$ *for each root and choose the one that leads to the smallest value for* $\mathcal{J}_4(\phi)$.

Table 2.1: Summary of the closed-form CFO estimator using the new factorization method.

To complete our discussion, we need to examine closely the computational complexity of the proposed algorithm. Since $Q = 1$, the computational complexity due to (2.20), (2.21) and (2.22) is negligible as compared to the complexity of computing the 5 polynomial coefficients d_0 to d_4. Every coefficient d_q requires the computation of $b_{i,q}(k)$ in (2.16), where we can easily notice that $\mathbf{C}_q$ is just a diagonal matrix and both $\mathbf{w}_{l_i}^H$ and $\mathbf{y}(k)$ are just vectors. As a result, the computational complexity for obtaining the polynomial coefficients can be shown to be about $O(dKN)$, that is, it is similar to that of the method in [64] when $Q = 1$. The ESPRIT method in [68] is proposed as a low-complexity method for the CFO estimator in [37]. The method is based on the estimation and computation of a certain matrix $\mathbf{A}$, its pseudo inverse and the construction of another matrix called Δ. These operations have at least the following computational complexities $O(K(N-M)(M+1)^2)$, $O(P^3)+O(MP^2)$ and $O((MP)^2)$, where $M \geq P$ and P is the number of data subcarriers. In practice, both M and P are of comparable size as N. Hence, it should be obvious that the computational complexity of the proposed method is much lower than that of the methods in [37] and [68]. It is worth to note that the computational complexity using the new factorization method with $Q = 1$ is similar to that of the previous method in [64] with $Q = 2$. As we are going to show later using simulations, the performance using the new factorization method with $Q = 1$ is better than that of [64] with $Q = 2$.

2.4 Successive Blind CFO Estimation and Compensation

The performance of the closed-form CFO estimator using the new factorization method depends on the accuracy of the Taylor series approximation of the cost function in (2.2), which is determined by the number of terms used in the summation as well as the residual CFO values. As we only use $Q = 1$ (low cost) in the proposed method, the accuracy of the approximation is degraded when the actual CFO value is relatively large. As a result, there will be some performance degradation in the Mean Square Error (MSE) of the CFO estimation compared to the method in [37]. To reduce this degradation and further improve the performance of the proposed method, we present, in this section, an effective successive CFO estimation and compensation algorithm.

In the first iteration of the algorithm, we use the proposed method to find an initial estimate of the CFO, say $\hat{\phi}_0$. Then, the CFO compensation can be performed on the received signal $\mathbf{r}^k$. To this end, let us define the CFO compensation matrix in the first iteration as $\mathbf{T}_1 = \mathrm{diag}(1, e^{-j\hat{\phi}_0}, \cdots, e^{-j(N-1)\hat{\phi}_0})$. The time-domain received signal after the CFO compensation can thus be written as

$$\begin{aligned}
\tilde{\mathbf{r}}^k &= \mathbf{T}_1 e^{-j\hat{\phi}_0(k-1)(N+N_g)}\mathbf{r}^k \\
&= \mathbf{E}_1\mathbf{W}_P\mathbf{H}\mathbf{s}^k e^{j\phi_1(k-1)(N+N_g)} + \left(\mathbf{n}^k\right)', \qquad (2.23)
\end{aligned}$$

where $\mathbf{E}_1 = \mathrm{diag}(1, e^{j\phi_1}, e^{j2\phi_1}, \cdots, e^{j(N-1)\phi_1})$ denotes the residual CFO matrix with $\phi_1 = \phi_0 - \hat{\phi}_0$ representing the residual CFO after the first iteration. The noise vector $\left(\mathbf{n}^k\right)' = \mathbf{T}_1 e^{-j\hat{\phi}_0(k-1)(N+N_g)}\mathbf{n}^k$.

Let us consider the residual CFO after the first iteration $\mathbf{E}_1 e^{j\phi_1(k-1)(N+N_g)}$ in (2.23). It is obvious that when the CFO estimation is perfect, we should have $\hat{\phi}_0 = \phi_0$ and $\phi_1 = 0$. In this case, we have $\mathbf{E}_1 e^{j\phi_1(k-1)(N+N_g)} = \mathbf{I}$. Next, we consider the case where the CFO is not perfectly estimated ($\hat{\phi}_0 \neq \phi_0$) but it is close enough to ϕ_0 for the following condition to hold

$$|\phi_1| = \left|\phi_0 - \hat{\phi}_0\right| < |\phi_0|. \qquad (2.24)$$

Note that the mean of the noise term $\mathbf{n}'(k)$ after CFO compensation is $\mathrm{E}(\mathbf{n}'(k)) = 0 = \mathrm{E}(\mathbf{n}(k))$, and its covariance matrix can be calculated as

$$\begin{aligned}
\mathbf{R} &= \mathrm{E}\left(\mathbf{T}_1 e^{-j\hat{\phi}_0(k-1)(N+N_g)}\mathbf{n}^k\left(\mathbf{n}^k\right)^H e^{j\hat{\phi}_0(k-1)(N+N_g)}\mathbf{T}_1^H\right) \\
&= \mathbf{T}_1 e^{-j\hat{\phi}_0(k-1)(N+N_g)}\mathrm{E}\left(\mathbf{n}^k\left(\mathbf{n}^k\right)^H\right) e^{j\hat{\phi}_0(k-1)(N+N_g)}\mathbf{T}_1{}^H \\
&= \sigma_n^2\mathbf{T}_1 e^{-j\hat{\phi}_0(k-1)(N+N_g)}\mathbf{I}e^{j\hat{\phi}_0(k-1)(N+N_g)}\mathbf{T}_1^H \\
&= \sigma_n^2\mathbf{I}, \qquad (2.25)
\end{aligned}$$

and is seen to be equal to the covariance matrix of $\mathbf{n}^k$. This means that the noise power remains constant after carrier offset compensation and the CFO estimation and compensation process does not introduce any noise amplification. In the second iteration, since (2.24) holds, it is obvious that the residual CFO after the first iteration $e^{j\phi_1}$ can be represented more accurately using the first order Taylor series approximation as compared to $e^{j\phi_0}$ and therefore, our estimation method will lead to a better estimate for ϕ_1. That is, after the second iteration, we get the residual CFO after the second iteration ϕ_2 such that $|\phi_2| = |\phi_1 - \hat{\phi}_1| = |\phi_0 - (\hat{\phi}_0 + \hat{\phi}_1)|$ is very small. Now if after every iteration, we have the residual CFO smaller than that after the previous iteration, i.e.,

$$|\phi_{i+1}| = |\phi_i - \hat{\phi}_i| < |\phi_i|, \tag{2.26}$$

then eventually, as the iteration number goes to infinity, we have the residual CFO

$$\lim_{i\to\infty} |\phi_{i+1}| = 0 \ \text{ and } \ \lim_{i\to\infty} \left[\mathbf{E}_{i+1} e^{j\phi_{i+1}(k-1)(N+N_g)}\right] = \mathbf{I}.$$

The question now is how can we ensure, or at least monitor the algorithm such that the condition in (2.26) is met after each iteration so as to guarantee convergence. In the successive algorithm, we can monitor the convergence through the amplitude of the residual CFO estimate $|\hat{\phi}_i|$ from the second iteration onwards. If $|\hat{\phi}_i| < |\hat{\phi}_{i-1}|$, then the algorithm is moving in the right direction[1]. We can also use $|\hat{\phi}_i|$ to stop the algorithm should we find that $|\hat{\phi}_i|$

[1]Ideally, we should monitor the amplitude of the actual residual CFO $|\phi_i|$ for different iterations. If $|\phi_i| < |\phi_{i-1}|$, then the algorithm is converging. However, we do not know $|\phi_i|$ as it requires the knowledge of the true CFO value ϕ_0. To overcome this, an alternative approach is to monitor the amplitude of the CFO estimates $|\hat{\phi}_i|$ at different iterations. If the algorithm is converging, then we should expect the amplitude of the residual CFO estimate

is too small and reiterating the estimator one more time will not lead to any significant improvement in the CFO estimation.

Our objective is to minimize the computational complexity while improving the CFO estimation. Therefore, we need to keep the order of Taylor series approximation as small as possible and the number of iterations as low as possible. If $|\hat{\phi}_i| > |\hat{\phi}_{i-1}|$, we know that the successive algorithm is likely to diverge. In this case, we need to have a better estimate to ensure convergence. This can be achieved, for example, by increasing the order of Taylor series approximation in iteration $[i-1]$. In the simulations, we have found that under practical conditions, the first-order Taylor series approximation is adequate.

Given that the convergence condition is continuously monitored and enforced through iterations, the proposed successive CFO estimation and compensation algorithm approaches the performance of the algorithm in [37]. The proposed successive algorithm is summarized in Table 2.2. Here η is a small threshold value for CFO. When the estimated residual CFO gets smaller than this value, there is no point in going on with the iterations as the improvement will be marginal.

The computational complexity of the successive algorithm is roughly n_{itn} times the complexity of the closed-form CFO estimator, where n_{itn} is the number of iterations. As we are going to show later in the simulation results, the performance of the successive algorithm converges to that of the algorithm in [37] in 2 to 3 iterations for practical CFO values. Therefore, the complexity of the successive algorithm is still much lower than that of the ESPRIT method

$|\hat{\phi}_i|$ to decrease as the number of iterations increases.

Initialization
Set iteration number $i = 1$ and the CFO threshold η.
Algorithm:
1) Substitute $\mathbf{r}^k$ into cost function (2.2) and solve for the residual CFO estimate for the i^{th} iteration $\hat{\phi}_i$ using the method in Table 2.1.
2) Perform CFO compensation and update the new $\tilde{\mathbf{r}}^k$ according to (2.23).
3) If $\hat{\phi}_i < \eta$, exit iteration, else go to 4)
4) If $\{|\hat{\phi}_i| < |\hat{\phi}_{i-1}|$ and $i > 1\}$ or $\{i = 1\}$
$i = i + 1$, go back to 1).
Else
Go back to iteration $[i - 1]$ and increase the order of Taylor series approximation.

Table 2.2: Summary of the proposed successive CFO estimation and compensation algorithm.

in [68].

2.5 Decision-directed Successive Algorithm

Due to averaging, the MSE of the CFO estimation gets smaller as the number of null subcarriers, i.e., d used in cost function (2.2), gets larger. In practice, we cannot afford to have many null subcarriers in one OFDM symbol as this reduces the bandwidth efficiency. However, if the CFO estimation is accurate in the initial iteration, by performing CFO compensation and OFDM detection on a set of high SNR data subcarriers, we are able to obtain relatively accurate estimates $\hat{\mathbf{s}}^k$ of the transmitted signals $\mathbf{s}^k$ on these high-SNR subcarriers. Here, in order to keep the computational complexity low, we limit ourselves to the case where only 1 OFDM symbol is used for CFO estimation, i.e. $K = 1$ as in (2.2)and later in the simulation results section, we will show that $K = 1$ gives us good performance for all the proposed algorithms. In this case, we can drop the OFDM symbol index k in all the following formulations. Let us denote the selected high-SNR data subcarriers as $\mathbf{d}$ and the set of null subcarriers as $\mathbf{l}$. We can thus use a decision-directed method and re-formulate the cost function as

$$\mathcal{J}(z) = \sum_{i \in \mathbf{d}} \left\| \mathbf{w}_i^H \mathbf{Z}^{-1} \mathbf{r} - h_i \hat{s}_i \right\|^2 + \sum_{i \in \mathbf{l}} \left\| \mathbf{w}_i^H \mathbf{Z}^{-1} \mathbf{r} \right\|^2, \tag{2.27}$$

where h_i, $\hat{s}_i$ are the channel response and detected signal on subcarrier i. The two terms in the summation in (2.27) correspond to the cost function on the selected data subcarriers and the null subcarriers. Using Taylor series expansion as before, the decision-directed cost function is given by

$$\mathcal{J}(\phi) = \sum_{i \in \mathbf{d}} \left\| \mathbf{w}_i^H \sum_{n=0}^{+\infty} \frac{(j\phi)^n}{n!} \mathbf{D}_d^n \mathbf{r} - h_i \hat{s}_i \right\|^2 + \mathcal{J}_{4Q}(\phi), \tag{2.28}$$

where $\mathbf{D}_d = \text{diag}(0, -1, -2, \cdots, 1-N)$ and here we use subscript d to denote decision-directed. The function $\mathcal{J}_{4Q}(\phi)$ is the same cost function on the null subcarriers given in (2.17). Comparing (2.28) to (2.3), we can see that for the data subcarriers, we can no longer bring $e^{-j\phi\frac{(N-1)}{2}}$ out of the modulus operation. Therefore, in the Taylor series summation, we do not have the 2^n term in the denominator. As a result, the amplitudes of higher-order terms do not decay as fast as for (2.2) and we need to include more terms in the Taylor series summation in order to get a good approximation of $\mathbf{Z}^{-1}$.

Suppose we use M terms in the Taylors series approximation and set $a_{i,n} =$

$\mathbf{w}_i^H \mathbf{D}_d^n \mathbf{r}$, then the cost function in (2.28) can be expanded as

$$\mathcal{J}(\phi) = \sum_{i \in \mathbf{d}} \left[\sum_{n=0}^{M} \sum_{m=0}^{M} \frac{(j\phi)^n}{n!} \frac{((j\phi)^m)^*}{m!} a_{i,n} a_{i,m}^* - 2\mathcal{R}e \left(\sum_{n=1}^{M} \frac{(j\phi)^n}{n!} a_{i,n} \left(h(i)s(i)\right)^* \right) + |h_i s_i|^2 \right] + \mathcal{J}_{4Q}(\phi), \tag{2.29}$$

where $\mathcal{R}e(\bullet)$ denotes the real part of a complex number. Here, we assume the channel to be known at the receiver [2]. In practice, the decision-directed method is only invoked starting from the second iteration onwards as the detected symbol is only available after the first iteration. That means that an initial CFO estimate is already obtained in the first iteration. Therefore, what the decision-directed method needs to estimate is only the residual CFO, which is much smaller than ϕ_0. Note that the cost function of data subcarriers is a function of ϕ with order $2M$. In practice, we can set $M = 2$ such that the cost functions of the data subcarriers and the null subcarriers are both of order 4. The overall cost function in (2.29) is therefore also order 4 and we can use the proposed closed-form solution to find the ϕ that minimizes the total cost. However, the coefficients of the polynomial need to be re-calculated according to (2.29). Note that to ensure convergence of the algorithm, we again need to monitor the amplitude of the CFO estimate $|\hat{\phi}_i|$ after different iterations.

The complexity of the decision-directed blind CFO estimation technique is higher because more subcarriers are used in the cost function calculation. In

[2] The channel can also be estimated blindly using blind channel estimation methods such as [74].

practice, the size of $\mathbf{d}$ should be chosen such that a good trade-off between complexity and performance is achieved. The decision-directed CFO estimation algorithm can be summarized as shown in Table 2.3.

Initialization
set iteration number $i = 1$ and the threshold CFO η
Algorithm:
1) Substitute $\mathbf{r}$ into (2.2) and solve for $\hat{\phi}_i$ using the method in Table 2.1.
2) Perform CFO compensation and update the new $\tilde{\mathbf{r}}$ according to (2.23).
3) If $\hat{\phi}_i < \eta$, exit iteration, else go to 4).
4) If $\{|\hat{\phi}_i| < |\hat{\phi}_{i-1}|$ and $i > 1\}$ or $\{i = 1\}$
4.1) Form the set of subcarriers used in CFO estimation by combining null subcarriers and the chosen set of high-SNR data subcarriers.
4.2) Perform OFDM detection on the set of chosen data subcarriers to obtain $\hat{s}_i$.
4.3) Increment iteration number i=i+1.
4.4) Substitute $\mathbf{r}$ into cost function in (2.29) and solve for $\hat{\phi}_i$ that minimizes (2.29). Go to 2).
Else
4.5) Go back to iteration $[i-1]$ and increase the order of Taylor series approximation.

Table 2.3: Summary of the proposed decision-directed successive CFO estimation and compensation algorithm.

2.6 Simulation Results

Computer simulations were performed to study the performance of the proposed low-complexity blind CFO estimation algorithms using frequency-domain null subcarriers. We use an OFDM system with $N = 64$ subcarriers and length-16 cyclic prefix. We define the subcarrier spacing as $\omega = 2\pi/N$. To assess the performance of the proposed method, we define the estimation MSE

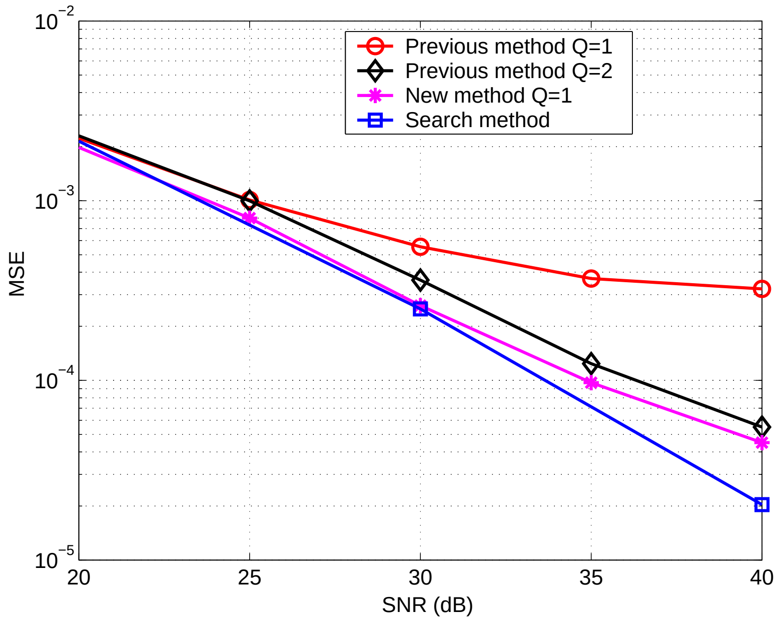

Fig. 2.1: MSE of CFO estimation using the new method ($-0.25\omega \leq \phi_0 \leq 0.25\omega$).

as [68]

$$\text{MSE} = \frac{1}{N_s}\sum_{i=1}^{N_s}\left(\frac{\hat{\phi}-\phi_0}{\omega}\right)^2, \tag{2.30}$$

where $\hat{\phi}$ and ϕ_0 represent the estimated and actual CFO values, respectively, and N_s denotes the total number of Monte Carlo trials. In all the simulations, we only use 1 OFDM symbol to perform CFO estimation, i.e $K = 1$ in all the cost functions. We use channel model A of the HiperLan II channel models [75] in all the simulations. It is a multi-path Rayleigh fading channel with exponential power delay profile and root mean square (RMS) delay spread equal to 50 ns.

2.6.1 Simulation Results for the New Factorization Method

According to the specifications given in IEEE 802.11a, the null subcarriers are placed consecutively from subcarriers 27 to 37 [17]. Figure 2.1 shows the MSE of the new factorization method. Here, the actual CFO for each OFDM symbol is modeled as a uniformly-distributed random variable between $[-0.25\omega, 0.25\omega]$. We compare the performance of the new method with that of the previous method in [64]. We can see that the new method with $Q = 1$ has a better MSE performance than the previous low-complexity method in [64] with both $Q = 1$ and $Q = 2$. Using the new method with $Q = 1$, the cost function is a 4th order polynomial. From a complexity point of view, this is similar to the method in [64] with $Q = 2$. However, due to the 4^n term in the denominator of the Taylor Series expansion, the new method achieves better performance. Also shown in the same figure is the MSE performance of the original algorithm in [37] with the CFO estimate obtained using search method, which is also the ML performance [48]. Only at high SNR regions, the new method suffers some degradation as compared to the search method in [37].

In [67], a study shows that if the null subcarriers are placed consecutively as in the IEEE 802.11a standard, then the CFO value that minimizes (2.2) might not be unique. It was also shown in [48] that the optimal placement of the null subcarriers to minimize the Cramer-Rao bound is to place them evenly spaced across the whole OFDM symbol. Such null subcarrier placement guarantees unique identifiability of CFO up to $2\pi d/N$ where d is the number of null subcarriers. We thus adopted this null subcarrier placement in the

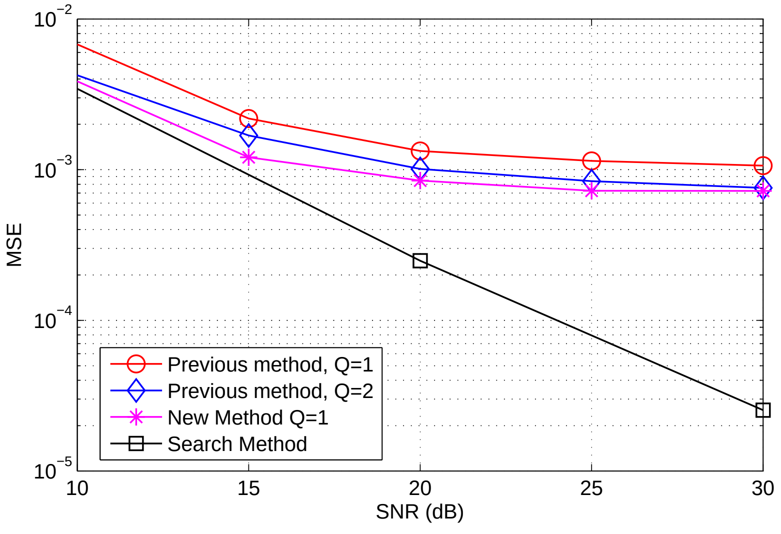

Fig. 2.2: MSE of CFO estimation using the new method for evenly placed null subcarriers ($-0.5\omega \leq \phi_0 \leq 0.5\omega$).

subsequent simulations. We use a total of 11 subcarriers (same number as the consecutive null subcarrier case) spaced 6 subcarriers apart, that is we placed the null subcarriers at the following locations $[1, 7, \cdots, 55, 61]$.

The MSE of the new method using evenly-spaced null subcarriers for $-0.5\omega \leq \phi_0 \leq 0.5\omega$ is shown in Figure 2.2. In this case, we purposely set the CFO value larger such that the degradation due to lower-order approximation in the cost function is more visible. We can see that the new method with $Q = 1$ still performs better than the previous method in [64] with $Q = 1$ and $Q = 2$. For evenly spaced null-subcarrier placements, the performance gain by using the new method is not as large as in the case of consecutive null subcarriers. The symbol error rate (SER) of the three schemes using QPSK modulation is compared in Figure 2.3. Here, we first use the proposed blind method to obtain the CFO estimate. The estimated offset is then compensated from the received

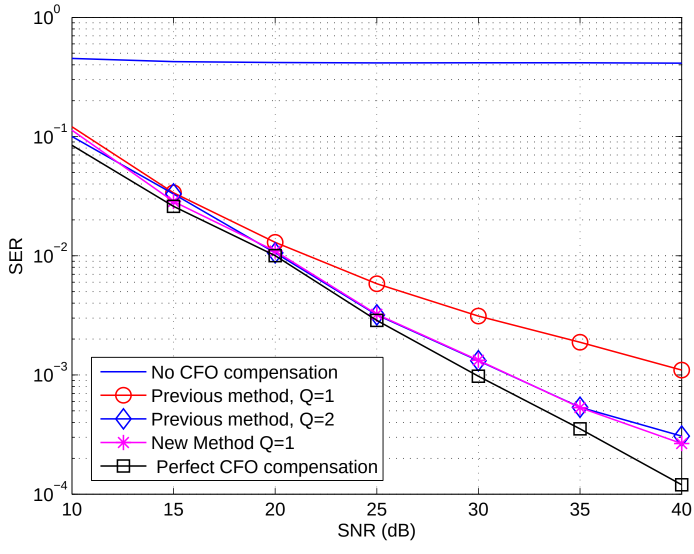

Fig. 2.3: SER with CFO estimation using the new method for evenly placed null subcarriers using QPSK modulation ($-0.5\omega \leq \phi_0 \leq 0.5\omega$).

signal, and OFDM detection is carried out to detect the transmitted data. To separate issues of channel estimation from CFO estimation, we assume that the channel estimation is perfect. We can see that without CFO estimation and compensation, the OFDM system fails. Using the new method with $Q = 1$, the performance is about 8 dB better than for the previous method in [64] (Q=1) at SER of 10^{-3}. The new method with $Q = 1$ achieves similar performance as the previous method in [64] for $Q = 2$.

One major observation from Figure 2.2 is the error floor effect in the high-SNR region. This is due to the inaccuracy of the first-order approximation of the cost function used. The same observation can be made from the SER performance in Figure 2.3. We will show later that this error floor can be effectively removed using the proposed successive CFO estimation and compensation algorithm.

2.6.2 Simulation Results for the Successive CFO Estimation and Compensation Algorithm

The performance of the successive CFO estimation method is evaluated using computer simulations following the same simulation setup as before. Figure 2.4 shows the MSE performance of the successive CFO estimation and compensation algorithm for $-0.7\omega \leq \phi_0 \leq 0.7\omega$. Here we purposely increase the value of the CFO such that the worst-case CFO of $\pm 0.64\omega$ specified by IEEE 802.11a [17] is included. We can see that the performance is improved significantly using the proposed successive algorithm (Table 2.2). The MSE after the first iteration has a floor of 3×10^{-3}. Using the proposed successive method, this floor is removed after the second iteration. Hence, in practice, the successive method can be stopped after the second iteration and the extra complexity introduced is very low. If we compare the MSE after convergence with the MSE of the search method in [37], we can see that after two iterations, the proposed method achieves almost the same MSE performance as that in [37]. We have implemented the convergence monitoring mechanism shown in Table 2.2 in the algorithm. We found that $Q = 1$ is good enough to guarantee convergence for all considered SNR values. Figure 2.5 also shows the SER performance of the successive algorithm using QPSK modulation. We can see that the SER performance takes only 2 iterations to achieve a performance similar to the case where we have a perfect estimation and compensation of the CFO.

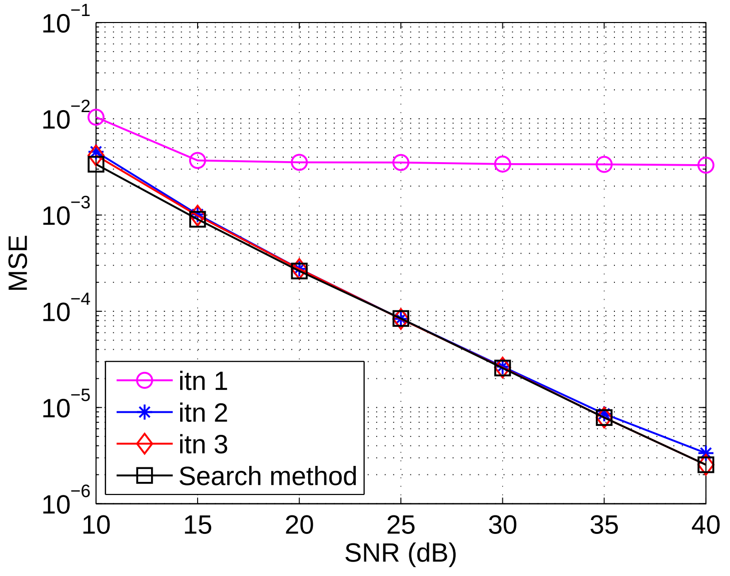

Fig. 2.4: MSE of CFO estimation using the successive CFO estimation and compensation algorithm ($-0.7\omega \leq \phi_0 \leq 0.7\omega$).

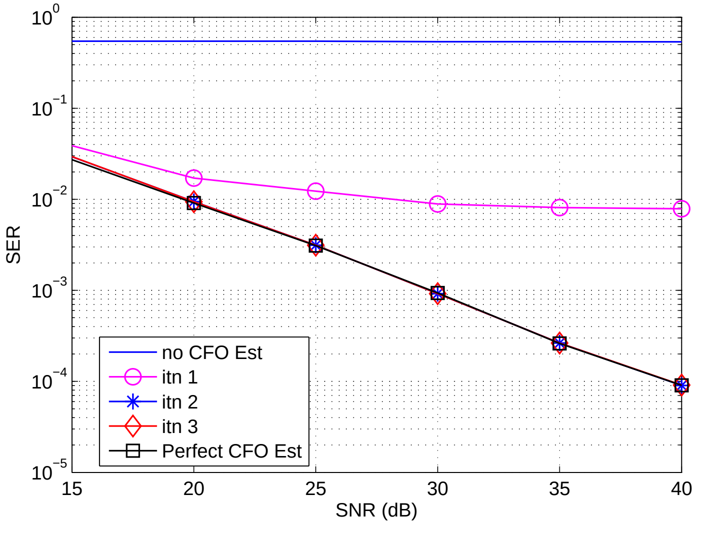

Fig. 2.5: SER with CFO estimation using the successive CFO estimation and compensation algorithm for QPSK modulation($-0.7\omega \leq \phi_0 \leq 0.7\omega$).

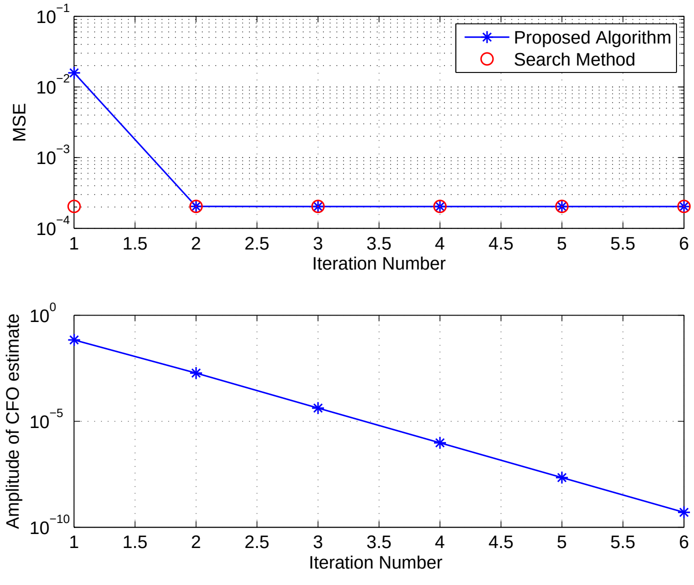

Fig. 2.6: Convergence behavior of the successive algorithm ($\phi_0 = 0.7\omega$, SNR=20dB).

Figure 2.6 shows the convergence behavior of the successive algorithm for a particular channel realization at an SNR of 20 dB. The actual CFO value is fixed at $\phi_0 = 0.7\omega$. From the upper figure in Figure 2.6, we can see that the MSE of the CFO estimation converges to that using the search method in 2 iterations, which is consistent with the results shown in Figure 2.4. The lower figure in Figure 2.6 plots the amplitude of the CFO estimates $|\hat{\phi}_i|$ for different iterations. We can see that the amplitude of $|\hat{\phi}_i|$ is indeed decreasing as the number of iterations i increases, which is an indication of the convergence of the algorithm as explained earlier.

As the successive CFO estimation and compensation algorithm is generic, it is applicable to the previous low-complexity method in [64] as well. Figure 2.7

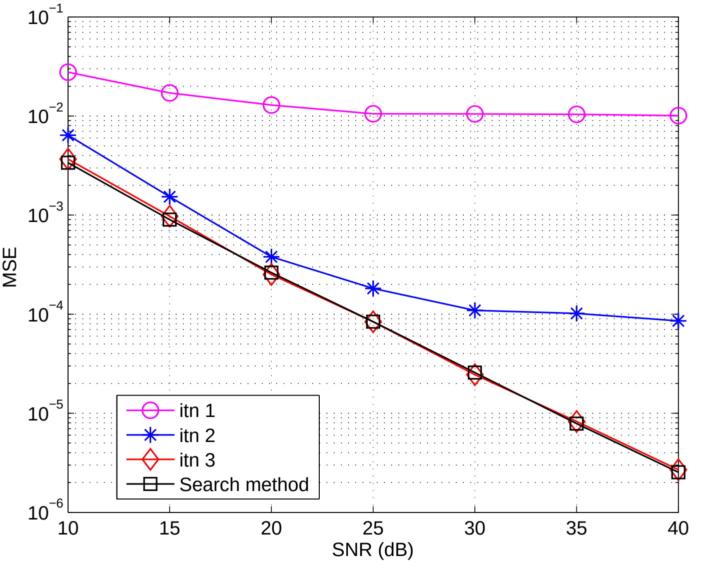

Fig. 2.7: CFO estimation using the previous method with $Q = 1$ and the successive algorithm $(-0.7\omega \leq \phi_0 \leq 0.7\omega)$.

shows the performance of the successive algorithm when used in combination with the low-complexity method in [64] for $Q = 1$. The successive method again significantly improves the performance of blind CFO estimation and effectively removes the error floor in the high-SNR region. In this case, the MSE also converges after 3 iterations to the same MSE as the search method in [37]. Figure 2.8 shows the SER performance of the successive algorithm combined with the low-complexity method in [64] for $Q = 1$ using QPSK modulation. We can see that the SER performance converges to that with perfect CFO compensation after 3 iterations.

From the MSE and SER performances, we can observe that the performance degradation due to the first-order approximation in Taylor series can be effectively reduced using the successive algorithm.

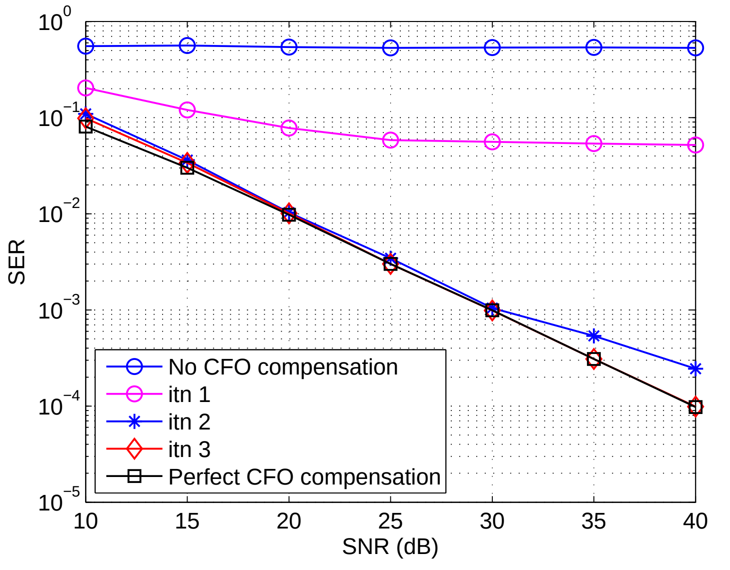

Fig. 2.8: SER with CFO estimation using the previous method with $Q = 1$ and the successive algorithm with QPSK modulation ($-0.7\omega \leq \phi_0 \leq 0.7\omega$).

2.6.3 Simulation Results for the Decision-directed Algorithm

Simulations were also carried out to study the performance of the decision-directed CFO estimation algorithm in Table 2.3. Figure 2.9 shows the MSE of the CFO estimation. Here, in the first iteration, we use the proposed closed-form approximation method to get the initial CFO estimate. The estimated CFO is then compensated. We then use a zero-forcing one-tap equalizer on each subcarrier to equalize the effect of the frequency selective channel. The estimate of the transmitted signal is obtained using a minimum Euclidean distance detector. From the second iteration onwards, we use both the null subcarriers and the reliable data subcarriers to perform CFO estimation. As we have more subcarriers available to perform CFO estimation, we expect better performance compared to the non-decision-directed method. This is

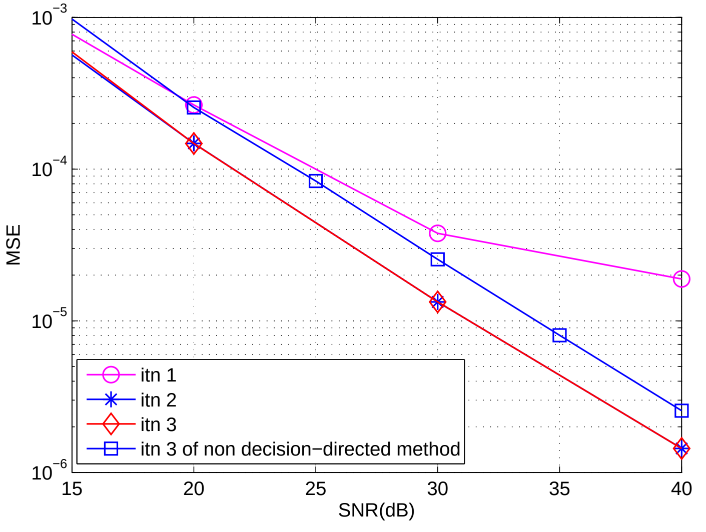

Fig. 2.9: CFO estimation using decision-directed algorithm with $Q = 1$ $(-0.25\omega \leq \phi_0 \leq 0.25\omega)$.

also evident from Figure 2.9. In this simulation, we choose the 11 highest-SNR data subcarriers combined with the 11 null subcarriers for CFO estimation. We use $M = 2$ and $Q = 1$ in the cost function (2.29). As we use twice the number of subcarriers for CFO estimation, we expect a performance gain of 3 dB compared to non-decision-directed method. This is confirmed by Figure 2.9.

The best performance is achieved when all the subcarriers are used for CFO estimation. However, the complexity of such a method is high and error propagation due to wrong decisions will be worse compared to using only high-SNR subcarriers. Therefore, a trade-off between complexity and MSE performance should be found.

2.7 Conclusions

In this chapter, we developed a new factorization method to approximate the cost function for blind CFO estimation in OFDM systems using null subcarriers. Using this new method, we further derived closed-form solutions for the CFO estimate using a first-order Taylor series approximation. This new CFO estimator reduces the computational complexity of the CFO estimation significantly. We also proposed a successive CFO estimation and compensation algorithm which further improves the performance of the new CFO estimator. Indeed, using the proposed successive algorithm, we were able to achieve similar performance as the method in [37] yet at a much lower computational complexity. A decision-directed extension of the successive algorithm was also given, which achieves even better performance at the cost of slightly higher computational complexity.

Chapter 3

Optimal Null Subcarrier Placement for Blind CFO Estimation

3.1 Introduction

In Chapter 2, we studied the blind CFO estimation algorithm using null subcarriers by Liu and Tureli [37] and proposed new algorithms to reduce the computational complexity when the CFO is small. In this chapter, we present a mathematical analysis on the relationship between the placement of null subcarriers and the performance of the CFO estimation. A previous work in [67] showed that consecutively placed null subcarriers at both ends of the spectrum does not guarantee unique solution for the CFO estimates. The identifiability of the CFO estimator in [37] with different null subcarrier placement is further studied in [48]. Moreover, it was also shown that equally spaced null subcarrier placement minimizes the Cramer Rao bound (CRB) of the CFO estimation. As the CRB is not always achievable for practical CFO estimation schemes, in this chapter, we study the relationship between the null subcarrier placement and the following two more practical performance-related parameters

- SNR of the CFO estimation;
- Theoretical MSE of the CFO estimation, which is a linear approximation of the actual MSE of CFO estimation in the high SNR region.

Based on the obtained relationship, we find the null subcarrier placement that maximizes the SNR and minimizes the theoretical MSE, respectively. We show that the two optimization problems are equivalent and a single optimal null subcarrier placement exists. For the case when the number of subcarriers is divisible by the number of null subcarriers, the exact optimal placement can be found. Interestingly, this is also the null subcarrier placement that minimizes the CRB as given in [48]. When the number of subcarriers is not divisible by the number of null subcarriers, it is difficult to prove the optimality of the null subcarrier placement due to the integer constraints on the null subcarrier positions. However, we will develop a heuristic procedure on how to place the null subcarriers where good performance can still be achieved. We verify that the null subcarrier placement obtained using the proposed heuristic procedure is indeed optimal using exhaustive computer search when the number of null subcarriers is small. We also extend the optimization problem to a practical OFDM system where guard bands are required at both ends of the spectrum. In this case, if given a few more null subcarriers that can be inserted freely in the OFDM symbol, we show how to place them to guarantee the SNR optimality in the CFO estimation. We show from computer simulations that with the proposed null subcarrier placement, the performance of the CFO estimation can be significantly improved. We further show that for practical OFDM systems with guard bands, introduction of a few extra null subcarriers leads to much better performance of the blind CFO estimation.

The rest of this chapter is organized as follows. In Section 3.2, we study the relationship between the null subcarrier placement and the SNR of the CFO estimation. We find the null subcarrier placement that maximizes this SNR, which we call $\mathrm{SNR_{CFO}}$ to distinguish it from the SNR of the received signal. In Section 3.3, we derive the theoretical MSE of the CFO estimation and obtain its relationship with the null subcarrier placement. We then show that the null subcarrier placement that minimizes the theoretical MSE also maximizes the $\mathrm{SNR_{CFO}}$. Optimal null subcarrier placement for practical OFDM systems with guard bands is studied in Section 3.4. In Section 3.5, we present computer simulation results and conclusions are drawn in Section 3.6.

3.2 Placement of Null Subcarriers Based on $\mathrm{SNR}_{\mathrm{CFO}}$ Maximization

For an OFDM system with a CFO value of ε_0, the received frequency domain signal on a null subcarrier l_i of OFDM symbol m can be written as

$$\begin{aligned} y_{l_i}^m &= \mathbf{w}_{l_i}^H \mathbf{r}^m = \sum_{n=0, n \notin \mathbf{l}^m}^{N-1} h_n^m s_n^m C_{n-l_i}^m(\varepsilon_0) + n_{l_i}^m \\ &= \mathrm{ICI}_{l_i}^m(\varepsilon_0) + n_{l_i}^m, \end{aligned} \tag{3.1}$$

where $\mathbf{w}_{l_i}^H$ is row l_i of the DFT matrix, and $\mathbf{r}^m$ is the time domain received signal for the m^{th} OFDM symbol given in (2.1). We use $h_{l_i}^m$ and $s_{l_i}^m$ to denote the channel response and transmitted data on subcarrier l_i of OFDM symbol m. Vector $\mathbf{l}^m$ contains indices of all the null subcarriers in OFDM symbol m. The ICI due to CFO of ε_0 on subcarrier l_i is denoted as $\mathrm{ICI}_{l_i}^m(\varepsilon_0)$ and $n_{l_i}^m$ is the AWGN noise. The value of $C_k^m(\varepsilon_0)$ is given by [76]

$$\begin{aligned} C_k^m(\varepsilon_0) &= \frac{\sin\left[\pi(k+\varepsilon_0)\right]}{N \sin\left[\frac{\pi}{N}(k+\varepsilon_0)\right]} \exp\left(j\pi(k+\varepsilon_0)(1-1/N)\right) \\ & \quad \exp\left(j2\pi\varepsilon_0(m-1)(1+N_g/N)\right). \end{aligned} \tag{3.2}$$

Using (3.1), the cost function in (2.2), which is the summation of the received signal power over all the null subcarriers, can be equivalently re-written as

$$\begin{aligned}
\mathcal{J}(\varepsilon) &= \sum_{m=1}^{K}\sum_{i=1}^{d}\left|\mathbf{w}_{l_i}^{H}\mathrm{diag}(1, e^{-j2\pi\varepsilon/N}, e^{-j2\pi 2\varepsilon/N}, \cdots, e^{-j2\pi(N-1)\varepsilon/N})\mathbf{r}^{m}\right|^{2} \\
&= \sum_{m=1}^{K}\sum_{i=1}^{d}\left|\mathrm{ICI}_{l_i}^{m}(\varepsilon_0-\varepsilon)+n_{l_i}^{m}\right|^{2} \\
&= \sum_{m=1}^{K}\sum_{i=1}^{d}\left|\sum_{n=0, n\notin \mathbf{l}^{m}}^{N-1} h_n^m s_n^m C_{n-l_i}^{m}(\varepsilon_0-\varepsilon)+n_{l_i}^{m}\right|^{2}.
\end{aligned} \tag{3.3}$$

Correspondingly, the estimate of the CFO is given by

$$\hat{\varepsilon} = \arg\min_{\varepsilon} \mathcal{J}(\varepsilon). \tag{3.4}$$

Note that the received signal on a null subcarrier l_i in (3.1) is the sum of $\mathrm{ICI}_{l_i}^{m}$ and $n_{l_i}^{m}$. In these two terms, $\mathrm{ICI}_{l_i}^{m}$ is the useful signal term which we can use to estimate the CFO ε_0, and $n_{l_i}^{m}$ is the noise term, which is uncorrelated with $\mathrm{ICI}_{l_i}^{m}$. Therefore, using (3.1) we can define an objective function, called SNR$_{\mathrm{CFO}}$ as

$$\mathrm{SNR}_{\mathrm{CFO}} = \frac{\mathrm{E}\left(\sum_{m=1}^{K}\sum_{i=1}^{d}\left|\mathrm{ICI}_{l_i}^{m}(\varepsilon_0)\right|^{2}\right)}{\mathrm{E}\left(\sum_{m=1}^{K}\sum_{i=1}^{d}\left|n_{l_i}^{m}\right|^{2}\right)}, \tag{3.5}$$

where E denotes statistical expectation. Note that the objective function can be interpreted as the SNR of the CFO estimation. The power of ICI on subcarrier l_i in OFDM symbol m can be written as

$$\begin{aligned}
\mathrm{E}\left|\mathrm{ICI}_{l_i}^m(\varepsilon_0)\right|^2 &= \mathrm{E}\left\{\left|\sum_{n=0,n\notin\mathbf{l}^m}^{N-1} h_n^m s_n^m C_{n-l_i}^m(\varepsilon_0)\right|^2\right\} \\
&= \left\{\sum_{n=0,n\notin\mathbf{l}^m}^{N-1} \mathrm{E}|h_n^m s_n^m|^2 \frac{\sin^2\left[\pi(n-l_i+\varepsilon_0)\right]}{N^2\sin^2\left[\frac{\pi}{N}(n-l_i+\varepsilon_0)\right]}\right\}. \quad (3.6)
\end{aligned}$$

We note from (3.6) that the power of ICI for the m^{th} OFDM symbol depends only on the signals in OFDM symbol m and is not affected by the other OFDM symbols. We also assume that the channels from different OFDM symbols have the same statistical distribution and are independent of the transmitted signal. As a result, $\mathrm{E}|h_n^m s_n^m|^2$ becomes independent of the OFDM symbol index m. As the noise in OFDM symbol m is also independent of the noise in other OFDM symbols, the $\mathrm{SNR}_{\mathrm{CFO}}$ optimization from the null subcarrier placements for K OFDM symbols can be performed on each OFDM symbol independently. Therefore, the optimization only needs to be performed for one OFDM symbol. From now on, for ease of notation, we drop the OFDM symbol index m. In this case, the null subcarrier placement $\mathbf{l}$ that maximizes the $\mathrm{SNR}_{\mathrm{CFO}}$ in (3.5) can be found by

$$\mathbf{l} = \arg\max_{\mathbf{l}}(\mathrm{SNR}_{\mathrm{CFO}}) = \arg\max_{\mathbf{l}}\left[\frac{\mathrm{E}\left(\sum_{i=1}^{d}|\mathrm{ICI}_{l_i}(\varepsilon_0)|^2\right)}{\mathrm{E}\left(\sum_{i=1}^{d}|n_{l_i}|^2\right)}\right]. \quad (3.7)$$

The noise variance is the same for all the subcarriers, therefore, the denominator of (3.7) is independent of the null subcarrier selection $\mathbf{l}$. Accordingly, the optimization of the null subcarrier placement reduces to

$$\begin{aligned}
\mathbf{l} &= \arg\max_{\mathbf{l}} \mathrm{E}\left(\sum_{i=1}^{d} |\mathrm{ICI}_{l_i}(\varepsilon_0)|^2\right) \\
&= \arg\max_{\mathbf{l}} \mathrm{E}\left\{\sum_{i=1}^{d} \left|\sum_{n=0,n\notin\mathbf{l}}^{N-1} h_n s_n C_{n-l_i}(\varepsilon_0)\right|^2\right\} \\
&= \arg\max_{\mathbf{l}} \sum_{i=1}^{d} \left\{\sum_{n=0,n\notin\mathbf{l}}^{N-1} \mathrm{E}|h_n s_n|^2 \frac{\sin^2\left[\pi(n-l_i+\varepsilon_0)\right]}{N^2\sin^2\left[\frac{\pi}{N}(n-l_i+\varepsilon_0)\right]}\right\} \\
&= \arg\max_{\mathbf{l}} \sum_{i=1}^{d} \left\{\sum_{n=0,n\notin\mathbf{l}}^{N-1} \frac{1}{\sin^2\left[\frac{\pi}{N}(n-l_i+\varepsilon_0)\right]}\right\}, \qquad (3.8)
\end{aligned}$$

as $\mathrm{E}|h_n s_n|^2 = \mathrm{E}\{|h_n|^2\}\mathrm{E}\{|s_n|^2\}$ is independent of the null subcarrier placement. Here, without *apriori* knowledge of the channels, we assume that the channels at different subcarriers h_n have the same average power and this makes $\mathrm{E}\{|h_n|^2\}$ independent of the subcarrier index n. The numerator $\sin^2\left[\pi(n-l_i+\varepsilon_0)\right]$ is equal to $\sin^2(\pi\varepsilon_0)$. Hence, it is also independent of the null subcarrier placement. In practice, ε_0 is normally modeled as a random variable with a uniform distribution [68] as follows

$$p(\varepsilon_0) = \begin{cases} \frac{1}{2\theta}, & \varepsilon_0 \in [-\theta, \theta) \\ 0, & \text{elsewhere}, \end{cases} \qquad (3.9)$$

where θ is the magnitude of the worst case CFO. In this case, the cost function, averaging over the random variable ε_0, can be written as

$$\begin{aligned}
\mathbf{l} &= \arg\max_{\mathbf{l}} \left\{ \int_{-\theta}^{+\theta} \sum_{i=1}^{d} \left[\sum_{n=0, n\notin \mathbf{l}}^{N-1} \frac{1}{\sin^2\left[\frac{\pi}{N}(n - l_i + \varepsilon_0)\right]} \right] p(\varepsilon_0) d\varepsilon_0 \right\} \\
&= \arg\max_{\mathbf{l}} \left\{ \sum_{i=1}^{d} \sum_{n=0, n\notin \mathbf{l}}^{N-1} \frac{1}{2\theta} \frac{N}{\pi} f(n - l_i) \right\}, \qquad (3.10)
\end{aligned}$$

where $f(k)$ is given by

$$\begin{aligned}
f(k) &= \left[\cot\left(\frac{\pi}{N}(k-\theta)\right) - \cot\left(\frac{\pi}{N}(k+\theta)\right) \right] \\
& \quad \text{for} \quad k = -(N-1), -(N-2) \cdots, -1, 1, 2, \cdots, N-1. \qquad (3.11)
\end{aligned}$$

Note that $k = n - l_i \neq 0$ for $n \notin \mathbf{l}$. It can be easily shown that $f(k)$ has the following two properties:

1. $f(k)$ is periodic with period N, i.e. $f(k) = f(k+N)$. Therefore, for the subsequent optimization, we only need to consider the function $f(k)$ over one period, i.e. $k = 1, 2, \cdots, N-1$.
2. $f(k)$ is an even function of k, i.e. $f(k) = f(-k)$ for any integer k.

Discarding the constants in (3.10), we can re-write the optimization problem in the following form

$$\begin{aligned}
\mathbf{l} &= \arg\max_{\mathbf{l}} \left\{ \sum_{i=1}^{d} \sum_{n=0, n\notin \mathbf{l}}^{N-1} f(n - l_i) \right\} \\
&= \arg\max_{\mathbf{l}} \sum_{i=1}^{d} \left\{ \sum_{n=0}^{N-1} f(n - l_i) - \sum_{n\in \mathbf{l}, n\neq l_i} f(n - l_i) - f(0) \right\}. \qquad (3.12)
\end{aligned}$$

We can notice that the third term in (3.12), that is $f(0)$, is independent of $\mathbf{l}$ and hence can be dropped. Now, we prove that the first term in the summation $c_1 = \sum_{n=0}^{N-1} f(n-l_i)$ in (3.12) is also independent of l_i.

Proof. Let k be any arbitrary positive integer between 1 and $N-1$, then

$$\sum_{n=0}^{N-1} f(n-l_i) = \sum_{n=0}^{k-1} f(n-l_i) + \sum_{n=k}^{N-1} f(n-l_i).$$

Using the periodicity of $f(k)$, we can write

$$\begin{aligned}\sum_{n=0}^{N-1} f(n-l_i) &= \sum_{n=N}^{N+k-1} f(n-l_i) + \sum_{n=k}^{N-1} f(n-l_i) \\ &= \sum_{m=0}^{N-1} f(m+k-l_i).\end{aligned} \tag{3.13}$$

Since (3.13) holds for arbitrary $k \in [1, N-1]$, it holds for $k = l_i$. Substituting $k = l_i$ in (3.13), we get

$$c_1 = \sum_{n=0}^{N-1} f(n-l_i) = \sum_{m=0}^{N-1} f(m+l_i-l_i) = \sum_{m=0}^{N-1} f(m).$$

This proves that c_1 is independent of l_i. $\square$

Therefore, the cost function in (3.12) can be simplified to

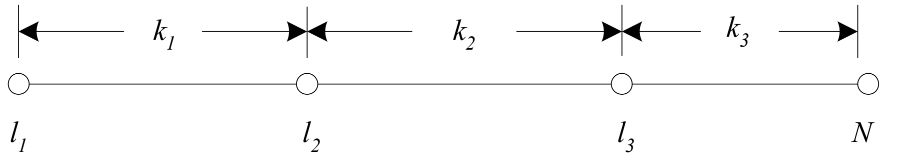

Fig. 3.1: Illustration of the placement of 3 null-subcarriers.

$$\mathbf{l} = \arg\min_{\mathbf{l}} \left\{ \sum_{i=1}^{d} \sum_{n \in \mathbf{l}, n \neq l_i} f(n - l_i) \right\} = \arg\min_{\mathbf{l}} \left\{ \sum_{i=1}^{d} \sum_{j=1, j \neq i}^{d} f(l_i - l_j) \right\}. \quad (3.14)$$

Notice that the new cost function in (3.14) depends only on the spacing, not the absolute positions, of the null subcarriers. Let us define the spacing between the i^{th} and $(i+1)^{\text{th}}$ null subcarriers as $k_i = l_{i+1} - l_i$ for $i = 1, 2...d-1$ and $k_d = N + l_1 - l_d$. For illustration, we first give the new formulation of (3.14) for the simple case of $d = 3$ and then generalize the result to arbitrary d.

Figure 3.1 illustrates the problem of placing $d = 3$ null subcarriers. Without loss of generality, we place l_1 at subcarrier 0. From (3.14), the optimization of the placement of the null subcarriers l_1, l_2 and l_3 is equivalent to the optimization of the spacing between these null subcarriers, that is $k_1 = l_2 - l_1$, $k_2 = l_3 - l_2$ and $k_3 = N + l_1 - l_3 = N - l_3$ as $l_1 = 0$. Note that there is now a constraint on the values of k_1, k_2 and k_3, i.e. $k_1 + k_2 + k_3 = N$. We can now re-write the cost function in (3.14) as

$$\mathbf{l} = \arg \min_{k_1, k_2, k_3} \mathcal{J}(k_1, k_2, k_3),$$
$$\text{subject to:} \quad k_1 + k_2 + k_3 = N,$$

where

$$
\begin{aligned}
& \mathcal{J}(k_1,k_2,k_3) = \sum_{i=1}^{3} \sum_{j=1,j\neq i}^{3} \{f(l_i - l_j)\} \\
= \quad & f(l_1-l_2)+f(l_1-l_3)+f(l_2-l_3)+f(l_2-l_1)+f(l_3-l_1)+f(l_3-l_2) \\
= \quad & \{f(k_1)+f(k_1+k_2)\}+\{f(k_2)+f(k_2+k_3)\}+\{f(k_3)+f(k_3+k_1)\}\,.
\end{aligned}
\tag{3.15}
$$

Here we made use of the evenness property of $f(k)$, e.g. $f(l_1-l_2)=f(-k_1)=f(k_1)$.

To extend the formulation in (3.15) to arbitrary number (d) of null subcarriers, we first define $p_{i,m} = \sum_{j=0}^{m-1} k_{[(i+j-1) \bmod d]+1}$ for $i = 1, 2, \cdots d$ and $m = 1, 2, \cdots d-1$. Here, we use $[i \bmod d]$ for integers i and d to denote the integer remainder of i/d. The subscript i indicates the k index of the first term in the summation, because $[(i+0-1) \bmod d]+1 = i$. The subscript m indicates the total number of terms in the summation. Therefore, $p_{i,m}$ is actually the spacing between the i^{th} null-subcarrier and its m^{th} neighbouring null subcarrier to the right in the cyclic sense[1]. Therefore, the contribution to the total cost function due to a particular null subcarrier i is the summation of $f(l_i-l_j)$ from all its $d-1$ neighbouring null subcarriers, i.e. $\sum_{j=1,j\neq i}^{d} f(l_i-l_j)$. As $p_{i,m}$ is the spacing between the i^{th} null subcarrier and its m^{th} neighbouring null subcarrier, we can write $\sum_{j=1,j\neq i}^{d} f(l_i-l_j) = \sum_{m=1}^{d-1} f(p_{i,m})$. Summing this over all the d null subcarriers, i.e. d possible values of i, the new cost

[1] The length of the cycle is d as there are only d null subcarriers.

function can be written as

$$\mathcal{J}(k_1, k_2, \cdots, k_d) = \sum_{i=1}^{d} \sum_{m=1}^{d-1} f(p_{i,m}) = \sum_{m=1}^{d-1} \left\{ \sum_{i=1}^{d} f(p_{i,m}) \right\}$$
$$\text{subject to:} \quad \sum_{i=1}^{d} k_i = N. \tag{3.16}$$

Notice that the optimization problem in (3.16) has all variables being positive integers. Such an integer programming problem is difficult to solve analytically. Therefore, we first relax the constraints on all k_i's being positive integers and assume them to be positive real numbers. This approach has been commonly used in finding the optimal bit allocations for multiuser or multicarrier systems, see for example [77]. For ease of analysis, we also assume that $\theta < 1$ so that $k - \theta > 0$ and $k + \theta < N$ are satisfied for all possible values of k. It can be easily shown that if $\theta < 1$ is satisfied, the double derivative of $f(k)$ with respect to k, $\frac{d^2}{dk^2} f(k) > 0$ for $1 < k < N - 1$. Therefore, $f(k)$ is a convex function for $1 < k < N-1$ and $\theta < 1$. It is stated in [78] that if $f(k)$ is convex for $k_1, k_2, \cdots, k_d$, and given $\lambda_1, \lambda_2, \cdots, \lambda_d$ with $\lambda_1 + \lambda_2 + \cdots + \lambda_d = 1$, then

$$f(\lambda_1 k_1 + \lambda_2 k_2 + \cdots + \lambda_d k_d) \leq \lambda_1 f(k_1) + \lambda_2 f(k_2) + \cdots + \lambda_d f(k_d). \tag{3.17}$$

This relationship is also known as the Jensen inequality. By setting $\lambda_1 = \lambda_2 = \cdots = \lambda_d = \frac{1}{d}$, we have

$$\frac{1}{d} \sum_{i=1}^{d} f(p_{i,m}) \geq f\left(\frac{1}{d} \sum_{i=1}^{d} p_{i,m} \right) = f\left(\frac{mN}{d} \right) \quad \text{for } \ m = 1, 2, \cdots d - 1. \tag{3.18}$$

Here we make use of the fact that $\sum_{i=1}^{d} p_{i,m} = mN$ because $\sum_{i=1}^{d} k_i = N$. When $k_1 = k_2 = \cdots = k_d = \frac{N}{d}$, the equality in (3.18) holds for all the values of m. Therefore, we get

$$\mathcal{J}(k_1, k_2, \cdots, k_d) = \sum_{m=1}^{d-1} \left\{ \sum_{i=1}^{d} f(p_{i,m}) \right\} \geq \sum_{m=1}^{d-1} d \left\{ f\left(\frac{mN}{d} \right) \right\}. \tag{3.19}$$

This cost function is minimized when $k_1 = k_2 = \cdots = k_d = \frac{N}{d}$. This means that the null subcarriers should be placed evenly-spaced across the whole OFDM symbol.

If $\frac{N}{d}$ is an integer, the null subcarriers should be placed $\frac{N}{d}$ apart to maximize $\mathrm{SNR}_{\mathrm{CFO}}$. Therefore, in system design when we can freely choose the number of null subcarriers d, we should always choose d such that $\frac{N}{d}$ is an integer to ensure the optimality of null subcarrier placement. However, for systems where N is not divisible by d, it turns out difficult to prove the optimality of a particular null subcarrier placement because of the integer constraints on the values of k_i's. However, from the optimal solution for real k_i, we know that to maximize the $\mathrm{SNR}_{\mathrm{CFO}}$, the spacing between the null subcarriers should be as even as possible. In the following, we propose a heuristic procedure to achieve this.

Let $k_l = \lfloor \frac{N}{d} \rfloor$ and $k_u = \lceil \frac{N}{d} \rceil$ where k_l and k_u are both integers. Here we use $\lfloor x \rfloor$ to denote the largest integer that is smaller than or equal to x, while $\lceil x \rceil$ denotes the smallest integer that is larger than or equal to x. We know that to achieve close to even spacing between the null subcarriers, all the k_i values should be chosen as either k_l or k_u. Next we determine how many k_i's should take the value k_l and how many k_i's should take the value k_u and we use n_l and n_u to denote these two numbers respectively. The values of n_l and n_u can be obtained by solving

$$\begin{cases} n_l + n_u = d \\ n_l \times k_l + n_u \times k_u = N. \end{cases}$$

Now the problem of placing the null subcarriers is equivalent to placing these n_l k_l's and n_u k_u's as evenly as possible. It is obvious that if we place all the k_l's consecutively and all the k_u's consecutively, the spacing between the null subcarriers will not be very even. They should be placed alternately in some way. Without loss of generality, let us assume $n_l \geq n_u$. If $\frac{n_l}{n_u} = q$ is an integer, we should group q k_l's followed by one k_u into one group and place n_u of such groups as illustrated in Table 3.1. Otherwise, we let $q_l = \lfloor \frac{n_l}{n_u} \rfloor$. In this case, we should have two kinds of placing groups. The type 1 group consists of q_l k_l's followed by one k_u and the type 2 group consists of $q_l + 1$ k_l's followed by one k_u. The number of type 1 groups g_l and number of type 2 groups g_u can be obtained by solving

$$\begin{cases} g_l + g_u = n_u \\ g_l \times q_l + g_u \times (q_l + 1) = n_l. \end{cases}$$

These two types of groups should be placed alternately. A summary of this heuristic placement method is given in Table 3.1.

Let us illustrate this procedure with an example. Suppose we want to place

• Find k_l, k_u and solve for the corresponding n_l n_u.
• **if** n_l is divisible by n_u, i.e. $\frac{n_l}{n_u} = q$ then
{ • The spacing between null subcarriers should be

$$\overbrace{[\underbrace{k_l, k_l, \cdots, k_l}_{q}, \underbrace{k_u}_{1}, \cdots, \underbrace{k_l, k_l, \cdots, k_l}_{q}, \underbrace{k_u}_{1}]}^{n_u \text{groups}}$$

}
else{
• calculate $q_l = \lfloor \frac{n_l}{n_u} \rfloor$ and g_l and g_u from $g_l + g_u = n_u$ and $g_l \times q_l + g_u \times (q_l + 1) = n_l$
• The spacing between the null subcarriers should be

$$[\overbrace{\underbrace{k_l, k_l, \cdots, k_l}_{q_l}, \underbrace{k_u}_{1}}^{\text{type 1 group}}, \overbrace{\underbrace{k_l, k_l, \cdots, k_l}_{q_l+1}, \underbrace{k_u}_{1}}^{\text{type 2 group}}, \overbrace{\underbrace{k_l, k_l, \cdots, k_l}_{q_l}, \underbrace{k_u}_{1}}^{\text{type 1 group}} \cdots\cdots]$$

}

Table 3.1: Heuristic null subcarrier placement when N is not divisible by d ($n_l > n_u$).

10 null subcarriers for an OFDM system with $N = 64$ subcarriers. We first calculate $k_l = \lfloor \frac{64}{10} \rfloor = 6$ and $k_u = \lceil \frac{64}{10} \rceil = 7$. We can also get $n_l = 6$, $n_u = 4$. Now we need to place these 6 k_l's and 4 $k_u's$ as evenly as possible. Next we determine $q_l = \lfloor 1.5 \rfloor = 1$, $g_l = 2$ and $g_u = 2$. In this case, the k_i's should be divided into two types of groups. The type one group consists of one (q_l) k_l followed by one k_u, while the type 2 group consists of two ($q_l + 1$) k_l followed by one k_u. And these two types of groups should be placed alternately. Therefore, the spacing between the null subcarriers should be [6 7 6 6 7 6 7 6 6 7]. Hence, one possible null subcarrier placement using this heuristic approach is [0 6 13 19 25 32 38 45 51 57].[2]

The null subcarrier placement for $d = 4$ to $d = 11$ null subcarriers for an

[2]Because the positions of the null subcarriers can be cyclically shifted without affecting the value of the cost function, there are multiple solutions to the null subcarrier placement. What we have here is just one possible placement.

OFDM system with $N = 64$ subcarriers using the proposed heuristic method is listed in Table 3.2. For the case of $d = 5$ and 6, we have verified that the null subcarrier placement using the heuristic method is the same as the optimal placement obtained through exhaustive computer search[3].

d	k_i	index of null subcarriers
5	[13 13 13 13 12]	[0 13 26 39 52]
6	[11 11 10 11 11 10]	[0 11 22 32 43 54]
7	[9 9 9 9 9 9 10]	[0 9 18 27 36 45 54]
8	[8 8 8 8 8 8 8 8]	[0 8 16 24 32 40 48 56]
9	[7 7 7 7 7 7 7 7 8]	[0 7 14 21 28 35 42 49 56]
10	[6 7 6 6 7 6 7 6 6 7]	[0 6 13 19 25 32 38 45 51 57]
11	[6 6 6 6 5 6 6 6 6 6 5]	[0 6 12 18 24 29 35 41 47 53 59]

Table 3.2: Heuristic null subcarrier placement for d=4 to 11 for N=64 OFDM systems

Note that our previous derivation is based on the assumption that $\theta < 1$ to ensure that $f(k)$ is convex for $k = 1, 2, \cdots N - 1$. This is a valid assumption for most indoor communication systems operating in the 2.4GHz and 5GHz bands, such as wireless local area network (LAN) systems [17]. According to the IEEE 802.11a standard [17], the tolerance of transmit and receive center frequency should be ± 20 ppm. Therefore, the worst case CFO is 40 ppm, which is about 200 KHz for a 5.2 GHz center frequency. This worst case CFO corresponds to the value of $\theta = 0.66$. Moreover, for indoor applications, due to low mobility and high carrier frequency (5GHz for IEEE 802.11a system), the CFO due to doppler shift is negligible. Therefore, this is a valid assumption in practice, especially for indoor wireless LAN based applications due to the high-quality oscillators currently used.

[3]The complexity of exhaustive computer search grows exponentially with the number of null subcarriers. Although this could be done offline, the complexity is still not practical for systems with large number of null subcarriers and data subcarriers.

It is shown in [48] that the evenly spaced null subcarrier placement will introduce an ambiguity in the CFO estimation of uN/d where u is a positive integer. However, the CFO is uniquely identifiable in $[-\frac{N}{2d}, \frac{N}{2d})$ [48]. In a practical OFDM system, the number of null subcarriers is normally kept below 15% of the total number of subcarriers to ensure high spectral efficiency [17]. In such a case, the SNR-optimal subcarrier placement results in the null subcarrier spacing $N/d \geq 6$. Therefore, using the SNR-optimal null subcarrier placement, the CFO is uniquely identifiable within $[-\frac{N}{2d}, \frac{N}{2d})$, which is normally larger than $[-3, 3)$. In modern wireless communication systems, especially wireless LAN systems, the practical values of CFO are normally within ± 1 subcarrier spacing. Therefore, knowing that the CFO is very small, we can limit the search range for the CFO values that minimizes (2.2), for example within [-1, +1]. In this case, the ambiguity in CFO estimation can be avoided.

3.3 Placement of Null Subcarriers Based on the Theoretical MSE Minimization

In this section, we first derive the theoretical MSE of the CFO estimation, which is a linear approximation of the actual MSE in the high SNR region. Then we find the relationship between the null subcarrier placement and the theoretical MSE. Based on this, we formulate the theoretical MSE optimization problem of the null subcarrier placement and find the optimal null subcarrier placement.

Let us define $\Delta\varepsilon = \varepsilon_0 - \hat{\varepsilon}$ as the CFO estimation error. Using a first-order approximation, we get [66]

$$0 = \left.\frac{\partial \mathcal{J}(\varepsilon)}{\partial \varepsilon}\right|_{\varepsilon=\hat{\varepsilon}} \approx \left.\frac{\partial \mathcal{J}(\varepsilon)}{\partial \varepsilon}\right|_{\varepsilon=\varepsilon_0} - \Delta\varepsilon \left.\frac{\partial \mathcal{J}^2(\varepsilon)}{\partial \varepsilon^2}\right|_{\varepsilon=\varepsilon_0}, \tag{3.20}$$

where $\mathcal{J}(\varepsilon)$ is the cost function given in (3.3) and $\hat{\varepsilon}$ is the CFO estimate that minimizes $\mathcal{J}(\varepsilon)$. As a result, the linear approximation of the CFO estimation error can be obtained as

$$\Delta\varepsilon = \frac{\left.\frac{\partial \mathcal{J}(\varepsilon)}{\partial \varepsilon}\right|_{\varepsilon=\varepsilon_0}}{\left.\frac{\partial^2 \mathcal{J}(\varepsilon)}{\partial \varepsilon^2}\right|_{\varepsilon=\varepsilon_0}}. \tag{3.21}$$

Evaluating the first derivative of $\mathcal{J}(\varepsilon)$ with respect to ε at $\varepsilon = \varepsilon_0$, we get

$$\begin{aligned} &\left.\frac{\partial \mathcal{J}(\varepsilon)}{\partial \varepsilon}\right|_{\varepsilon=\varepsilon_0} \\ = \quad & -2\Re\left\{\sum_{m=1}^{K}\sum_{i=1}^{d}\sum_{n=0,n\notin \mathbf{l}}^{N-1} h_n^m s_n^m (n_{l_i}^m)^* \frac{\pi}{N\sin\left[\frac{\pi}{N}(n-l_i^m)\right]} \exp\left[-j\pi\frac{n-l_i^m}{N}\right]\right\}, \end{aligned} \tag{3.22}$$

where $\Re(\bullet)$ denotes the real part of a complex number. Similarly, at high SNR, we can write

$$\begin{aligned} &\left.\frac{\partial \mathcal{J}^2(\varepsilon)}{\partial \varepsilon^2}\right|_{\varepsilon=\varepsilon_0} \\ \approx \quad & 2\sum_{m=1}^{K}\sum_{i=1}^{d}\sum_{k=0,k\notin \mathbf{l}^m}^{N-1}\sum_{n=0,n\notin \mathbf{l}^m}^{N-1} \frac{h_k^m (h_n^m)^* s_k^m (s_n^m)^* \pi^2 \exp\left(-j\pi\frac{k-n}{N}\right)}{N^2\sin\left(\frac{\pi}{N}(k-l_i^m)\right)\sin\left(\frac{\pi}{N}(n-l_i^m)\right)}. \end{aligned} \tag{3.23}$$

Details on the derivation of (3.22) and (3.23) are given in the Appendix. Substituting (3.22) and (3.23) into (3.21), we get in the high SNR region, the CFO estimation error $\Delta\varepsilon$ can be approximated as

$$\Delta\varepsilon = -\frac{\Re\left\{\sum_{m=1}^{K}\sum_{i=1}^{d}\sum_{n=0,n\notin\mathbf{l}}^{N-1} h_n^m s_n^m (n_{l_i}^m)^* \frac{\exp\left[-j\pi\frac{n-l_i^m}{N}\right]}{\sin\left[\frac{\pi}{N}(n-l_i^m)\right]}\right\}}{\sum_{m=1}^{K}\sum_{i=1}^{d}\sum_{k=0,k\notin\mathbf{l}^m}^{N-1}\sum_{n=0,n\notin\mathbf{l}^m}^{N-1} \frac{h_k^m(h_n^m)^* s_k^m (s_n^m)^* \pi \exp\left(-j\pi\frac{k-n}{N}\right)}{N\sin\left(\frac{\pi}{N}(k-l_i^m)\right)\sin\left(\frac{\pi}{N}(n-l_i^m)\right)}}. \tag{3.24}$$

Assuming the noise on different subcarriers to be independent and identically distributed (i.i.d.) with zero-mean and variance σ_n^2, we can show that $\mathrm{E}_n(\Delta\varepsilon) = 0$. Therefore, the linearized estimator is unbiased. This also means that the MSE of the CFO estimation is equal to the variance of $\Delta\varepsilon$. The squared error of the CFO estimator can be obtained from (3.21) as

$$\begin{aligned}(\Delta\varepsilon)^2 &= \frac{\mathrm{Num}}{\mathrm{Den}} \\ &= \frac{\left(\Re\left\{\sum_{m=1}^{K}\sum_{i=1}^{d}\sum_{n=0,n\notin\mathbf{l}}^{N-1} h_n^m s_n^m (n_{l_i}^m)^* \frac{\exp\left[-j\pi\frac{n-l_i^m}{N}\right]}{\sin\left[\frac{\pi}{N}(n-l_i^m)\right]}\right\}\right)^2}{\left(\sum_{m=1}^{K}\sum_{i=1}^{d}\sum_{k=0,k\notin\mathbf{l}^m}^{N-1}\sum_{n=0,n\notin\mathbf{l}^m}^{N-1} \frac{h_k^m(h_n^m)^* s_k^m (s_n^m)^* \pi \exp\left(-j\pi\frac{k-n}{N}\right)}{N\sin\left(\frac{\pi}{N}(k-l_i^m)\right)\sin\left(\frac{\pi}{N}(n-l_i^m)\right)}\right)^2}.\end{aligned} \tag{3.25}$$

As the noise is i.i.d., we can take the expectation of the numerator with respect to the noise and get

$$\mathrm{E}_n\left(\mathrm{Num}\right) = \frac{\sigma_n^2}{2}\sum_{m=1}^{K}\sum_{i=1}^{d}\sum_{k=0,k\notin\mathbf{l}^m}^{N-1}\sum_{n=0,n\notin\mathbf{l}^m}^{N-1} \frac{h_k^m(h_n^m)^* s_k^m (s_n^m)^* \exp\left[-j\pi\frac{k-n}{N}\right]}{\sin\left[\frac{\pi}{N}(k-l_i^m)\right]\sin\left[\frac{\pi}{N}(n-l_i^m)\right]}, \tag{3.26}$$

and hence

$$\mathrm{E}_n\left[(\Delta\varepsilon)^2\right] = \frac{N^2\sigma_n^2}{2\pi^2\sum_{m=1}^{K}\sum_{i=1}^{d}\sum_{k=0,k\notin\mathbf{l}^m}^{N-1}\sum_{n=0,n\notin\mathbf{l}^m}^{N-1}\frac{h_k^m(h_n^m)^* s_k^m(s_n^m)^*\exp\left[-j\pi\frac{k-n}{N}\right]}{\sin\left[\frac{\pi}{N}(k-l_i^m)\right]\sin\left[\frac{\pi}{N}(n-l_i^m)\right]}}. \tag{3.27}$$

Let us assume that the transmitted signal s_k^m is i.i.d. with zero-mean and unit-variance, i.e. $\mathrm{E}[s_k^m(s_n^m)^*] = \delta(k-n)$, where $\delta(\bullet)$ denotes the dirac delta function. Averaging $\mathrm{E}_n\left[(\Delta\varepsilon)^2\right]$ over transmitted signal leads us to

Lemma 1: In the high SNR region, the theoretical MSE of the CFO estimation for a realization of a multipath channel $\mathbf{h}$ for K OFDM symbols is

$$\mathrm{MSE}(\varepsilon|\mathbf{h}) = \mathrm{E}_{n,s}\left[(\Delta\varepsilon)^2|\mathbf{h}\right] = \frac{N^2\sigma_n^2}{2\pi^2\sum_{m=1}^{K}\sum_{i=1}^{d}\sum_{n=0,n\notin\mathbf{l}^m}^{N-1}|h_n^m|^2\frac{1}{\sin^2\left[\frac{\pi}{N}(n-l_i^m)\right]}}. \tag{3.28}$$

Now we average the theoretical MSE over different realizations of channel $\mathbf{h}$. Similar as before, we assume that channel response on each subcarrier is zero-mean with unit variance, i.e. $\mathrm{E}(h_n^m)$=0 and $\mathrm{E}(|h_n^m|^2)$=1 for $n = 0, 1, \cdots, N-1$ and $m = 1, \cdots, K$, we get the following result:

Lemma 2: In the high SNR region, the theoretical MSE of the CFO estimation is

$$\mathrm{MSE}(\varepsilon) = \mathrm{E}_{n,s,h}\left[(\Delta\varepsilon)^2\right] = \frac{N^2\sigma_n^2}{2\pi^2\sum_{m=1}^{K}\sum_{i=1}^{d}\sum_{n=0,n\notin\mathbf{l}^m}^{N-1}\frac{1}{\sin^2\left[\frac{\pi}{N}(n-l_i^m)\right]}}. \tag{3.29}$$

Now, let us look at the null subcarrier optimization problem again. The null subcarrier placement that minimizes the theoretical MSE can be formulated as

$$\mathbf{l} = \arg\min_{\mathbf{l}} (\text{MSE}) = \arg\max_{\mathbf{l}} \left(\sum_{m=1}^{K} \sum_{i=1}^{d} \sum_{n=0, n \notin \mathbf{l}^m}^{N-1} \frac{1}{\sin^2 \left[\frac{\pi}{N} (n - l_i^m) \right]} \right). \quad (3.30)$$

If $\sum_{i=1}^{d} \sum_{n=0, n \notin \mathbf{l}^m}^{N-1} \frac{1}{\sin^2 \left[\frac{\pi}{N} (n - l_i^m) \right]}$ is maximized for every value of m, i.e. for each OFDM symbol, then the cost function in (3.30) is maximized. Therefore, the optimization problem over K OFDM symbols is equivalent to the optimization in one OFDM symbol given by

$$\begin{aligned} \mathbf{l} &= \arg\min_{\mathbf{l}} (\text{MSE}) = \arg\max_{\mathbf{l}} \sum_{i=1}^{d} \left(\sum_{n=0, n \notin \mathbf{l}}^{N-1} \frac{1}{\sin^2 \left[\frac{\pi}{N} (n - l_i) \right]} \right) \\ &= \arg\max_{\mathbf{l}} \left(\sum_{i=1}^{d} \sum_{n=0, n \notin \mathbf{l}}^{N-1} g(n - l_i) \right), \end{aligned} \quad (3.31)$$

where $g(k) = \frac{1}{\sin^2 \left[\frac{\pi}{N} (n - l_i) \right]}$. It is straight-forward to show that $g(k)$ is also periodic with period of N. Using a similar approach as in Section 3.2, the cost function in (3.31) can be simplified to

$$\begin{aligned} \mathbf{l} &= \arg\max_{\mathbf{l}} \left\{ c_1 - \sum_{i=1}^{d} \sum_{n \in \mathbf{l}, n \neq l_i} g(n - l_i) \right\} \\ &= \arg\min_{\mathbf{l}} \left\{ \sum_{i=1}^{d} \sum_{j=1, j \neq i}^{d} g(l_i - l_j) \right\}. \end{aligned} \quad (3.32)$$

It can also be shown that $g(x)$ is a convex function of real number x for $1 < x < N - 1$. Therefore, the cost function in (3.32) is essentially of the same form as the cost function in (3.14) as $g(x)$ and $f(x)$ are both convex.

This means the optimal null subcarrier placement $\mathbf{l}$ that minimize both cost functions are the same. Thus we have proven

Proposition: The null subcarrier placement that maximizes the SNR of CFO estimation defined in (3.5) also minimizes the theoretical MSE of the CFO estimation given in (3.29).

3.4 Practical Considerations

For practical OFDM systems, it is usually necessary to place some null subcarriers consecutively at both ends of the spectrum as guard bands. We call these null subcarriers the guard null subcarriers. In this section, we show that given the fixed positions of the guard null subcarriers, if there are a few null subcarriers to place freely in the OFDM symbol for the purpose of CFO estimation, which we call free null subcarriers, how we should place them to maximize $\mathrm{SNR}_{\mathrm{CFO}}$.

Figure 1.12 illustrates an OFDM system having two guard bands with d_1 and d_2 null subcarriers respectively. Here, we have re-arranged the OFDM subcarrier index from $-N/2+1$ to $N/2$ such that the purpose of the guard bands is more obvious. However, such re-arrangement does not affect the formulation of the cost function due to the circular symmetry of the OFDM system. Suppose that we have d_n free null subcarriers that we can place freely between subcarrier $-N/2+d_1$ and $N/2-d_2+1$, the whole set of all the null subcarriers becomes

$$\mathbf{l} = [l_1, l_2, \cdots, l_{d_1}, l_{d_1+1}, \cdots, l_{d_1+d_n}, l_{d_1+d_n+1}, \cdots, l_d],$$

where $d = d_1 + d_2 + d_n$ is the total number of null subcarriers. Again we define $k_i = l_{i+1} - l_i$ as the spacing between null subcarrier l_{i+1} and null subcarrier l and $p_{i,m} = \sum_{j=0}^{m-1} k_{[(i+j-1) \bmod d]+1}$ as the spacing between the i^{th} null-subcarrier and its m^{th} neighbouring null subcarrier to the right in the cyclic sense. Notice that given the positions of the guard null subcarriers fixed at both ends of the spectrum, the positions of the free null subcarriers are uniquely determined by the following quantities:

- The spacing k_{d_1} between the left most free null subcarrier l_{d_1+1} and the right most guard null subcarrier in the left guard band l_{d_1},
- The spacing $k_{d_1+d_n}$ between the right most free null subcarrier $l_{d_1+d_n}$ and the left most guard null subcarrier in the right guard band $l_{d_1+d_n+1}$,
- The spacing $k_{d_1+1} \cdots k_{d_1+d_n-1}$ between the free null subcarriers.

Following a similar procedure as in Section 3.2, we obtain the cost function of null subcarrier placement for an OFDM system with guard band as

$$\begin{aligned} \mathcal{J}(k_{d_1}, k_{d_1+1}, \cdots, k_{d_1+d_n}) &= \sum_{i=1}^{d} \sum_{m=1}^{d-1} f(p_{i,m}) \\ \text{subject to:} \quad \sum_{i=1}^{d} k_i &= N. \end{aligned} \tag{3.33}$$

Comparing (3.33) with (3.16), we can see that the summation is still across all the d null subcarriers, including both the guard and free null subcarriers. However, for this problem, we cannot reach the same optimal solution as in Section 3.2 because that solution requires the k_i's to be equal for all $i = 1, 2, \cdots, d$, which means the null subcarriers should be placed evenly across the whole OFDM symbol. This is impossible for our problem as we do not have the freedom to place all the null subcarriers freely due to the fixed-positions of the guard null subcarriers. As a result, the closed-form optimal solution for (3.33) is difficult to find. However, in practice, the number of free null subcarriers d_n must be kept small to minimize the loss of in transmission data rate as they occupy the useful spectrum of the data subcarriers. Therefore, it is usually possible to resort to computer search to find the optimal placement of these subcarriers offline. Table 3.3 shows the optimal placement of d_n free null subcarriers with different d_n values for an IEEE 802.11a compliant system obtained by computer search. In such a system, there are total $N = 64$ subcarriers. Subcarriers $[-31 : -27, 27 : 32]$ are used as guard bands, i.e. $d_1 = 5$ and $d_2 = 6$. Here the θ value used is 0.5.

d_n	Free Null Subcarrier Index
2	[-7, 7]
3	[-12, 0, 12] [6]
4	[-15, -5, 5, 15]

Table 3.3: SNR-optimal free null subcarrier placement for IEEE 802.11a systems

In the case where the offline computer search is not feasible, for example, when the number of subcarriers is high or in MIMO-OFDM systems, we hereby propose a suboptimal solution for the null subcarrier placement. From (3.10), we

[6] In practise, the DC subcarrier is normally subject to large interference from DC offset and other RF impairments and therefore not reliable for CFO estimation. As a result, we could replace the 0 subcarrier with subcarrier 1 or -1 for practical implementations.

can see that $f(k)$ is proportional to the power of ICI on a particular subcarrier due to another subcarriers that is k away. The ICI power on a particular subcarrier due to another subcarrier decreases as the spacing between these two subcarriers increases. Therefore, $f(k)$ is monotonically decreasing as the magnitude of k increases. As a result, the ICI power on one particular null subcarrier l_i due to all the other null subcarriers $\sum_{m=1}^{d-1} f(p_{i,m})$ is dominated by the contribution from its two nearest neighbours. Therefore, we could make the following approximation

$$\sum_{m=1}^{d-1} f(p_{i,m}) \approx f(p_{i,1}) + f(p_{i,d-1}) = f(k_i) + f(k_{i-1}).$$

Therefore, the cost function in (3.33) can be approximated by

$$\begin{aligned}
\mathcal{J}(k_{d_1}, k_{d_1+1}, \cdots, k_{d_1+d_n}) &= \sum_{i=1}^{d} \sum_{m=1}^{d-1} f(p_{i,m}) \approx \sum_{i=1}^{d} (f(k_i) + f(k_{i-1})) \\
&= 2\sum_{i=1}^{d} f(k_i) = 2\left[(d_1 + d_2 - 1)f(1) + \sum_{i=d_1}^{d_1+d_n} f(k_i)\right],
\end{aligned} \tag{3.34}$$

because the spacing between the guard null subcarriers is 1. Substituting this into the optimization problem, we get the sub-optimal solution given by

$$[k_{d_1}, \cdots, k_{d_1+d_n}] = \arg\min \left[\sum_{i=d_1}^{d_1+d_n} f(k_i)\right]. \tag{3.35}$$

Due to the convexity of $f(k)$, we have

$$\sum_{i=d_1}^{d_1+d_n} f(k_i) \geq (d_n+1) f\left(\frac{\sum_{i=d_1}^{d_1+d_n}(k_i)}{d_n+1}\right) = (d_n+1) f\left(\frac{N-d_1-d_2+1}{d_n+1}\right) \tag{3.36}$$

where the equality holds when $k_i = \frac{N-d_1-d_2+1}{d_n+1}$ for $i = d_1, \cdots, d_1+d_n$. Therefore, our suboptimal solution shows that the free null subcarriers should be evenly distributed across the data subcarriers of the OFDM symbol. For an IEEE 802.11a system with 4 free null subcarriers, the sub-optimal solution leads to the placement of the null subcarriers at [-16 -5 5 16], which is very close to the optimal placement of [-15 -5 5 15] given by computer search. Later we will show using computer simulations that the performance difference between the sub-optimal and the optimal placement is marginal.

For indoor wireless communication systems with bursty transmission, such as wireless LAN systems, channel tracking within a packet is not so important due to the low mobility and the short packet duration, which is usually smaller than the coherence time of the channel. Therefore, the pilot subcarriers are mainly used for residual frequency offset estimation and correction. For these systems, it makes practical sense to replace these pilots by null subcarriers. Firstly the replacement of pilot subcarriers by null subcarriers does not reduce the transmission rate. Secondly, the residual frequency offset could be estimated from the null subcarriers using the method in [37], or the low complexity methods in [64] [79] [80]. Moreover, replacing pilots with null subcarriers provides savings in transmission power as the transmission power of null subcarriers is zero.

3.5 Simulation Results

Computer simulations were performed for an OFDM system with 64 subcarriers and length-16 cyclic prefix. According to the specifications given in IEEE 802.11a, there is a total of 11 null subcarriers placed consecutively from subcarriers 27 to 37 [17]. To achieve a fair comparison, we also use 11 null subcarriers in our simulations. We only use 1 OFDM symbol for CFO estimation, i.e. $K = 1$. We use channel model A of the HiperLan II channel models [75] in all the simulations. This is a multipath Rayleigh fading channel with exponential power delay profile and root mean square (RMS) delay spread equal to 50 ns. To assess the performance of the proposed null subcarrier placement, we define the estimation MSE as [68]

$$\text{MSE} = \frac{1}{N_s} \sum_{i=1}^{N_s} (\varepsilon_0 - \hat{\varepsilon})^2 \, , \tag{3.37}$$

where $\hat{\varepsilon}$ and ε_0 represent the estimated and the actual CFO's, respectively, and N_s denotes the total number of Monte Carlo trials.

A comparison between the MSE obtained through simulations and the theoretical MSE obtained from (3.29) is depicted in Figure 3.2. The SNR on the x-axis is the SNR of the received signal, not the CFO estimation SNR we are trying to optimize. The CFO value we use in the simulation is uniformly distributed between -0.5 and $+0.5$. We compare the theoretical MSE and the MSE obtained from simulations for both the consecutive null subcarriers placed from 27 to 37 according to IEEE 802.11a, and the proposed null subcarrier placement according to Table 3.2. From the comparison, we can see

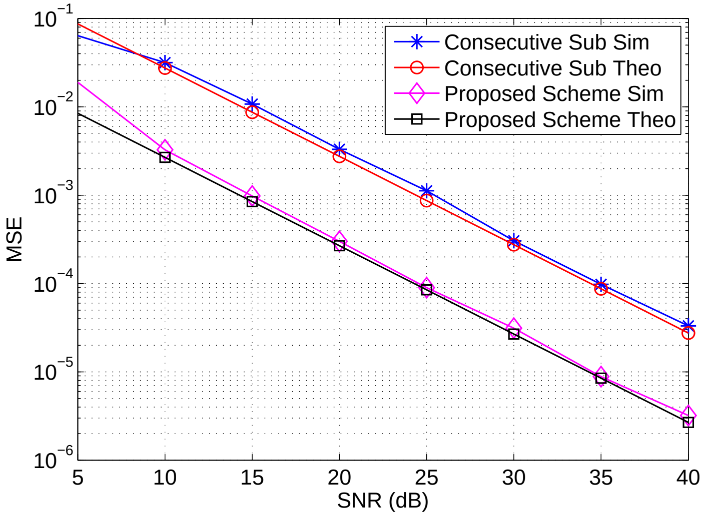

Fig. 3.2: Comparison between the theoretical MSE and the MSE obtained from simulations.

that the theoretical MSE approximates the actual MSE very closely for SNR larger than 10 dB.

Figure 3.3 shows the performance of the blind carrier offset estimation using the method in [37] with null subcarriers placed with different spacings. Without loss of generality, we always place the first null subcarrier at 0. By "n-sub spacing', we mean that the null subcarriers are placed n subcarriers apart like $[0, n, \cdots, (d-1)n]$. Just as above, the proposed scheme places the null subcarriers according to Table 3.2. We can see that with the proposed null subcarrier placement, the CFO estimation accuracy is improved significantly. The performance gain, compared to the consecutive null subcarrier placement, is as large as 10 dB. We can also see that the further apart the null-subcarriers are placed, the better the MSE performance. Although we can not prove the optimality of the null subcarrier placement obtained using the

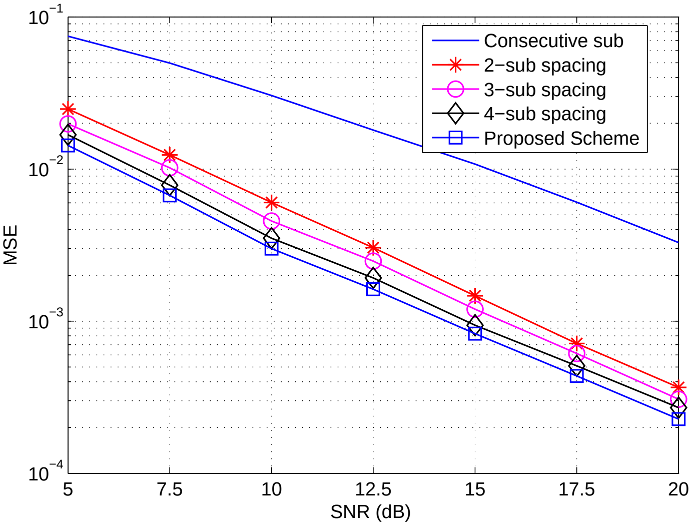

Fig. 3.3: MSE performance of the CFO estimation using different null subcarrier placements.

heuristic procedure in Table 3.1, from the results, we can see that it still leads to very good performance in CFO estimation. Figure 3.4 shows the symbol error rate (SER) performance of OFDM systems with CFO estimation using different null subcarrier placements. In this simulation, the CFO is estimated using the method in [37] and compensated. We use QPSK modulation and assume perfect channel estimation. A performance gain of about 3.5 dB can be achieved using the proposed placement compared to consecutively-placed null subcarriers.

Figure 3.5 shows the improvement in CFO estimation achieved by introducing a few optimally-placed free null subcarriers besides the guard null subcarriers. The system follows IEEE 802.11a specifications with 11 guard null subcarriers. The CFO value we used in the simulation is again uniformly distributed between -0.5 and $+0.5$. We can see by introducing 2 extra free null sub-

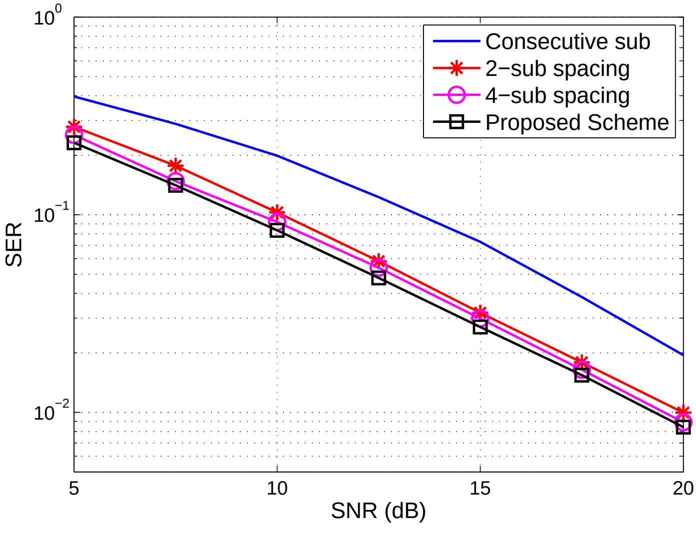

Fig. 3.4: SER performance with CFO estimation using different null subcarrier placements (QPSK modulation).

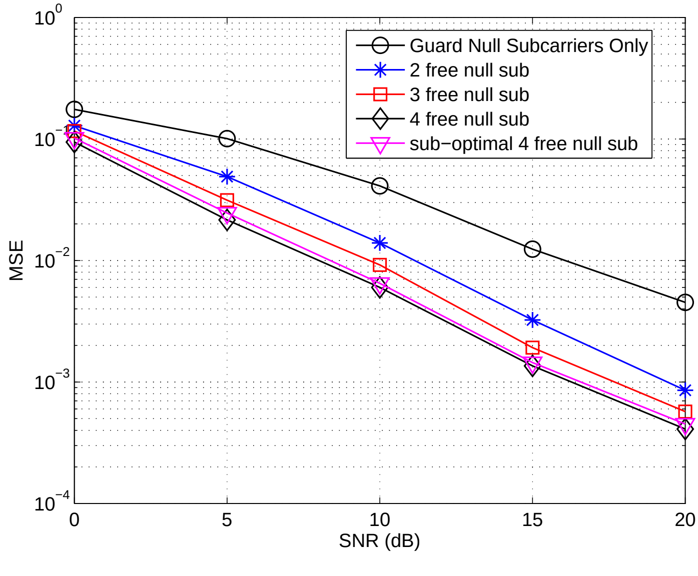

Fig. 3.5: MSE performance of the CFO estimation for OFDM systems with guard bands and different number of optimally-placed free null subcarriers.

carriers, the performance of the CFO estimation can be improved by 5 dB compared to using guard null subcarriers alone. The performance can be further improved by introducing more free null subcarriers. The gain, on the other hand, becomes smaller as the number of free null subcarriers increases. We also compared the performance of using 4 free null subcarriers with the optimal placement by computer search and the sub-optimal placement by using the approximated cost function. The results show that the performance difference between these two placement is rather marginal.

3.6 Conclusion

In this chapter, we formulated the optimization of null subcarrier placement for blind CFO estimation in an OFDM system using the $\mathrm{SNR}_{\mathrm{CFO}}$ maximization criterion. We showed that for small CFO values, this leads to a convex optimization problem, and that the optimal placement is achieved by placing the null subcarriers evenly across the OFDM symbol. We proved that this optimal null subcarrier placement also minimizes the theoretical MSE of the CFO estimation. For systems where the number of subcarriers is divisible by the number of null subcarriers, this optimal placement can be achieved. Otherwise, based on a heuristic procedure, we showed how to place the null subcarriers such that a good performance in CFO estimation can still be attained. We also studied the optimal free null subcarrier placement for practical OFDM systems with fixed guard bands. We demonstrated using computer simulations that the performance of CFO estimation is improved significantly by using the proposed null subcarrier placements.

Appendix: Derivation of Linear Approximation of CFO Estimation Errors

Proof of (3.22): Differentiating $\mathcal{J}(\varepsilon)$ with respect to ε, we can write

$$
\begin{aligned}
&\frac{\partial \mathcal{J}(\varepsilon)}{\partial \varepsilon} = \\
&\sum_{m=1}^{K}\sum_{i=1}^{d}\left(\sum_{\substack{k=0,\\ k\notin \mathbf{l}^m}}^{N-1}\sum_{\substack{n=0,\\ n\notin \mathbf{l}^m}}^{N-1} h_k^m (h_n^m)^* s_k^m (s_n^m)^* \frac{\partial C_{k-l_i}^m(\varepsilon_0-\varepsilon)}{\partial \varepsilon}\left(C_{n-l_i}^m(\varepsilon_0-\varepsilon)\right)^* + \right.\\
&\sum_{\substack{k=0,\\ k\notin \mathbf{l}^m}}^{N-1}\sum_{\substack{n=0,\\ n\notin \mathbf{l}^m}}^{N-1} h_k^m (h_n^m)^* s_k^m (s_n^m)^* C_{k-l_i}^m(\varepsilon_0-\varepsilon)\frac{\partial \left(C_{n-l_i}^m(\varepsilon_0-\varepsilon)\right)^*}{\partial \varepsilon} + \\
&\left.\sum_{\substack{k=0,\\ k\notin \mathbf{l}^m}}^{N-1} h_k^m s_k^m (n_{l_i}^m)^* \frac{\partial C_{k-l_i}^m(\varepsilon_0-\varepsilon)}{\partial \varepsilon} + \sum_{\substack{n=0,\\ n\notin \mathbf{l}^m}}^{N-1} (h_n^m)^* (s_n^m)^* n_{l_i}^m \frac{\partial \left(C_{n-l_i}^m(\varepsilon_0-\varepsilon)\right)^*}{\partial \varepsilon}\right),
\end{aligned}
\tag{3.38}
$$

where $C_k^m(\varepsilon)$ is given in (3.2) and

$$
\begin{aligned}
&\frac{\partial C_{n-l_i}^m(\varepsilon_0-\varepsilon)}{\partial \varepsilon} = \\
&-\left\{ j\pi\left(1-\frac{1}{N}\right)\frac{\sin\left(\pi(n-l_i+\varepsilon_0-\varepsilon)\right)}{N\sin\left(\frac{\pi}{N}(n-l_i+\varepsilon_0-\varepsilon)\right)}\exp\left(j\pi(n-l_i+\varepsilon_0-\varepsilon)\left(1-\frac{1}{N}\right)\right) + \right.\\
&\left[\frac{\pi\cos\left(\pi(n-l_i+\varepsilon_0-\varepsilon)\right)}{N\sin\left(\frac{\pi}{N}(n-l_i+\varepsilon_0-\varepsilon)\right)} - \frac{\pi\sin\left(\pi(n-l_i+\varepsilon_0-\varepsilon)\right)\cos\left(\frac{\pi}{N}(n-l_i+\varepsilon_0-\varepsilon)\right)}{N^2\sin^2\left(\frac{\pi}{N}(n-l_i+\varepsilon_0-\varepsilon)\right)}\right]\\
&\left.\exp\left(j\pi(n-l_i+\varepsilon_0-\varepsilon)\left(1-\frac{1}{N}\right)\right)\right\}\exp\left(j2\pi(\varepsilon_0-\varepsilon)(m-1)(1+N_g/N)\right) - \\
&\left(j2\pi(m-1)(1+N_g/N)\right)\frac{\sin\left[\pi(k+\varepsilon_0-\varepsilon)\right]}{N\sin\left[\frac{\pi}{N}(k+\varepsilon_0-\varepsilon)\right]}\exp\left(j\pi(k+\varepsilon_0-\varepsilon)(1-\frac{1}{N})\right)\\
&\exp\left(j2\pi(\varepsilon_0-\varepsilon)(m-1)(1+N_g/N)\right).
\end{aligned}
\tag{3.39}
$$

At $\varepsilon = \varepsilon_0$, we get

$$
\begin{aligned}
& \left.\frac{\partial \mathcal{J}(\varepsilon)}{\partial \varepsilon}\right|_{\varepsilon=\varepsilon_0} \\
= \quad & -\sum_{m=1}^{K} \sum_{i=1}^{d} \sum_{\substack{n=0, \\ n \notin \mathbf{l}}}^{N-1} h_n^m s_n^m (n_{l_i}^m)^* \frac{\pi}{N \sin\left[\frac{\pi}{N}(n - l_i^m)\right]} \exp\left[-j\pi \frac{n - l_i^m}{N}\right] - \\
& \sum_{m=1}^{K} \sum_{i=1}^{d} \sum_{\substack{n=0, \\ n \notin \mathbf{l}}}^{N-1} (h_n^m)^* (s_n^m)^* n_{l_i}^m \frac{\pi}{N \sin\left[\frac{\pi}{N}(n - l_i^m)\right]} \exp\left[j\pi \frac{n - l_i^m}{N}\right] \\
& = -2\Re\left\{ \sum_{m=1}^{K} \sum_{i=1}^{d} \sum_{\substack{n=0, \\ n \notin \mathbf{l}}}^{N-1} h_n^m s_n^m (n_{l_i}^m)^* \frac{\pi}{N \sin\left[\frac{\pi}{N}(n - l_i^m)\right]} \exp\left[-j\pi \frac{n - l_i^m}{N}\right] \right\},
\end{aligned}
$$

which gives us (3.22).

Proof of (3.23): Differentiating (3.38) one more time, we obtain

$$\begin{aligned}
&\frac{\partial^2 \mathcal{J}(\varepsilon)}{\partial \varepsilon^2} \\
= &\sum_{m=1}^{K}\sum_{i=1}^{d}\left(2\sum_{\substack{k=0,\\ k\notin \mathbf{l}^m}}^{N-1}\sum_{\substack{n=0,\\ n\notin \mathbf{l}^m}}^{N-1} h_k^m (h_n^m)^* s_k^m (s_n^m)^* \frac{\partial C_{k-l_i}^m(\varepsilon_0-\varepsilon)}{\partial \varepsilon}\frac{\partial \left(C_{n-l_i}^m(\varepsilon_0-\varepsilon)\right)^*}{\partial \varepsilon} + \right.\\
&\left.\sum_{\substack{k=0,\\ k\notin \mathbf{l}^m}}^{N-1} h_k^m s_k^m (n_{l_i}^m)^* \frac{\partial^2 C_{k-l_i}^m(\varepsilon_0-\varepsilon)}{\partial \varepsilon^2} + \sum_{\substack{n=0,\\ n\notin \mathbf{l}}}^{N-1} (h_n^m)^*(s_n^m)^* n_{l_i}^m \frac{\partial^2 \left(C_{n-l_i}^m(\varepsilon_0-\varepsilon)\right)^*}{\partial \varepsilon^2}\right).
\end{aligned} \tag{3.40}$$

Similarly to [66], we can assume high SNR. i.e. $|h_n s_n|^2 \gg |n_{l_i}|^2$. In this case, the second and third terms in (3.40) are much smaller than the first term and hence can be dropped in the approximation. Again at $\varepsilon = \varepsilon_0$, we get the following approximation

$$\begin{aligned}
&\left.\frac{\partial \mathcal{J}^2(\varepsilon)}{\partial \varepsilon^2}\right|_{\varepsilon=\varepsilon_0} \\
\approx\ & 2\sum_{m=1}^{K}\sum_{i=1}^{d}\sum_{\substack{k=0,\\ k\notin \mathbf{l}^m}}^{N-1}\sum_{\substack{n=0,\\ n\notin \mathbf{l}^m}}^{N-1} h_k^m (h_n^m)^* s_k^m (s_n^m)^* \frac{\partial C_{k-l_i}^m(\varepsilon_0-\varepsilon)}{\partial \varepsilon}\frac{\partial \left(C_{n-l_i}^m(\varepsilon_0-\varepsilon)\right)^*}{\partial \varepsilon} \\
=\ & 2\sum_{m=1}^{K}\sum_{i=1}^{d}\sum_{\substack{k=0,\\ k\notin \mathbf{l}^m}}^{N-1}\sum_{\substack{n=0,\\ n\notin \mathbf{l}^m}}^{N-1} h_k^m (h_n^m)^* s_k^m (s_n^m)^* \frac{\pi^2 \exp\left(-j\pi\frac{k-n}{N}\right)}{N^2 \sin\left(\frac{\pi}{N}(k-l_i^m)\right)\sin\left(\frac{\pi}{N}(n-l_i^m)\right)},
\end{aligned} \tag{3.41}$$

which leads to (3.23).

Chapter 4

CFO Estimation for MIMO-OFDM Systems

4.1 Introduction

Multiple-input multiple-output systems increase the capacity of rich scattering wireless fading channels enormously by using multiple antennas at both the transmitter and the receiver [24] [25] [81]. Most of the early studies on the capacity of MIMO systems were based on the assumption of flat-fading channels. For frequency-selective fading channels, combining MIMO with OFDM provides an effective solution. MIMO-OFDM transforms a frequency selective MIMO system to a number of flat fading MIMO systems on different subcarriers. Therefore, MIMO-OFDM has been adopted in various industrial standards for wireless communications, such as IEEE 802.11n high-throughput wireless LAN [5], IEEE 802.16 WiMAX [19] and 3GPP long term evolution (3GPP-LTE) [26].

Similar to single-input single-output (SISO) OFDM systems, carrier frequency offset (CFO) is still a major impairment for MIMO-OFDM systems. It destroys the orthogonality between different subcarriers and causes inter-carrier interference (ICI). ICI can cause severe degradation to the system performance if not properly compensated. Therefore, accurate estimation and compensation of CFO is essential for both SISO and MIMO OFDM systems. For single-user MIMO-OFDM systems, all the transmit antennas are driven by a centralized local oscillator (LO) and so are all the receive antennas. As a result, the CFO between the transmitter LO and the receiver LO is a single scalar parameter. Hence, the CFO estimation in this system is very similar to SISO-OFDM systems. Some CFO estimation algorithms for MIMO-OFDM systems are proposed in [34] [49] [50] [82].

Channel estimation for MIMO-OFDM systems is more complicated than for SISO-OFDM systems. For a MIMO-OFDM system with n_t transmit and n_r receive antennas, $n_r \times n_t$ channel responses must be estimated per subcarrier. To estimate the channel responses between a certain receive antenna and different transmit antennas using training sequences, the receiver must be able to distinguish between the training sequences from different transmit antennas. Therefore, for training-based channel estimation, some orthogonality among training sequences from different transmit antennas is required. In [52], a frequency-domain orthogonal training sequence design is proposed. The training sequences from different transmit antennas occupy different subcarriers. The length of the training sequence must be at least n_t OFDM symbols to get the channel estimate on all the subcarriers. Another approach uses orthogonal Walsh-Hadamard spreading codes to spread one training sequence to different OFDM symbols such that the training sequences from different transmit antennas are orthogonal in the code domain [5] [83]. This approach again requires a training sequence of at least n_t OFDM symbols. Both approaches require significantly larger overhead for channel estimation compared to SISO-OFDM systems. In [82], a time domain training sequence design is proposed for MIMO-OFDM systems. This time domain approach requires only training sequences of length $n_t \times L$, where L is the length of the channel impulse response and is much smaller than the OFDM symbol length. However, the proposed training sequences are impulses in time and hence have very high peak to average power ratio (PAPR).

In this chapter, we propose to use constant amplitude zero autocorrelation (CAZAC) sequences, which have constant amplitude elements and zero autocorrelation for any nonzero circular shifts, for joint CFO and channel estimation for MIMO-OFDM systems. We first formulate the Maximum-Likelihood (ML) CFO and channel estimator. Similar to [49] [50], we show that ML CFO estimate can be obtained with low computational complexity by transmitting two periods of the same training sequence. After compensating the estimated CFO, the channel estimation can be performed in the time domain. The advantages of the proposed training sequences are:

- One training sequence for both CFO and channel estimation.

- No calculation of matrix inversion is required to obtain channel estimates.
- Significantly reduced training overhead. The minimum length required for channel estimation is only $n_t \times L$.
- The PAPR of the training sequence in time domain is 1.

The residual CFO after CFO compensation degrades the performance of the channel estimation. In this chapter, we also derive an approximation on the mean square error (MSE) of channel estimation in the presence of the residual CFO. We show from computer simulations that this approximation is accurate. From the approximation, we can see that the degradation caused by the residual CFO in the channel estimation is negligible.

In the study of MIMO and MIMO-OFDM systems, a common assumption used in the literature is that the channel responses between different transmit and receive antennas are statistically independent. In practice, due to the close proximity among the antennas, the channel responses are spatially correlated [53] [55] [84]. The spatial correlation is related to the propagation environment. It is a function of the distributions of angle of arrival (AOA) at the receive antennas and the angle of departure (AOD) at the transmit antennas. Besides this spatial correlation, the electromagnetic (EM) fields at closely-placed antennas also interact with each other and cause mutual coupling among the antennas [56] [57]. This coupling changes the spatial correlation and also the power of the transmitted/received signals at the antennas. In this chapter, we present a study on the effects of spatial correlation and mutual coupling and in particular, their impacts on the performance of the CFO estimation. The simulation results show that spatial correlation degrades the performance of the CFO estimation. Mutual coupling has two effects. Firstly it reduces the spatial correlation, which is beneficial. On the other hand, it also reduces the power of the desired signal, which is detrimental. Simulations results show that the combined effects of mutual coupling introduces additional degradation on CFO estimation.

The rest of this chapter is organized as follows. In Section 4.2, we develop the system model for the MIMO-OFDM system and derive the ML CFO and channel estimators. We then propose the CAZAC training sequence and derive the simplified ML CFO and channel estimators in Section 4.3. We also show that using the proposed training sequence, the training overhead can be significantly reduced compared to conventional frequency-domain training. In Section 4.4 we analyze the MSE of the channel estimation in the presence of the residual CFO. An accurate closed-form approximation on the MSE is derived. Simulation results on the performance of the joint CFO and channel estimator are presented in Section 4.5. In Section 4.6, we study the effect of spatial correlations and its impact on the performance of CFO estimation. The effect of mutual coupling is studied in Section 4.7. The concluding remarks are given in Section 4.8.

4.2 System Model

In a single-user MIMO-OFDM system, the CFO can be quantified by a single parameter ϕ. We assume perfect timing synchronization has been achieved.

In this case, the received signal at the i^{th} receive antenna can be written as

$$r_i(k) = e^{j\phi k}\frac{1}{\sqrt{n_t}}\sum_{m=1}^{n_t}\sum_{d=0}^{L-1} h_{i,m}(d)s_m(k-d) + n_i(k), \tag{4.1}$$

where k is the time index, n_t is the number of transmit antennas, L is the length of the impulse response of the multi-path channel, $h_{i,m}(d)$ is the d^{th} tap of the channel impulse response between the i^{th} receive antenna and the m^{th} transmit antenna, s_m is the transmitted signal from the m^{th} transmit antenna and $n_i(k)$ is the AWGN noise. Here we assume that the power of s_m for all m is 1, and $1/\sqrt{n_t}$ is used to normalize the total transmission power from all antennas to 1. We consider a training sequence of length N and cyclic prefix (CP) of length L. After removing the cyclic prefix, we can write the received signal at the i^{th} receive antenna in an equivalent matrix form as

$$\mathbf{r}_i = \frac{1}{\sqrt{n_t}}\sum_{m=1}^{n_t} \mathbf{E}(\phi)\mathbf{S}_m\mathbf{h}_{i,m} + \mathbf{n}_i \tag{4.2}$$

where $\mathbf{E}(\phi)$ is the CFO matrix, which is a diagonal matrix with diagonal elements equal to $[1, \exp(j\phi), \cdots, \exp(j(N-1)\phi)]$. We use $\mathbf{S}_m$ to denote the transmitted signal matrix from the m^{th} transmit antenna. This is a circulant matrix with the first column defined by $[s_m(0), s_m(1), \cdots, s_m(N-1)]^T$, where we use superscript T to denote vector/matrix transpose. Here we assume $N > L$, so the channel vector between the m^{th} transmit antenna and the i^{th} receive antenna $\mathbf{h}_{i,m}$ is a $N \times 1$ vector obtained by appending the $L \times 1$ channel impulse response $[h_{i,m}(0), \cdots, h_{i,m}(L-1)]^T$ vector with $N-L$ zeros, i.e. $\mathbf{h}_{i,m} = [h_{i,m}(0), \cdots, h_{i,m}(L-1), 0, \cdots, 0]^T$. The AWGN noise at the i^{th}

receive antenna is denoted as $\mathbf{n}_i$.

Gathering the received signal from all the receive antennas, we get

$$\boldsymbol{\mathcal{R}} = \mathbf{E}(\phi)\boldsymbol{\mathcal{S}}\boldsymbol{\mathcal{H}} + \boldsymbol{\mathcal{N}}, \tag{4.3}$$

where

$$\boldsymbol{\mathcal{R}} = [\mathbf{r}_1 \cdots, \mathbf{r}_{n_r}]_{\{N \times n_r\}},$$

$$\boldsymbol{\mathcal{S}} = \frac{1}{\sqrt{n_t}} [\mathbf{S}_1, \cdots, \mathbf{S}_{n_t}]_{\{N \times (N \times n_t)\}}$$

$$\boldsymbol{\mathcal{H}} = \begin{bmatrix} \boldsymbol{\mathcal{H}}_1 \\ \vdots \\ \boldsymbol{\mathcal{H}}_{n_t} \end{bmatrix}_{\{(N \times n_t) \times n_r\}},$$

with $\boldsymbol{\mathcal{H}}_i = [\mathbf{h}_{1,i}, \cdots, \mathbf{h}_{n_r,i}]_{\{N \times n_r\}}$. For ease of understanding, we use a subscript inside curved brackets to denote dimensions of matrices. The noise matrix is given by $\boldsymbol{\mathcal{N}} = [\mathbf{n}_1, \cdots, \mathbf{n}_{n_r}]$.

Because the noise is Gaussian and uncorrelated, the likelihood function for the CFO ϕ and the channel matrix $\boldsymbol{\mathcal{H}}$ can be written as

$$\Lambda(\tilde{\phi}, \tilde{\boldsymbol{\mathcal{H}}}) = \frac{1}{(\pi\sigma_n^2)^{N \times n_r}} \exp\left\{ -\frac{1}{\sigma_n^2} \left\| \boldsymbol{\mathcal{R}} - \mathbf{E}(\tilde{\phi})\boldsymbol{\mathcal{S}}\tilde{\boldsymbol{\mathcal{H}}} \right\|^2 \right\}, \tag{4.4}$$

where $\tilde{\phi}$ and $\tilde{\boldsymbol{\mathcal{H}}}$ are trial values for ϕ and $\boldsymbol{\mathcal{H}}$ and σ_n^2 is the variance of the receiver AWGN noise. The maximum-likelihood estimates for CFO and channel can be obtained by finding the $\tilde{\phi}$ and $\tilde{\boldsymbol{\mathcal{H}}}$ that maximize (4.4).

4.3 CAZAC Sequences for Joint CFO and Channel Estimation

We propose to use constant amplitude zero autocorrelation (CAZAC) sequences for joint CFO and channel estimation in MIMO-OFDM systems. Each element of a CAZAC sequence has a amplitude equal to one, i.e. constant amplitude. The autocorrelation of a length-N CAZAC sequence $\mathbf{s}_1$ satisfies

$$R(k) = \sum_{n=0}^{N-1} s_1(n) s_1^*(n \ominus k) = \begin{cases} N & k = 0; \\ 0 & k \neq 0. \end{cases} \tag{4.5}$$

where $\ominus$ denotes circular subtraction and superscript * denotes complex conjugation. This means that the CAZAC sequence is orthogonal to all non-zero circular shifts. Let $\mathbf{S}_1$ be a circulant matrix with the first column equal to $[s_1(0), s_1(1), \cdots, s_1(N-1)]^T$. The autocorrelation property of the CAZAC sequence can be written in an equivalent matrix form as

$$\mathbf{S}_1^H \mathbf{S}_1 = N\mathbf{I}, \tag{4.6}$$

where superscript H denotes conjugate transpose. This means that $\mathbf{S}_1$ is both a unitary (subject to a normalization constant N) and a circulant matrix. Commonly used CAZAC sequences include the Frank-Zadoff sequences [85], the Chu sequences [86] and the S&H sequences [87].

We use $\mathbf{s}_1$ as the training sequence from the first transmit antenna. The training sequence from the m^{th} transmit antenna is a circularly shifted version of $\mathbf{s}_1$, i.e. $s_m(n) = [s_1(n \ominus \tau_m)]^T$, where τ_m is the shift value. It is straightforward to show that the cross-correlation between the training sequences from different transmit antennas satisfies

$$\mathbf{S}_i^H \mathbf{S}_j = \mathfrak{I}^{\tau_j - \tau_i} \tag{4.7}$$

where $\mathfrak{I}^{\tau_j - \tau_i}$ denotes a matrix resulting from circularly shifting the one elements of the identify matrix to the right by $\tau_j - \tau_i$. Note that the matrix $\mathbf{S}_m$ can be obtained by circularly shifting the rows of $\mathbf{S}_1$ τ_m rows downwards. Hence, we have

$$\mathbf{S}_m \mathbf{h}_{i,m} = \mathbf{S}_1 \mathbf{h}_{i,m}^{\tau_m}, \tag{4.8}$$

where $\mathbf{h}_{i,m}^{\tau_m} = [h_{i,m}(N-\tau_m), \cdots, h_{i,m}(0), \cdots h_{i,m}(N-\tau_m-1)]^T$ is obtained by circularly shifting $\mathbf{h}_{i,m}$ τ_m rows downwards. Making use of this property, we can rewrite the received signal at receive antenna i as

$$\mathbf{r}_i = \frac{1}{\sqrt{n_t}} \mathbf{E}(\phi) \sum_{m=1}^{n_t} \mathbf{S}_m \mathbf{h}_{i,m} = \frac{1}{\sqrt{n_t}} \mathbf{E}(\phi) \mathbf{S}_1 \sum_{m=1}^{n_t} \mathbf{h}_{i,m}^{\tau_m}. \tag{4.9}$$

Collecting the received signals from all receive antennas, we get

$$\boldsymbol{\mathcal{R}} = \frac{1}{\sqrt{n_t}} \mathbf{E}(\phi) \mathbf{S}_1 \mathcal{H} + \boldsymbol{\mathcal{N}}, \tag{4.10}$$

where

$$\mathcal{H} = \left[\sum_{m=1}^{n_t} \mathbf{h}_{1,m}^{\tau_m}, \sum_{m=1}^{n_t} \mathbf{h}_{2,m}^{\tau_m}, \cdots, \sum_{m=1}^{n_t} \mathbf{h}_{n_r,m}^{\tau_m} \right]_{\{N \times n_r\}}.$$

From (4.10), we can see that by using CAZAC training sequence, the channel impulse responses are contained in a smaller matrix $\mathcal{H}$ of size $N \times n_r$ as compare to the $(N \times n_t) \times n_r$ channel matrix $\boldsymbol{\mathcal{H}}$ in the more general received signal model in (4.3).

Without loss of generality, let us examine the first column of the $\mathcal{H}$ matrix, $\sum_{m=1}^{n_t} \mathbf{h}_{1,m}^{\tau_m}$. We know that only the first L elements in the $N \times 1$ vector $\mathbf{h}_{1,m}$ are nonzero. We choose the length of the CAZAC sequence N such that $N \geq n_t \times L$ and we can make $\tau_m - \tau_{m-1} \geq L$ for $m = 2, \cdots, n_t$. In this case, there will be no overlap between the non-zero channel impulse responses from different transmit antennas. As a result, after obtaining the estimate of the first column of $\mathcal{H}$, i.e. $\sum_{m=1}^{n_t} \mathbf{h}_{1,m}^{\tau_m}$, we can obtain the channel impulse responses from different transmit antennas by taking appropriate elements of the column. The same principle applies to the other columns of $\mathcal{H}$. In this case, the estimation of the channel impulse responses between all the transmit and receive antenna pairs is converted equivalently to the estimation of matrix $\mathcal{H}$.

In [38] and [39], CFO estimation methods using periodic training sequences were proposed. Here, we adopt a similar approach. We successively transmit two periods of training sequences in time, i.e. the training sequence from the i^{th} transmit antenna, $\mathbf{x}_i = [\mathbf{s}_i^T, \mathbf{s}_i^T]^T$, is of length $2N$. Assuming the channel does not change within the duration of $2N$, the received signal can be written as:

$$\boldsymbol{\mathcal{R}}_{\{2N \times n_r\}} = \mathbf{E}(\phi)_{\{2N \times 2N\}} \mathbf{X}_{\{2N \times N\}} \mathcal{H}_{\{N \times n_r\}} + \boldsymbol{\mathcal{N}}_{\{2N \times n_r\}}, \tag{4.11}$$

where

$$\mathbf{X} = \frac{1}{\sqrt{n_t}} \begin{bmatrix} \mathbf{S}_1 \\ \mathbf{S}_1 \end{bmatrix}.$$

Using the received signal model given in (4.11), the likelihood function of the CFO ϕ and the channel response $\mathcal{H}$ can be written as

$$\begin{aligned} \Lambda(\tilde{\phi}, \tilde{\mathcal{H}}) \quad = \quad & \frac{1}{(\pi\sigma_n^2)^{2N \times n_r}} \exp\left\{ -\frac{1}{\sigma_n^2} \mathbf{tr}\Big\{ [\boldsymbol{\mathcal{R}} - \mathbf{E}(\tilde{\phi})\mathbf{X}\tilde{\mathcal{H}}]^H \right. \\ & \left. [\boldsymbol{\mathcal{R}} - \mathbf{E}(\tilde{\phi})\mathbf{X}\tilde{\mathcal{H}}] \Big\} \right\} \end{aligned} \tag{4.12}$$

where $\mathbf{tr}$ denotes the trace of a matrix.

Following a similar approach as in [45], we find that by keeping $\tilde{\phi}$ fixed, the ML estimate of the channel $\mathcal{H}$ is given by

$$\hat{\mathcal{H}}(\tilde{\phi}) = \left(\mathbf{X}^H \mathbf{X}\right)^{-1} \mathbf{X}^H \mathbf{E}^H(\tilde{\phi}) \boldsymbol{\mathcal{R}}. \tag{4.13}$$

Substituting (4.13) into (4.12), and after some algebraic manipulations we get the ML estimator of the CFO ϕ is given by

$$\hat{\phi} = \arg\max_{\tilde{\phi}} \left\{ \mathbf{tr}\left\{ \boldsymbol{\mathcal{R}}^H \mathbf{E}(\tilde{\phi}) \mathbf{B} \mathbf{E}^H(\tilde{\phi}) \boldsymbol{\mathcal{R}} \right\} \right\}, \tag{4.14}$$

where

$$\begin{aligned}\mathbf{B} &= \mathbf{X}\left(\mathbf{X}^H\mathbf{X}\right)^{-1}\mathbf{X}^H = \frac{1}{2N}\begin{bmatrix}\mathbf{S}_1\\ \mathbf{S}_1\end{bmatrix}\mathbf{I}_{\{N\times N\}}\left[\mathbf{S}_1^H, \mathbf{S}_1^H\right]\\ &= \frac{1}{2}\begin{bmatrix}\mathbf{I}_{\{N\times N\}} & \mathbf{I}_{\{N\times N\}}\\ \mathbf{I}_{\{N\times N\}} & \mathbf{I}_{\{N\times N\}}\end{bmatrix}. \end{aligned} \tag{4.15}$$

We can also rewrite $\mathbf{E}(\phi)$ and $\mathcal{R}$ in the following form

$$\mathbf{E}(\phi) = \begin{bmatrix}\mathbf{E}_1(\phi) & \mathbf{0}\\ \mathbf{0} & e^{jN\phi}\mathbf{E}_1(\phi)\end{bmatrix},$$

where $\mathbf{E}_1(\phi) = \mathrm{diag}[1, e^{j\phi}, \cdots, e^{j(N-1)\phi}]$ and

$$\boldsymbol{\mathcal{R}} = \begin{bmatrix}\boldsymbol{\mathcal{R}}_1\\ \boldsymbol{\mathcal{R}}_2\end{bmatrix},$$

where $\boldsymbol{\mathcal{R}}_1$ denotes the first N rows of $\boldsymbol{\mathcal{R}}$ and $\boldsymbol{\mathcal{R}}_2$ denotes rows $N+1$ to $2N$ of $\boldsymbol{\mathcal{R}}$. Substituting these new expressions into (4.14), we can further simplify the cost function for CFO estimation to

$$\mathcal{J}(\tilde{\phi}) = \Re\left\{e^{jN\tilde{\phi}}\mathbf{tr}(\boldsymbol{\mathcal{R}}_2^H\boldsymbol{\mathcal{R}}_1)\right\}, \tag{4.16}$$

where $\Re(\bullet)$ denotes the real part of a complex number. Correspondingly, the

ML estimate of ϕ is given by

$$\hat{\phi} = \arg\max_{\tilde{\phi}} \Re\left\{e^{jN\tilde{\phi}}\mathbf{tr}(\boldsymbol{\mathcal{R}}_2^H \boldsymbol{\mathcal{R}}_1)\right\}. \tag{4.17}$$

Using scalar notations, the ML CFO estimator in (4.17) can be written equivalently as

$$\hat{\phi} = \frac{1}{N}\angle\left\{\sum_{k=1}^{N}\sum_{m=1}^{n_r} r_m^*(k) r_m(k+N)\right\}, \tag{4.18}$$

where $\angle(\bullet)$ denotes the angle of a complex number and $r_m(k)$ denotes the received signal from the m^{th} receive antenna at time k. This ML estimate is very similar in form to its SISO counterpart as shown in [39] [45] and it can be easily obtained using low-complexity correlation operations.

The performance of the ML CFO estimator for SISO-OFDM systems has been extensively studied in the literature [38], [39], [45]. Following a similar approach as in SISO-OFDM systems, we can show that the Cramer-Rao Bound (CRB) of the CFO estimation is given by [50]

$$E[(\hat{\phi} - \phi)^2] \geq \text{CRB} = \frac{1}{n_r N^3 \gamma}, \tag{4.19}$$

where γ is the SNR per receive antenna. Notice that the CRB decays with N^3 and hence in practice, only small values of N are needed.

Having obtained the CFO estimate $\hat{\phi}$, we can simply plug it into (4.13) to get the channel estimate as follows

$$
\begin{aligned}
\hat{\mathcal{H}} &= \left(\mathbf{X}^H\mathbf{X}\right)^{-1}\mathbf{X}^H\mathbf{E}^H(\hat{\phi})\boldsymbol{\mathcal{R}} = \frac{n_t}{2N}\mathbf{X}^H\mathbf{E}^H(\hat{\phi})\boldsymbol{\mathcal{R}} \\
&= \frac{\sqrt{n_t}}{2N}\left[\mathbf{S}_1^H, \mathbf{S}_1^H\right]\begin{bmatrix} \mathbf{E}_1^H(\hat{\phi}) & \mathbf{0} \\ \mathbf{0} & e^{-jN\hat{\phi}}\mathbf{E}_1^H(\hat{\phi}) \end{bmatrix}\begin{bmatrix} \boldsymbol{\mathcal{R}}_1 \\ \boldsymbol{\mathcal{R}}_2 \end{bmatrix} \\
&= \frac{\sqrt{n_t}}{2N}\left(\mathbf{S}_1^H\mathbf{E}_1^H(\hat{\phi})\boldsymbol{\mathcal{R}}_1 + e^{-jN\hat{\phi}}\mathbf{S}_1^H\mathbf{E}_1^H(\hat{\phi})\boldsymbol{\mathcal{R}}_2\right).
\end{aligned} \tag{4.20}
$$

From (4.20), we can see that the channel estimate can be obtained using simple matrix multiplications. Due to the orthogonal property of the $\mathbf{S}_1$ matrix, a complicated matrix inversion can be avoided. This provides a large saving in the computational complexity of channel estimation. Another advantage of this training sequence is the low overhead. For channel estimation alone, we only need training sequences of length N where $N \geq n_t \times L$. By comparison, the conventional frequency-domain channel estimation requires training sequence of length at least $n_t \times M$, where M is the length of the OFDM symbol. In a practical OFDM system, the length L of the channel impulse response is similar to the length of the cyclic prefix, which is much smaller than the length of the OFDM symbol M. Therefore, by using the proposed training sequence for channel estimation, we can reduce the training overhead by a factor of $(M/L - 1)$. Moreover, the training signal is constant-amplitude in time and therefore has peak to average power ratio (PAPR) equal to 1.

Notice that the constant amplitude property of CAZAC training sequences guarantees a PAPR equal to 1. This means that training sequence will not suffer from nonlinear distortions from the transmitter power amplifier. The ZAC property guarantees orthogonality between the estimated channel impulse responses from different transmit antennas. In this sense, all CAZAC sequences can be used for low-complexity joint CFO and channel estimation in MIMO-OFDM systems and are considered in this Chapter. However, there are still some practical considerations. For example, for sequence length $N = 16$, all elements of the Frank-Zadoff sequences are BPSK symbols while for $N = 64$, all elements are BPSK and QPSK symbols. This is simple to implement in practice. The disadvantage is that the Frank-Zadoff sequences exist only for sequence length $N = K^2$ where K is any positive integer greater than 1. In comparison, the Chu sequences exist for any sequence length N, however, the elements of Chu sequences have more possible phase angles, which requires more bits in binary representation.

4.4 MSE Analysis of Channel Estimation with Residual CFO

In practical systems, there exists some residual CFO after CFO compensation due to the inaccuracy of the CFO estimation. In this section, we examine how the residual CFO affects the performance of the channel estimation.

Substituting the expression for $\boldsymbol{\mathcal{R}}_1$ and $\boldsymbol{\mathcal{R}}_2$ into (4.20) and denoting the residual CFO $(\phi - \hat{\phi})$ by ϕ_d, we get

$$\begin{aligned}\hat{\mathcal{H}} &= \frac{1}{2N}\Big(\mathbf{S}_1^H\mathbf{E}_1(\phi_d)\mathbf{S}_1\mathcal{H} + \sqrt{n_t}\mathbf{S}_1^H\mathbf{E}_1^H(\hat{\phi})\boldsymbol{\mathcal{N}}_1 \\ &+ e^{jN\phi_d}\mathbf{S}_1^H\mathbf{E}_1(\phi_d)\mathbf{S}_1\mathcal{H} + e^{-jN\hat{\phi}}\sqrt{n_t}\mathbf{S}_1^H\mathbf{E}_1^H(\hat{\phi})\boldsymbol{\mathcal{N}}_2\Big),\end{aligned} \tag{4.21}$$

where $\boldsymbol{\mathcal{N}}_1$ contains the first N rows of $\boldsymbol{\mathcal{N}}$ in (4.11) and $\boldsymbol{\mathcal{N}}_2$ contains rows $N+1$ to $2N$ of $\boldsymbol{\mathcal{N}}$. As $\mathbf{E}_1^H(\hat{\phi})$ is a unitary matrix, $\mathbf{E}_1^H(\hat{\phi})\boldsymbol{\mathcal{N}}_1$ is statistically the same as $\boldsymbol{\mathcal{N}}_1$. Similarly $e^{-jN\hat{\phi}}\mathbf{E}_1^H(\hat{\phi})\boldsymbol{\mathcal{N}}_2$ is statistically the same as $\boldsymbol{\mathcal{N}}_2$. Therefore, for ease of notation, we still use $\boldsymbol{\mathcal{N}}_1$ and $\boldsymbol{\mathcal{N}}_2$ to denote the new noise. With this simplification of notation, the channel estimate can be rewritten as

$$\hat{\mathcal{H}} = \frac{1}{2N}\left(1 + e^{jN\phi_d}\right)\mathbf{S}_1^H\mathbf{E}_1(\phi_d)\mathbf{S}_1\mathcal{H} + \frac{\sqrt{n_t}}{2N}(\mathbf{S}_1^H\boldsymbol{\mathcal{N}}_1 + \mathbf{S}_1^H\boldsymbol{\mathcal{N}}_2). \tag{4.22}$$

The MSE of the channel estimation is given by

$$\text{MSE} = \frac{1}{Nn_r}\mathbf{tr}\left\{\text{E}\left[(\mathcal{H} - \hat{\mathcal{H}})^H(\mathcal{H} - \hat{\mathcal{H}})\right]\right\}, \tag{4.23}$$

where E[$\bullet$] denotes statistical expectation over the AWGN noise.

When the CFO estimation is perfect, i.e. $\phi_d = 0$, it can be easily shown that

$$\begin{aligned}\text{MSE} &= \frac{n_t}{4N^2}\frac{1}{Nn_r}\mathbf{tr}\left\{\text{E}\left[\boldsymbol{\mathcal{N}}_1^H\mathbf{S}_1\mathbf{S}_1^H\boldsymbol{\mathcal{N}}_1\right] + \text{E}\left[\boldsymbol{\mathcal{N}}_2^H\mathbf{S}_1\mathbf{S}_1^H\boldsymbol{\mathcal{N}}_2\right]\right\} \\ &= \frac{n_t\sigma_n^2}{2N}.\end{aligned} \tag{4.24}$$

Making use of the Taylor's series expansion, we can write the exponential function as $e^{\phi} = 1 + \sum_{k=1}^{\infty} \frac{\phi^k}{k!}$. Substituting this into (4.22), we get

$$\hat{\mathcal{H}} = \frac{1+\delta}{N}\mathbf{S}_1^H(\mathbf{I} + \Delta(\phi_d))\mathbf{S}_1\mathcal{H} + \frac{\boldsymbol{\mathcal{N}}'}{N}, \tag{4.25}$$

where $\delta = 1/2\sum_{k=1}^{\infty} \frac{(jN\phi_d)^k}{k!}$ and $\boldsymbol{\Delta}(\phi_d)$ is a diagonal matrix with the n^{th} element equal to $\sum_{k=1}^{\infty} \frac{(j(n-1)\phi_d)^k}{k!}$. Here we use one AWGN noise matrix $\boldsymbol{\mathcal{N}}'$ to denote $\frac{\sqrt{n_t}}{2}(\mathbf{S}_1^H\boldsymbol{\mathcal{N}}_1 + \mathbf{S}_1^H\boldsymbol{\mathcal{N}}_2)$. Note that the variance of each element of $\boldsymbol{\mathcal{N}}'$ is $\frac{Nn_t}{2}\sigma_n^2$. Using this new expression, we can write the difference between the channel estimate and the actual channel as

$$\hat{\mathcal{H}} - \mathcal{H} = \frac{\boldsymbol{\mathcal{N}}'}{N} + \mathcal{H}\delta + \frac{1+\delta}{N}\mathbf{S}_1^H\boldsymbol{\Delta}(\phi_d)\mathbf{S}_1\mathcal{H}. \tag{4.26}$$

Here the first term $\frac{\mathcal{N}'}{N}$ is the estimation error caused by the AWGN noise while the last two terms in the summation describe the extra estimation error caused by the residual CFO error ϕ_d.

Using (4.26), we can show that the MSE of the channel estimation is given by

$$\begin{aligned} \text{MSE} &= \frac{1}{N^3 n_r}\Big\{N^2|\delta|^2\mathbf{tr}\left\{\boldsymbol{\Psi}_{\mathcal{H}}\right\} + 2N\Re\left[(\delta^* + |\delta|^2)\mathbf{tr}\left[\boldsymbol{\Delta}(\phi_d)\mathbf{S}_1\boldsymbol{\Psi}_{\mathcal{H}}\mathbf{S}_1^H\right]\right] \\ &+ |1+\delta|^2\mathbf{tr}\left[\boldsymbol{\Delta}(\phi_d)^H\boldsymbol{\Delta}(\phi_d)\mathbf{S}_1\boldsymbol{\Psi}_{\mathcal{H}}\mathbf{S}_1^H\right]\Big\} + \frac{n_t\sigma_n^2}{2N}. \end{aligned} \tag{4.27}$$

where $\boldsymbol{\Psi}_{\mathcal{H}} = \mathrm{E}(\mathcal{H}\mathcal{H}^H)$. The details of the derivation is given in the appendix of this chapter. Now let us assume that the channels between different transmit and receive antennas are uncorrelated in space and the different paths in the multi-path channel are also uncorrelated. We define $\mathbf{p}_{i,m} = [p_{i,m}(1), \cdots, p_{i,m}(N)]^T$ as the power delay profile of the channel between the m^{th} transmit antenna and the i^{th} receive antenna. Since the length of the channel impulse response is L, $p_{i,m}(N) = 0$ for $N > L-1$. Using this, we can write

$$\mathbf{\Psi}_{\mathcal{H}} = \mathrm{E}(\mathcal{H}\mathcal{H}^H) = \mathrm{diag}\left[\sum_{i=1}^{n_t}\left(\sum_{k=1}^{n_r}\mathbf{p}_{k,i}(n \ominus \tau_i)\right)\right], \tag{4.28}$$

where $\mathbf{p}_{k,i}(n \ominus \tau_i)$ denotes a vector obtained by circularly shift $\mathbf{p}_{k,i}$ τ_i elements downwards. We normalize the channel such that the total transmit signal power equals the receive signal power per receive antenna. As a result, the power of the channel taps between all the transmit and receive antenna pairs adds up to $n_t \times n_r$. Therefore, we have

$$\mathbf{tr}[\mathbf{\Psi}_{\mathcal{H}}] = n_t n_r.$$

We further define $\mathbf{F} = \mathbf{S}_1\mathbf{\Psi}_{\mathcal{H}}\mathbf{S}_1^H$. It can be shown that the i^{th} diagonal element of $\mathbf{F}$, $F(i,i)$ is given by

$$F(i,i) = \sum_{m=1}^{N}\Psi(j,j) = \mathbf{tr}[\mathbf{\Psi}_{\mathcal{H}}] = n_t n_r. \tag{4.29}$$

As $\mathbf{\Delta}(\phi_d)$ is a diagonal matrix, we have

$$\mathbf{tr}\left[\mathbf{\Delta}(\phi_d)\mathbf{S}_1\mathbf{\Psi}_{\mathcal{H}}\mathbf{S}_1^H\right] = n_t n_r \mathbf{tr}\left[\mathbf{\Delta}(\phi_d)\right],$$

and similarly

$$\mathbf{tr}\left[\mathbf{\Delta}(\phi_d)^H\mathbf{\Delta}(\phi_d)\mathbf{S}_1\mathbf{\Psi}_{\mathcal{H}}\mathbf{S}_1^H\right] = n_t n_r \mathbf{tr}\left[\mathbf{\Delta}(\phi_d)^H\mathbf{\Delta}(\phi_d)\right].$$

As we are going to show later from the simulations, the performance of CFO estimation reaches the CRB at SNRs of practical interest. Therefore, the residual CFO value ϕ_d is usually very small. We can use a first-order Taylor series expansion to get a good approximation of the exponential function, i.e. $\delta = 1/2\sum_{k=1}^{\infty}\frac{(jN\phi_d)^k}{k!} \approx jN\phi_d/2$ and $\mathbf{\Delta}(\phi_d) \approx \mathrm{diag}[0, j\phi_d, j2\phi_d, \cdots, j(N-1)\phi_d]$. Substituting these into (4.27), we get

$$\begin{aligned}
\mathrm{MSE} &= \frac{n_t\sigma_n^2}{2N} + 2\Re\left\{\frac{(N-1)\phi_d^2 n_t}{4} + \frac{jN(N-1)\phi_d^3 n_t}{8}\right\} \\
&+ \left(1+\frac{N^2\phi_d^2}{4}\right)\frac{n_t(N-1)(2N-1)\phi_d^2}{6N^2} + \frac{n_t N\phi_d^2}{4} \\
&= \frac{n_t\sigma_n^2}{2N} + \frac{n_t\left(9N^3-2N^2-6N+2\right)}{12N^2}\phi_d^2 + \frac{n_t(N-1)(2N-1)}{24}\phi_d^4 \\
&\approx \frac{n_t\sigma_n^2}{2N} + \frac{n_t\left(9N^3-2N^2-6N+2\right)}{12N^2}\phi_d^2. \qquad (4.30)
\end{aligned}$$

Here we drop the ϕ_d^4 term in the MSE expression because the estimation error ϕ_d is very small in practical SNR regions and higher-order terms have only negligible contribution to the overall MSE. As we are going to show later using simulations, the variance of ϕ_d touches the CRB at moderate to high SNR regions. Therefore, we can approximate ϕ_d^2 in (4.30) with the CRB expression, i.e.

$$\phi_d^2 \approx \frac{1}{n_r N^3\gamma}.$$

Table 4.1: Extra MSE caused by residual CFO for different training sequence lengths and different number of receive antennas .

Training Sequence Length	**2 Rx Ant**	**3 Rx Ant**
25	0.127 dB	0.085 dB
36	0.089 dB	0.060 dB
49	0.066 dB	0.044 dB

Substituting this into (4.30), we get the MSE of channel estimation in the presence of residual CFO ϕ_d given by

$$\begin{aligned} \text{MSE} &\approx \frac{n_t\sigma_n^2}{2N} + \frac{n_t\left(9N^3 - 2N^2 - 6N + 2\right)}{12N^5\gamma n_r} \\ &= \sigma_n^2\left(\frac{n_t}{2N} + \frac{n_t\left(9N^3 - 2N^2 - 6N + 2\right)}{12N^5 n_r}\right). \end{aligned} \tag{4.31}$$

The first term in (4.31) is the MSE due to the AWGN noise while the second term is the extra MSE caused by the residual CFO ϕ_d. The ratio between these two MSE terms amounts to

$$\frac{\text{MSE}_{RCFO}}{\text{MSE}_{AWGN}} = \frac{(9N^3 - 2N^2 - 6N + 2)}{6N^4 n_r}. \tag{4.32}$$

As N is larger than 32 in practical systems and the denominator is one order larger than the numerator, the MSE caused by the interference is usually negligible compared to the MSE caused by the AWGN noise. Computer simulations, which will be presented later, show that the approximation given by (4.31) is very close to actual MSE obtained from simulations.

Table 4.1 shows the extra MSE in channel estimation caused by the residual CFO ϕ_d obtained through the approximation in (4.31) for different sequence lengths and different number of receive antennas. From the table, we can see that the MSE degradation is indeed very marginal.

4.5 Simulation Results

We performed computer simulations to study the performance of the CFO and channel estimations using the proposed CAZAC sequences. We simulated a MIMO OFDM system with 2 transmit and 2 receive antennas. The number of subcarriers is equal to 64 with length 16 cyclic prefix. The CFO is fixed at half the subcarrier spacing, i.e. $\phi = 0.5 \times \frac{2\pi}{64}$. We use CAZAC sequences of length 36 and the circular shift between transmit antenna 1 and 2 is 18 taps. The total length of the training sequence is 72 as two periods of the same CAZAC sequence are transmitted for CFO estimation. The channel is a 16-tap multi-path fading channel with uniform power delay profile.

Figure 4.1 shows the performance of CFO estimation using the proposed training sequence. Here, the MSE of the CFO estimation is normalized with respect to the subcarrier spacing as follows

$$\text{MSE} = \frac{1}{N_s} \sum_{i=1}^{N_s} \left(\frac{\hat{\phi} - \phi}{2\pi/64} \right)^2 ,$$

where $\hat{\phi}$ and ϕ represent the estimated and actual CFO values, respectively, and N_s denotes the total number of Monte Carlo trials. In comparison, we

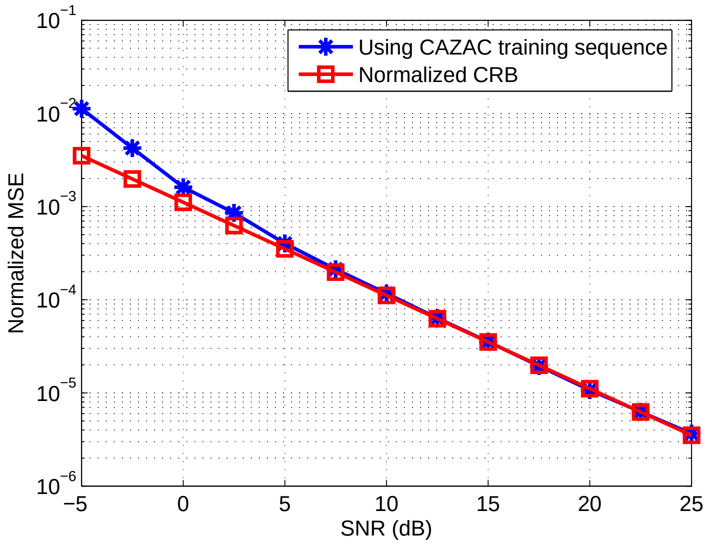

Fig. 4.1: MSE of CFO estimation using the proposed training sequence.

also plotted the CRB of the CFO estimation, again normalized with respect to the subcarrier spacing $2\pi/64$. We can see that the performance of the CFO estimator touches the CRB when SNR is larger than 5 dB.

Figure 4.2 shows the performance of channel estimation using the proposed CAZAC training sequences in the presence of a residual CFO ϕ_d. Comparing the channel estimation with perfect CFO compensation, we can see that the performance degradation due to the residual CFO ϕ_d is really negligible, which is consistent with the theoretical prediction. In the lower left corner of the figure, we plotted the zoomed-in MSE performance of the channel estimation. We can see that the theoretical MSE approximation by (4.31) is very accurate compared to the MSE obtained through simulations.

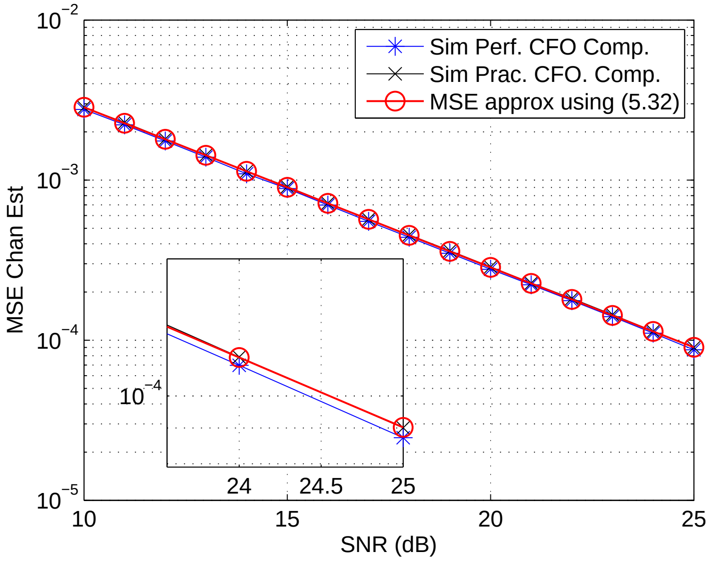

Fig. 4.2: Performance of channel estimation using the proposed CAZAC sequence in the presence of residual CFO.

4.6 Effect of Spatial Correlation on CFO Estimation

In this section, we study the spatial correlation among antennas related to the propagation environment and also its effects on the performance of the CFO estimation in MIMO systems. As the correlation effect is similar for different paths in a multi-path channel, in this section, we only consider the effect on one path, i.e. we only consider a flat fading channel. To simplify the analysis, we only look at the spatial correlation at the receive antennas, while assuming zero correlation among the transmit antennas. The spatial correlation is related to the propagation environment and is dependent on the distributions of angle of arrival (AOA) and angle of departure (AOD), which are specified by the power angular spectrum (PAS). We study how PAS affects the performance of CFO estimation. For a Laplacian PAS, which is a good model for the indoor propagation environment [88] [89], we also study how the performance of CFO estimation is affected by the mean AOA values.

We consider a MIMO system with N_t transmit and N_r receive antennas in flat fading channels. The received signal on n_r receive antennas can be written as

$$\mathbf{r} = \mathbf{H}\mathbf{s} + \mathbf{n} \tag{4.33}$$

where $\mathbf{s}$ is the transmitted signal from n_t transmit antennas, $\mathbf{H}$ is the $n_r \times n_t$ channel matrix with the i, j^{th} element $H_{i,j}$ as the channel response between the j^{th} transmit antenna and the i^{th} receive antenna and $\mathbf{n}$ is the AWGN noise. In practice, MIMO channels are correlated in the spatial domain. Such correlation can be modeled as [90]

$$\mathbf{H} = [\mathbf{R}_{\text{rx}}]^{1/2}\,\mathbf{H}_{\text{iid}}\left([\mathbf{R}_{\text{tx}}]^{1/2}\right)^{T}, \tag{4.34}$$

where $\mathbf{H}_{\text{iid}}$ is the channel matrix generated using independent, identically, distributed (i.i.d.) zero-mean complex Gaussian random variables. The transmit and receive correlation matrices are denoted as $\mathbf{R}_{\text{tx}}$ and $\mathbf{R}_{\text{rx}}$ respectively. For a 3×3 channel, the two matrices take on the following form [90]

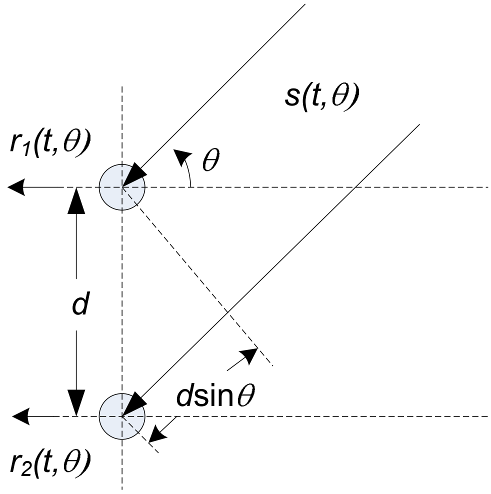

Fig. 4.3: Received signal for a two-element antenna array spaced d for a plane wave impinging at angle θ.

$$\mathbf{R}_{\mathrm{tx}} = \begin{bmatrix} 1 & \rho_{\mathrm{tx},1,2} & \rho_{\mathrm{tx},1,3} \\ \rho_{\mathrm{tx},2,1} & 1 & \rho_{\mathrm{tx},2,3} \\ \rho_{\mathrm{tx},3,1} & \rho_{\mathrm{tx},3,2} & 1 \end{bmatrix},$$

$$\mathbf{R}_{\mathrm{rx}} = \begin{bmatrix} 1 & \rho_{\mathrm{rx},1,2} & \rho_{\mathrm{rx},1,3} \\ \rho_{\mathrm{rx},2,1} & 1 & \rho_{\mathrm{rx},2,3} \\ \rho_{\mathrm{rx},3,1} & \rho_{\mathrm{rx},3,2} & 1 \end{bmatrix}, \tag{4.35}$$

where $\rho_{\mathrm{tx},i,j}$ is the correlation coefficient between the i^{th} and j^{th} transmit antennas and $\rho_{\mathrm{rx},i,j}$ is the correlation coefficient between the i^{th} and j^{th} receive antennas. The spatial correlation is determined by the PAS of AOA at the receiver and the PAS of the AOD at the transmitter.

In the derivation of the spatial correlation, we consider a two-antenna receiver for easy illustration. The results can be extended to more than two antennas straight-forwardly. Figure 4.3 illustrates a receiver with two antennas spaced d meters apart. There is a plane wave ($s(t,\theta)$) impinging at an AOA of θ. The received signal at the i^{th} receive antenna can be expressed as [91]

$$r_i(t,\theta) = \sqrt{G_i(\theta)}s(t,\theta)e^{j2\pi\left[f_c+(i-1)\frac{d}{\lambda}\sin\theta\right]}, \tag{4.36}$$

where $s(t,\theta)$ is the impinging signal, t is time and θ is the AOA of $s(t,\theta)$. The carrier frequency is denoted as f_c, d is the spacing between the antennas and λ is the wavelength. The power gain of the antenna at angle θ is denoted as $G(\theta)$. The covariance matrix of the received signal can be written as

$$\begin{aligned} \mathrm{R}_r &= \mathrm{E}_{t,\theta}\left(\begin{bmatrix} r_1(t,\theta) \\ r_2(t,\theta) \end{bmatrix}\begin{bmatrix} r_1^*(t,\theta) & r_2^*(t,\theta) \end{bmatrix}\right) \\ &= \begin{bmatrix} P_1 & \mathrm{E}_{t,\theta}\left(r_1(t,\theta)r_2^*(t,\theta)\right) \\ \mathrm{E}_{t,\theta}\left(r_1^*(t,\theta)r_2(t,\theta)\right) & P_2 \end{bmatrix}, \end{aligned} \tag{4.37}$$

where we use $\mathrm{E}_{t,\theta}$ to denote statistical expectation taken over both time t and the angle θ. The received signal power at each receive antenna is given by $P_i = \mathrm{E}_{t,\theta}\left(G_i(\theta)|s(t,\theta)|^2\right)$. The correlation coefficients of the received signals at the two antennas are defined as [92]

$$\rho_{1,2} = \frac{\mathrm{E}_{t,\theta}\left[r_1(t,\theta)r_2^*(t,\theta)\right] - \mathrm{E}_{t,\theta}\left[r_1(t,\theta)\right]\mathrm{E}_{t,\theta}\left[r_2^*(t,\theta)\right]}{\sqrt{P_1P_2}}. \tag{4.38}$$

We assume that the impinging signal $s(t,\theta)$ has zero mean over all angles, so that

$$\mathrm{E}_{t,\theta}\left[r_1(t,\theta)\right] = \mathrm{E}_\theta\left[\sqrt{G_1(\theta)}\mathrm{E}_t\left[s(t,\theta)\right]e^{j2\pi f_c}\right] = 0, \tag{4.39}$$

where E_θ and E_t denote expectations over angle θ and time t respectively. Similarly we have $\mathrm{E}_{t,\theta}\left[r_2(t,\theta)\right] = 0$. Therefore, the correlation coefficient can be simplified to

$$\rho_{1,2} = \frac{\mathrm{E}_{t,\theta}\left[r_1(t,\theta)r_2^*(t,\theta)\right]}{\sqrt{P_1 P_2}}, \tag{4.40}$$

and the covariance matrix can be re-written as

$$\mathbf{R}_r = \sqrt{P_1 P_2}\begin{bmatrix} 1 & \rho_{1,2} \\ \rho_{1,2}^* & 1 \end{bmatrix} = \sqrt{P_1 P_2}\mathbf{R}_{\mathrm{rx}}, \tag{4.41}$$

where $\mathbf{R}_{\mathrm{rx}}$ is the receiver correlation matrix as in (4.35). Denoting $D = 2\pi\frac{d}{\lambda}$, we can write

$$\begin{aligned}\mathrm{E}_{t,\theta}\left[r_1(t,\theta)r_2^*(t,\theta)\right] &= \mathrm{E}_{t,\theta}\left[\sqrt{G_1(\theta)G_2(\theta)}\left|s(t,\theta)\right|^2 e^{-jD\sin\theta}\right] \\ &= \mathrm{E}_\theta\left[\sqrt{G_1(\theta)G_2(\theta)}\mathrm{E}_t\left(\left|s(t,\theta)\right|^2\right)e^{-jD\sin\theta}\right].\end{aligned} \tag{4.42}$$

It is reasonable to assume that different antenna elements in an antenna array have the same radiation pattern, i.e. $G_1(\theta) = G_2(\theta) = G(\theta)$. In this case, we also have $P_1 = P_2 = P$. We use $P_s(\theta) = \mathrm{E}_t\left(\left|s(t,\theta)\right|^2\right)$ to denote the power of the impinging signal from angle θ. It is reasonable to assume that the power of the impinging signal is independent of θ and hence we will use P_s instead. We also use $\mathrm{PAS}(\theta)$ to denote the PAS of the received signal at angle θ. Then, we can rewrite the correlation coefficient in (4.40) as

$$\begin{aligned}
\rho_{1,2} &= \frac{\mathrm{E}_{t,\theta}\left[r_1(t,\theta)r_2^*(t,\theta)\right]}{P} \\
&= \frac{P_s \int_{-\pi}^{\pi} G(\theta)\mathrm{PAS}(\theta)e^{-jD\sin\theta}d\theta}{P} \\
&= \frac{\int_{-\pi}^{\pi} G(\theta)\mathrm{PAS}(\theta)e^{-jD\sin\theta}d\theta}{\int_{-\pi}^{\pi} G(\theta)\mathrm{PAS}(\theta)d\theta}. \qquad (4.43)
\end{aligned}$$

A common assumption used in the analysis of the spatial correlation is that the AOA is uniformly distributed between 0 and 360 degrees, i.e. PAS(θ)=$1/(2\pi)$ for all θ values. In this case, the correlation coefficient is given by

$$\rho_{1,2} = \frac{\int_{-\pi}^{\pi} e^{-jD\sin\theta}G(\theta)d\theta}{\int_{-\pi}^{\pi} G(\theta)d\theta}. \qquad (4.44)$$

Moreover, if the antenna is omni-directional, i.e. $G(\theta) = G$ for all the angles, $\rho_{1,2} = J_0(D)$ where J_0 is the Bessel function of the first kind and order 0.

It was found in [88] [89] that the PAS for indoor environments closely matches a Laplacian distribution and is given by

$$\mathrm{PAS}(\theta) = \frac{1}{\sqrt{2}\sigma}\exp\left(-\left|\frac{\sqrt{2}(\theta-\mu)}{\sigma}\right|\right) \qquad (4.45)$$

where σ is the angular spread, μ is the mean AOA and both are in degrees. For this PAS, there is no closed-form solution for the correlation coefficients. Therefore, we use numerical integration to calculate $\rho_{1,2}$.

Figure 4.4 shows the effect of angular spread on the correlation coefficients

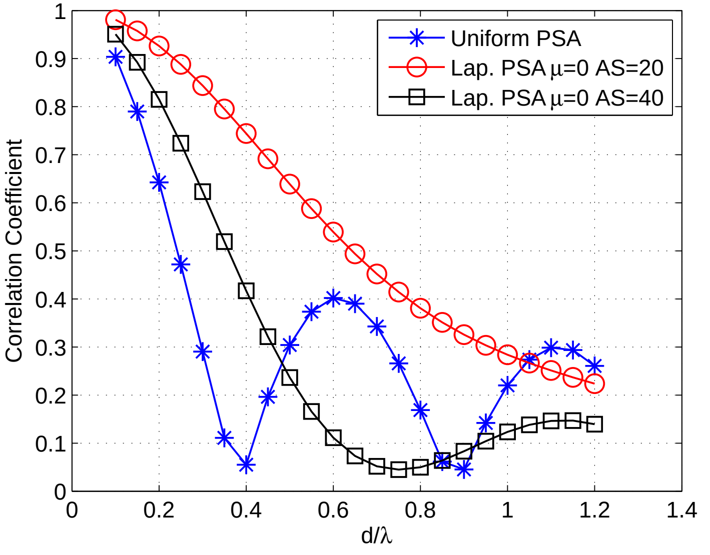

Fig. 4.4: Correlation coefficients for different angular spreads for a fixed mean AOA of 0^o.

for a fixed mean AOA of 0^o for the Laplacian-PAS given in (4.45), assuming omni-directional antenna elements. In comparison, we also plot the correlation coefficients for uniformly distributed AOA. From the figure, we can see that the correlation coefficients for Laplacian-distributed PAS are much higher than a uniform PAS. Comparing between different angular spread values, we can see that larger angular spreads lead to smaller correlations. In Figure 4.5, we plot the correlation coefficient for a fixed angular spread of 20^o and different mean AOA values for a Laplacian PAS. Again we assume all the antenna elements are omni-directional. We can see that for the same angular spread, the correlation becomes larger when the mean AOA becomes larger.

We use computer simulations to study the effects of different angular spreads and mean AOA values on the performance of CFO estimation for a 2×2 MIMO

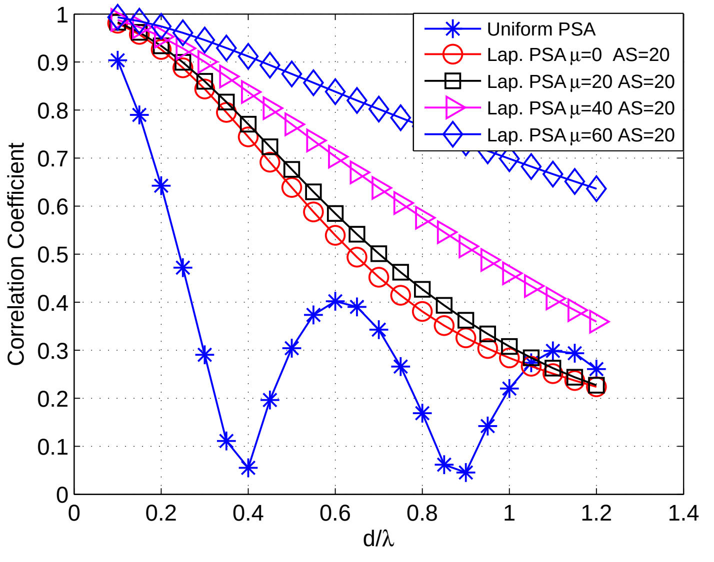

Fig. 4.5: Correlation coefficients for different mean AOA values for a fixed angular spread of 20°.

system for flat fading channels. The spacing between the 2 receive antennas is 0.5λ. We use two periods of length-16 CAZAC sequence as training sequence for CFO estimation. The CFO estimate is obtained using the estimator in (4.18). Figure 4.6 shows the MSE of CFO estimation for different angular spread values for a fixed mean AOA of 0°. From the figure, we can see that the performance of CFO estimation is degraded compared to that of the i.i.d. channel due to the spatial correlation. The degradation is larger for smaller angular spread values due to the larger spatial correlation. Figure 4.7 shows the performance of CFO estimation for different mean AOA (μ) values for a fixed angular spread of 20°. From the results, we can see that the performance degradation is larger for larger mean AOA values. This is because, as shown in Figure 4.5, the spatial correlation is larger for larger mean AOA values. The

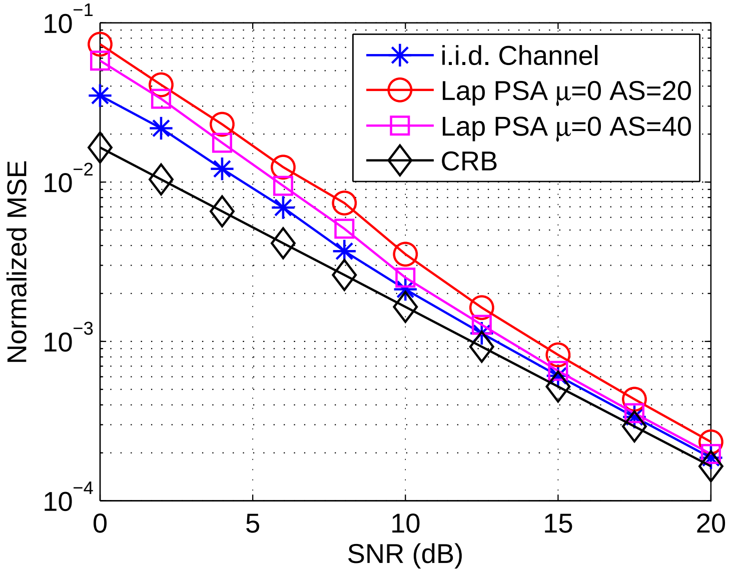

Fig. 4.6: MSE of CFO estimation for different angular spreads for a fixed mean AOA of 0^o.

performance difference for different μ values is small when μ is smaller than 40^o. When the mean AOA is larger than 40^o, the degradation due to larger mean AOA becomes more significant.

4.7 Effect of Antenna Mutual Coupling on CFO Estimation

Mutual coupling among different antenna elements in an antenna array is caused by the interactions of the EM waves received at different antenna elements. This effect is related to the antenna array and is independent of the propagation environment. The effects of mutual coupling were studied in [56]

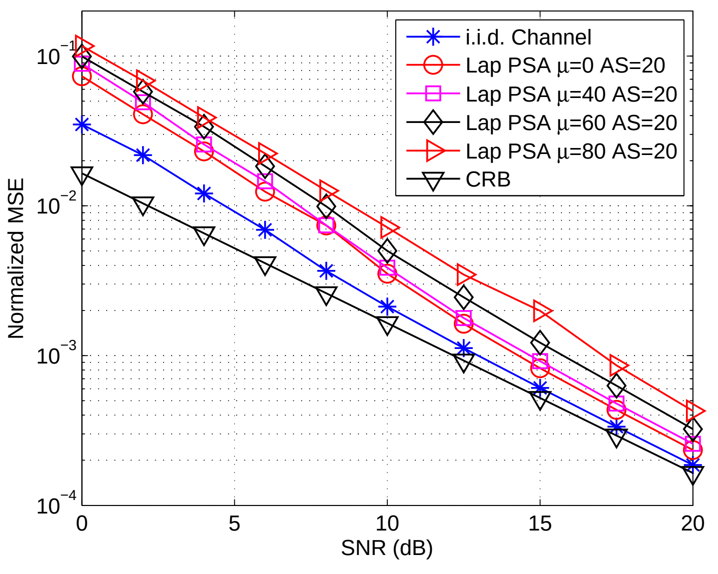

Fig. 4.7: MSE of CFO estimation for different mean AOA values for a fixed angular spread of 20°.

and [57]. It was shown that with mutual coupling among different antennas, the effective channel can be re-written as

$$\mathbf{H} = \left[\mathbf{C}_{\mathrm{rx}}\mathbf{R}_{\mathrm{rx}}\mathbf{C}_{\mathrm{rx}}^{H}\right]^{1/2}\mathbf{H}_{\mathrm{iid}}\left(\left[\mathbf{C}_{\mathrm{tx}}\mathbf{R}_{\mathrm{tx}}\mathbf{C}_{\mathrm{tx}}^{H}\right]^{1/2}\right)^{T}, \tag{4.46}$$

where $\mathbf{C}_{\mathrm{rx}}$ and $\mathbf{C}_{\mathrm{tx}}$ are the coupling matrices for the receiver and transmitter respectively. In this section, for simplicity of illustration, we only consider the effects of propagation environments and mutual coupling at the receiver. In this case, the effective channel can be simplified to

$$\mathbf{H} = \left[\mathbf{C}\mathbf{R}\mathbf{C}^{H}\right]^{1/2}\mathbf{H}_{\mathrm{iid}}. \tag{4.47}$$

Here we dropped the subscript of rx for simplicity of illustration. In [58] [59] [93], it was shown that mutual coupling reduces the spatial correlation between the antennas. On the other hand, mutual coupling also results in power loss on the desired signal when the two antennas are placed too close [94]. Next, we look at the overall effects of mutual coupling on the performance of CFO estimation in MIMO systems.

In this study, we consider a receiver with two dipole antennas with the following parameters:

- l: length of the dipole antenna;
- D: $D = 2\pi\frac{d}{\lambda}$ where d is the spacing between the two antennas and λ is the wavelength;
- $Z_s = R_s + jX_s$: self impedance of the antenna;
- $Z_m = R_m + jX_m$: mutual impedance between the antennas due to mutual coupling;
- $Z_{\text{load}} = R_{\text{load}} + jX_{\text{load}}$: loading impedance of the antennas.

From [56], the coupling matrix in (4.47) is given by

$$\mathbf{C} = (Z_{\text{load}} + Z_s)\begin{bmatrix} Z_{\text{load}} + Z_s & Z_m \\ Z_m & Z_{\text{load}} + Z_s \end{bmatrix}^{-1}. \tag{4.48}$$

In this study, we assume that the loading impedance is matched to the self impedance of the antenna, i.e. $Z_{\text{load}} = Z_s^*$. The mutual impedance Z_m is a function of the dipole length l, the antenna spacing D and the antenna placement configuration. The mutual impedance can be calculated numerically using the induced Electromagnetic Fields (EMF) method [95]. Combining the effect of coupling with the spatial correlation related to the propagation environment, we have

$$\begin{aligned}\mathbf{CRC^H} &= \begin{bmatrix} C_{1,1} & C_{1,2} \\ C_{2,1} & C_{2,2} \end{bmatrix} \begin{bmatrix} 1 & \rho_{1,2} \\ \rho_{2,1} & 1 \end{bmatrix} \begin{bmatrix} C^*_{1,1} & C^*_{2,1} \\ C^*_{1,2} & C^*_{2,2} \end{bmatrix} \\ &= P \begin{bmatrix} 1 & \tilde{\rho}_{1,2} \\ \tilde{\rho}_{2,1} & 1 \end{bmatrix}. \end{aligned} \tag{4.49}$$

From (4.49), we can see that there are two effects from mutual coupling. Firstly, the mutual coupling changes the spatial correlation. Secondly, the received signal power is scaled by P.

The effective correlation ($|\tilde{\rho}_{1,2}|$) as a function of the antenna spacing for a 2-antenna receiver is depicted in Figure 4.8. Here, we assume two dipole antennas with length $l = 0.5\lambda$ placed side by side. For such antennas, the self-impedance is $Z_s = (73 + j42)\,\Omega$ [95]. We also assume that the AOA has a uniform distribution from 0 to 360°. We can see that with the effect of mutual coupling, the spatial correlation between the antennas is reduced. The power P as a function of the antenna spacing is shown in Figure 4.9. The plot shows that the system suffers significant power loss if the two antennas are spaced too closely. The power loss becomes insignificant when the antenna spacing is about 1λ. In summary, the effect of mutual coupling is two-fold. Firstly it reduces the spatial correlation between the antennas, which is a desirable effect. On the other hand, it introduces extra power loss, which is undesirable.

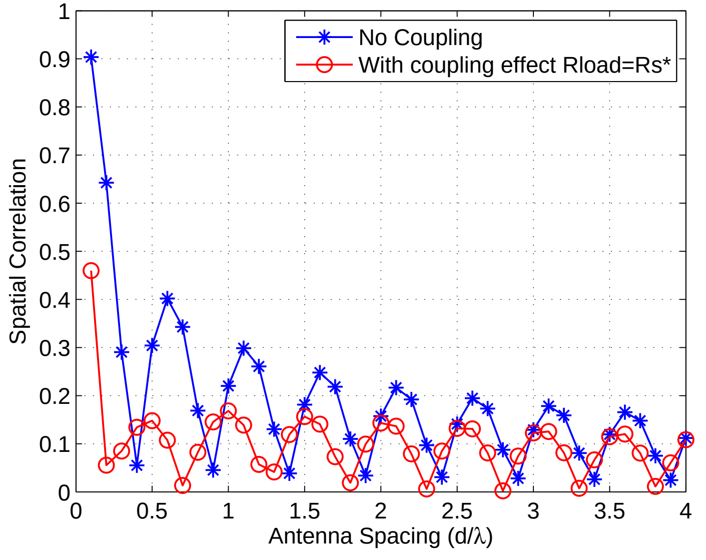

Fig. 4.8: Effective spatial correlation due to coupling for two $\lambda/2$ dipole antennas with $Z_{\text{load}} = Z_s^*$.

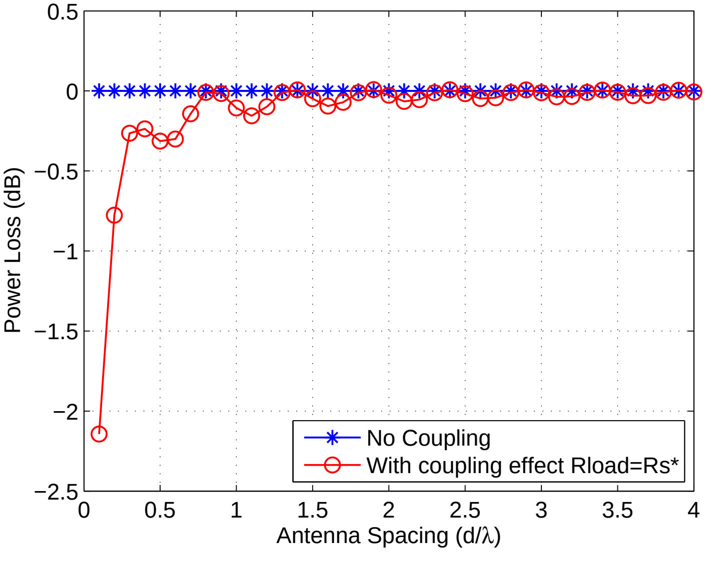

Fig. 4.9: Power loss due to coupling for two $\lambda/2$ dipole antennas with $Z_{\text{load}} = Z_s^*$.

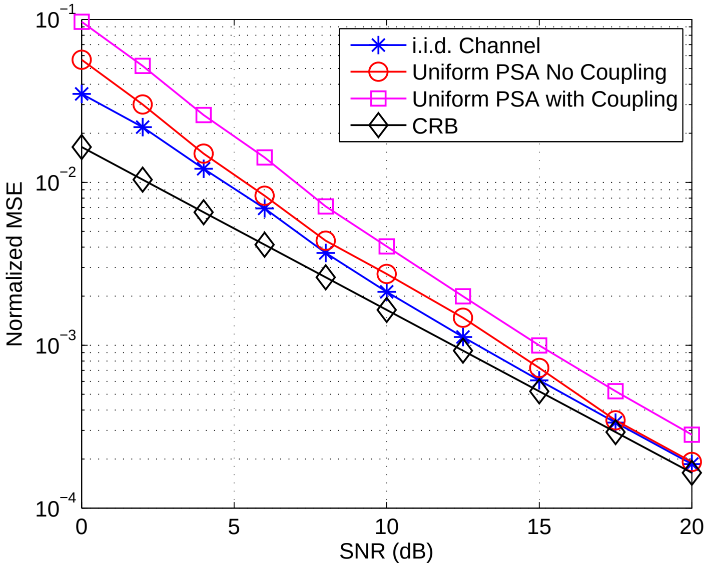

Fig. 4.10: Effects of mutual coupling on the performance of CFO estimation.

We used computer simulations to investigate the combined effect of mutual coupling on the performance of the CFO estimation. We simulated a 2×2 MIMO system for flat fading channels. We assume the transmit antennas are independent and only consider the effect of coupling at the receiver. The spacing between two receive antenna is 0.5λ. We also assume an uniformly distributed AOA at the receiver. The performance of CFO estimation with and without considering the effect of coupling is compared in Figure 4.10. We can see that the spatial correlation introduced by the propagation environment degrades the MSE performance as compared to the i.i.d. channel. Mutual coupling adds additional degradation to the performance. This means that the detrimental effect due to the power loss (as shown in Figure 4.9) is larger than the beneficial effect due to reduced spatial correlation (as shown in Figure 4.8).

4.8 Conclusions

In this chapter, we proposed to use CAZAC sequence as training sequences for joint CFO and channel estimation for MIMO-OFDM systems. We derived the corresponding maximum-likelihood (ML) joint CFO and channel estimator. We showed that using this sequence, the ML CFO estimate can be obtained using simple correlation operations. No matrix inversion needs to be performed to obtain the channel estimate. Moreover, the training overhead of the system can be significantly reduced compared to conventional frequency- domain training. We derived an accurate closed-form approximation on the MSE of channel estimation in the presence of the residual CFO. We showed that the extra degradation due to the residual CFO is negligible. We also studied the effects of spatial correlation and antenna mutual coupling on the performance of CFO estimation in MIMO systems. We showed that spatial correlation degrades the performance of CFO estimation. The mutual coupling has two effects. Firstly it reduces the spatial correlation, which is beneficial for CFO estimation. Secondly it introduces power loss on the received signal, which is detrimental. Computer simulations showed that the overall effect of mutual coupling adds additional degradation to the performance of CFO estimation.

Appendix: Derivation of MSE of Channel Estimation in the Presence of a Residual CFO ϕ_d

Using (4.26), we can write

$$\begin{aligned}
& (\hat{\mathcal{H}} - \mathcal{H})^H (\hat{\mathcal{H}} - \mathcal{H}) \\
= \; & \frac{1}{N^2} \Big\{ N^2 |\delta|^2 \mathcal{H}^H \mathcal{H} + N(\delta^* + |\delta|^2) \mathcal{H}^H \mathbf{S}_1^H \boldsymbol{\Delta}(\phi_d) \mathbf{S}_1 \mathcal{H} \\
+ \; & N \delta^* \mathcal{H}^H \boldsymbol{\mathcal{N}}' + N(\delta + |\delta|^2) \mathcal{H}^H \mathbf{S}_1^H \boldsymbol{\Delta}(\phi_d)^H \mathbf{S}_1 \mathcal{H} \\
+ \; & |1+\delta|^2 \mathcal{H}^H \mathbf{S}_1^H \boldsymbol{\Delta}(\phi_d)^H \boldsymbol{\Delta}(\phi_d) \mathbf{S}_1 \mathcal{H} + (1+\delta^*) \mathcal{H}^H \mathbf{S}_1^H \boldsymbol{\Delta}(\phi_d)^H \mathbf{S}_1 \boldsymbol{\mathcal{N}}' \\
+ \; & N \delta \boldsymbol{\mathcal{N}}'^H \mathcal{H} + (1+\delta) \boldsymbol{\mathcal{N}}'^H \mathbf{S}_1^H \boldsymbol{\Delta}(\phi_d) \mathbf{S}_1 \mathcal{H} + \boldsymbol{\mathcal{N}}'^H \boldsymbol{\mathcal{N}}' \Big\}. \qquad (4.50)
\end{aligned}$$

Taking expectation over the AWGN noise, we get

$$\begin{aligned}
\mathrm{E}_n \left[(\hat{\mathcal{H}} - \mathcal{H})^H (\hat{\mathcal{H}} - \mathcal{H}) \right] = \; & \frac{1}{N^2} \Big\{ N^2 |\delta|^2 \mathcal{H}^H \mathcal{H} + N(\delta^* + |\delta|^2) \mathcal{H}^H \mathbf{S}_1^H \boldsymbol{\Delta}(\phi_d) \mathbf{S}_1 \mathcal{H}. \\
+ \; & N(\delta + |\delta|^2) \mathcal{H}^H \mathbf{S}_1^H \boldsymbol{\Delta}(\phi_d)^H \mathbf{S}_1 \mathcal{H} \\
+ \; & |1+\delta|^2 \mathcal{H}^H \mathbf{S}_1^H \boldsymbol{\Delta}(\phi_d)^H \boldsymbol{\Delta}(\phi_d) \mathbf{S}_1 \mathcal{H} + \frac{N^2 n_t}{2} \sigma_n^2 \mathbf{I}_{n_r} \Big\}.
\end{aligned}$$

Here E_n denotes expectation over AWGN noise and $\mathbf{I}_{n_r}$ is an identity matrix of size $n_r \times n_r$. Thus, we can write the MSE of channel estimation conditioned on a particular channel realization $\mathcal{H}$ as

$$
\begin{aligned}
\mathrm{MSE}_{|\mathcal{H}} &= \frac{1}{Nn_r}\mathbf{tr}\left\{\mathrm{E}_n\left[(\hat{\mathcal{H}}-\mathcal{H})^H(\hat{\mathcal{H}}-\mathcal{H})\right]\right\} \\
&= \frac{1}{N^2}\frac{1}{Nn_r}\Bigg\{N^2|\delta|^2\mathbf{tr}(\mathcal{H}^H\mathcal{H}) \\
&+ 2N\Re\left[(\delta^*+|\delta|^2)\mathbf{tr}\left[\mathbf{\Delta}(\phi_d)\mathbf{S}_1\mathcal{H}\mathcal{H}^H\mathbf{S}_1^H\right]\right] \\
&+ |1+\delta|^2\mathbf{tr}\left[\mathbf{\Delta}(\phi_d)^H\mathbf{\Delta}(\phi_d)\mathbf{S}_1\mathcal{H}\mathcal{H}^H\mathbf{S}_1^H\right]\Bigg\} + \frac{n_t\sigma_n^2}{2N}.
\end{aligned}
\tag{4.51}
$$

Now averaging the MSE of the channel estimation over all the channel realizations, we get

$$
\begin{aligned}
\mathrm{MSE} &= \mathrm{E}_{\mathcal{H}}\left\{\mathrm{MSE}_{|\mathcal{H}}\right\} \\
&= \frac{1}{N^3n_r}\Bigg\{N^2|\delta|^2\mathbf{tr}\left\{\mathbf{\Psi}_{\mathcal{H}}\right\} + 2N\Re\left[(\delta^*+|\delta|^2)\mathbf{tr}\left[\mathbf{\Delta}(\phi_d)\mathbf{S}_1\mathbf{\Psi}_{\mathcal{H}}\mathbf{S}_1^H\right]\right] \\
&+ |1+\delta|^2\mathbf{tr}\left[\mathbf{\Delta}(\phi_d)^H\mathbf{\Delta}(\phi_d)\mathbf{S}_1\mathbf{\Psi}_{\mathcal{H}}\mathbf{S}_1^H\right]\Bigg\} + \frac{n_t\sigma_n^2}{2N},
\end{aligned}
\tag{4.52}
$$

where $\mathbf{\Psi}_{\mathcal{H}} = \mathrm{E}(\mathcal{H}\mathcal{H}^H)$.

Chapter 5

CFO Estimation for Multi-user MIMO-OFDM Uplink Using CAZAC Sequences

5.1 Introduction

The multi-user MIMO-OFDM system can be considered as an extension of the MIMO-OFDM system to the multi-user context. In the multi-user MIMO-OFDM system shown in Figure 5.1, multiple users, each with one or multiple antennas, transmit simultaneously using OFDM in the same frequency band. For clearness of illustration, in Figure 5.1, we only illustrate the case where each user has one transmit antenna. The receiver is a base station equipped

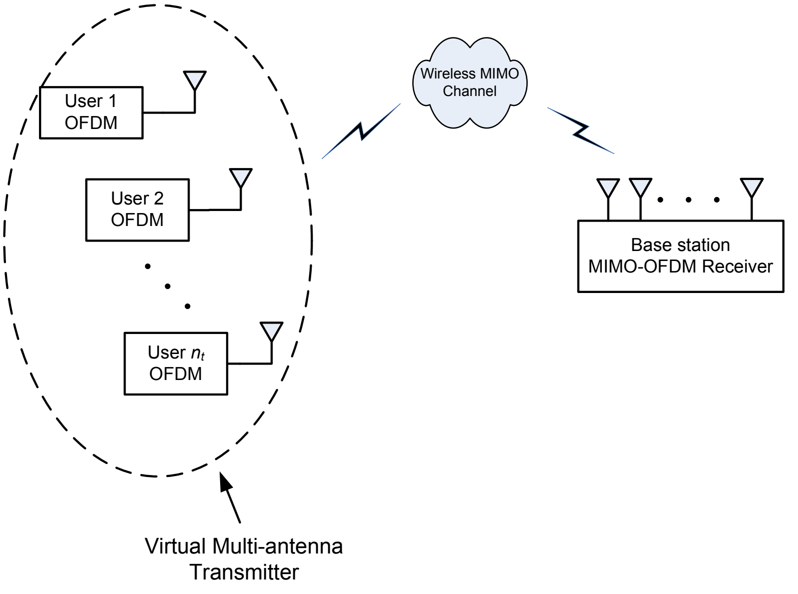

Fig. 5.1: Illustration of the multi-user MIMO-OFDM system.

with multiple antennas. It uses spatial processing techniques to separate the signals of different users. If we view the signals from different users as signals from different transmit antennas of a virtual transmitter, then the whole system can be viewed as an MIMO system. This system is also known as the virtual MIMO system [35].

As we discussed in previous chapters, in OFDM systems, CFO destroys the orthogonality between subcarriers and causes inter-carrier interference (ICI). To ensure good performance of OFDM systems, the CFO must be accurately estimated and compensated. For SISO-OFDM systems, it was shown in [38] and [39] that by using periodic training sequences, the maximum-likelihood (ML) CFO estimate can be obtained using simple correlation operations. Moreover, the mean square error (MSE) of the CFO estimate reaches the Cramer-Rao bound (CRB). A similar approach was used for single-user MIMO-OFDM systems [49] [34] [96], where all the transmit antennas are driven by a centralized local oscillator (LO) and so are all the receive antennas. In this case, the CFO is still a single parameter. For multi-user MIMO-OFDM systems, each user has its own LO, while the multiple antennas at the base station (receiver) are driven by a centralized LO. Therefore, in the uplink, the receiver needs to estimate multiple CFO values, one for each user. In [60] and [61], methods were proposed to estimate multiple CFO values for MIMO systems in flat fading channels. In [62], a semi-blind method was proposed to jointly estimate the CFO and channel for the uplink of multi-user MIMO-OFDM systems in frequency selective fading channels. An asymptotic Cramer-Rao bound for joint CFO and channel estimation in the uplink of MIMO-Orthogonal Frequency Division Multiple Access (OFDMA) system was derived in [97] and training strategies that minimize the asymptotic CRB were studied. In [98], a reduced-complexity CFO and channel estimator was proposed for the uplink of MIMO-OFDMA systems using an approximation of the ML cost function and a Newton search algorithm. It was also shown that the reduced-complexity method is asymptotically efficient. The joint CFO and channel estimation for multi-user MIMO-OFDM systems was studied in [63]. Training sequences that minimize the asymptotic CRB were also designed in [63].

It is known in the literature that the computational complexity for obtaining the ML CFO estimates in the uplink of multi-user MIMO-OFDM system grows exponentially with the number of users [63] [98]. A low-complexity algorithm was proposed in [63] for CFO estimation in the uplink of multi-user MIMO OFDM systems based on importance sampling. However, the complexity required to generate sufficient samples for importance sampling may still be high for practical implementations. In this chapter, we study algorithms that can further reduce the computational complexity of the CFO estimation. In particular, we propose a low-complexity CFO estimation algorithm using constant amplitude zero autocorrelation (CAZAC) training sequences. Following a similar approach as in [45], we first derive the ML estimator for the multiple CFO values in frequency selective-fading channels. Obtaining the ML estimates requires a search over all possible CFO values and the computational complexity is prohibitive for practical implementations. To reduce the computational complexity, we propose a sub-optimal algorithm using CAZAC training sequences. Using the proposed algorithm, the CFO estimates for different users can be obtained using simple correlation operations similar to single-user MIMO-OFDM systems. Moreover, the computational complexity of the algorithm grows only linearly with the number of users. However, we show that multiple CFO values in the uplink introduce multiple access interference (MAI) in the CFO estimation using the proposed algorithm. This causes an irreducible error floor in the MSE performance. We derive an expression for the signal to multiple access interference ratio (SIR) in the presence of multiple CFO values. To reduce the MAI, we find the training sequences that maximize the SIR. Note that the training sequence optimization problem we try to solve in this chapter is different from those in [63] and [97], where training sequences are optimized to minimize the CRB. In this chapter, we try to find the training sequences that maximize the SIR due to multiple CFO values specially for the proposed low-complexity CFO estimation algorithm using CAZAC training sequences. The optimal training sequences turn out to be dependent on the actual CFO values from different users. This is obviously not practical as it is not possible to know the CFO values and hence select the optimal training sequences in advance. To remove this dependency, we propose a new cost function, which is the Taylor's series approximation of the original cost function. The new cost function is independent of the actual CFO values and is an accurate approximation of the original SIR based cost function for small CFO values. Using the new cost function, we obtain the optimal training sequences for the following three classes of CAZAC sequences:

- the Frank & Zadoff sequences [85];
- the Chu Sequences [86];
- the polyphase sequences by Sueshiro and Hatori (S&H Sequences) [87].

Both the Frank & Zadoff sequences and the S&H sequences exist for sequence length $N = K^2$, where N is the length of the sequence and K is a positive integer larger than 1, while Chu sequences exist for any integer length $N > 1$. For both the Frank & Zadoff and the Chu sequences, there are a finite number of sequences for each sequence length. Therefore, the optimal sequences can be obtained using an off-line search among these sequences. However, for S& H sequences, there are infinitely many possible sequences. As the optimization problem for the S& H sequences cannot be solved analytically, we resort to a numerical method to obtain a near-optimal solution. To this end, we use the adaptive simulated annealing (ASA) technique [99]. For small sequence lengths, for example $N = 16$ and $N = 36$, we are able to use exhaustive search to verify that the solution obtained using ASA is globally optimal. We use computer simulations to evaluate the performance of the proposed CFO estimation algorithm using CAZAC sequences. We first compare the performance using CAZAC sequences with the performance using two other sequences with good correlation properties, namely, the IEEE 802.11n short training field (STF) [5] and the m sequences [100]. The results show that the error floor using CAZAC sequences is more than 10 times smaller compared to the other two sequences. Comparing among the three classes of CAZAC sequences, we find that the performance of the Chu sequences is better than the Frank & Zadoff sequences due to the larger degree of freedom in the sequence construction. The S&H sequences have the largest number of degree of freedom in the construction of the CAZAC sequences. However, the simulation results show that they have only very marginal performance gain compared to the Chu sequences. This makes Chu sequences a good choice for practical implementation due to its simple construction and flexibility in sequence lengths. By using the identified optimal sequences, the error floor in the CFO estimation is significantly lower compared to using a randomly selected CAZAC sequence.

The rest of this chapter is organized as follows. In Section 5.2, we present the system model and derive the ML estimator for the multiple CFO values. The sub-optimal CFO estimation algorithm using CAZAC sequences is proposed in Section 5.3. The training sequence optimization problem is formulated in Section 5.4 and methods are given to obtain the optimal training sequence. In Section 5.5, we present the computer simulation results and Section 5.6 concludes the chapter.

5.2 System Model

In this chapter, we study a multi-user MIMO-OFDM system with n_t users. For simplicity of illustration and analysis, we assume that each user has a single transmit antenna. The base station has n_r receive antennas, where $n_r \geq n_t$. The received signal at the i^{th} receive antenna can be written as

$$r_i(k) = \sum_{m=1}^{n_t} \left(e^{j\phi_m k} \sum_{d=0}^{L-1} h_{i,m}(d) s_m(k-d) \right) + n_i(k), \tag{5.1}$$

where ϕ_m is the CFO of the m^{th} user, k is the time index, and L is the length of the channel impulse response. The d-th tap of the channel impulse response between the m^{th} user and the i^{th} receive antenna is denoted as $h_{i,m}(d)$, s_m denotes the transmitted signal from the m^{th} user and n_i is the additive white Gaussian noise (AWGN) at the i^{th} receive antenna. Here we assume the initial phase for each user is absorbed in the channel impulse response. From (5.1), we can see that we have n_t different CFO values (ϕ_m's) to estimate. We consider a training sequence of length N and cyclic prefix (CP) of length L. The received signal after removal of CP can be written in an equivalent matrix form

$$\mathbf{r}_i = \sum_{m=1}^{n_t} \mathbf{E}(\phi_m)\mathbf{S}_m \mathbf{h}_{i,m} + \mathbf{n}_i \tag{5.2}$$

where $\mathbf{r}_i = [r_i(0), \cdots, r_i(N-1)]^T$ and superscript T denotes vector transpose. The CFO matrix of user m is denoted $\mathbf{E}(\phi_m)$ and is a diagonal matrix with diagonal elements equal to $[1, \exp(j\phi_m), \cdots, \exp(j(N-1)\phi_m)]$. We use $\mathbf{S}_m$ to denote the transmitted signal matrix for the m^{th} user. This is an $N \times N$ circulant matrix with the first column defined by $[s_m(0), s_m(1), s_m(2), \cdots, s_m(N-1)]^T$. Here we assume $N > L$ so the channel vector between the m^{th} user and the i^{th} receive antenna $\mathbf{h}_{i,m}$ is a $N \times 1$ vector by appending the $L \times 1$ channel impulse response $[h_{i,m}(0), \cdots, h_{i,m}(L-1)]^T$ vector with $N - L$ zeros.

Using this system model, the received signals from all n_r receive antennas can be written as

$$\boldsymbol{\mathcal{R}} = \boldsymbol{\mathcal{A}}(\boldsymbol{\phi})\boldsymbol{\mathcal{H}} + \boldsymbol{\mathcal{N}}, \tag{5.3}$$

where

$$\boldsymbol{\mathcal{R}} = [\mathbf{r}_1 \cdots, \mathbf{r}_{n_r}]_{\{N \times n_r\}},$$

$$\boldsymbol{\mathcal{A}}(\boldsymbol{\phi}) = [\mathbf{E}(\phi_1)\mathbf{S}_1, \cdots, \mathbf{E}(\phi_{n_t})\mathbf{S}_{n_t}]_{\{N \times (N \times n_t)\}}.$$

For clearness of presentation, we use subscripts inside curved brackets to denote the sizes of corresponding matrices. The vector $\boldsymbol{\phi} = [\phi_1, \cdots, \phi_{n_t}]$ is the CFO vector containing the CFO values from all users, and the channels of all users are stacked into the channel matrix $\boldsymbol{\mathcal{H}}$ given as

$$\boldsymbol{\mathcal{H}} = \begin{bmatrix} \boldsymbol{\mathcal{H}}_1 \\ \vdots \\ \boldsymbol{\mathcal{H}}_{n_t} \end{bmatrix}_{\{(N \times n_t) \times n_r\}},$$

with $\boldsymbol{\mathcal{H}}_i = [\mathbf{h}_{1,i}, \cdots, \mathbf{h}_{n_r,i}]_{\{N \times n_r\}}$ being the channel matrix for the i^{th} user. The AWGN noise matrix is given by $\boldsymbol{\mathcal{N}} = [\mathbf{n}_1, \cdots, \mathbf{n}_{n_r}]$.

Because the noise is Gaussian and uncorrelated, the likelihood function for the channel $\boldsymbol{\mathcal{H}}$ and CFO values $\boldsymbol{\phi}$ can be written as

$$\Lambda(\tilde{\boldsymbol{\mathcal{H}}}, \tilde{\boldsymbol{\phi}}) = \frac{1}{(\pi\sigma_n^2)^{N \times n_r}} \exp\left\{-\frac{1}{\sigma_n^2}\left\|\boldsymbol{\mathcal{R}} - \boldsymbol{\mathcal{A}}(\tilde{\boldsymbol{\phi}})\tilde{\boldsymbol{\mathcal{H}}}\right\|^2\right\}, \tag{5.4}$$

where $\tilde{\boldsymbol{\mathcal{H}}}$ and $\tilde{\boldsymbol{\phi}}$ are trial values for $\boldsymbol{\mathcal{H}}$ and $\boldsymbol{\phi}$ and σ_n^2 is the variance of the AWGN noise. Following a similar approach as in [45], we find that for a fixed CFO vector $\tilde{\boldsymbol{\phi}}$, the ML estimate of the channel matrix is given by

$$\hat{\boldsymbol{\mathcal{H}}}(\tilde{\boldsymbol{\phi}}) = \left[\boldsymbol{\mathcal{A}}^H(\tilde{\boldsymbol{\phi}})\boldsymbol{\mathcal{A}}(\tilde{\boldsymbol{\phi}})\right]^{-1} \boldsymbol{\mathcal{A}}^H(\tilde{\boldsymbol{\phi}})\boldsymbol{\mathcal{R}}, \tag{5.5}$$

where superscript H denotes matrix Hermitian. Substituting (5.5) into (5.4) and after some algebraic manipulations, we obtain that the ML estimate of the CFO vector $\boldsymbol{\phi}$ is given by

$$\hat{\boldsymbol{\phi}} = \arg\max_{\tilde{\boldsymbol{\phi}}} \left\{\mathbf{tr}\left(\boldsymbol{\mathcal{R}}^H\boldsymbol{\mathcal{B}}(\tilde{\boldsymbol{\phi}})\boldsymbol{\mathcal{R}}\right)\right\}, \tag{5.6}$$

with

$$\boldsymbol{\mathcal{B}}(\tilde{\boldsymbol{\phi}}) = \boldsymbol{\mathcal{A}}(\tilde{\boldsymbol{\phi}}) \left[\boldsymbol{\mathcal{A}}^H(\tilde{\boldsymbol{\phi}})\boldsymbol{\mathcal{A}}(\tilde{\boldsymbol{\phi}})\right]^{-1} \boldsymbol{\mathcal{A}}^H(\tilde{\boldsymbol{\phi}}),$$

and $\mathbf{tr}\,(\bullet)$ denotes the trace of a matrix. To obtain the ML estimate of the CFO vector $\boldsymbol{\phi}$, a search needs to be performed over the possible ranges of CFO values of all the users. The complexity of this search grows exponentially with the number of users and hence the search is not practical.

5.3 CAZAC Sequences for Multiple CFO's Estimation

To reduce the complexity of the CFO estimation for multi-user MIMO-OFDM systems, in this section, we propose a sub-optimal algorithm using CAZAC sequences as training sequences. CAZAC sequences are special sequences with constant amplitude elements and zero autocorrelation for any non-zero circular shifts. This means for a length-N CAZAC sequence, we have $s(n) = \exp(j\theta_n)$ and the auto-correlation

$$R(k) = \sum_{n=1}^{N} s(n)s^*(n \ominus k) = \begin{cases} N & k = 0; \\ 0 & k \neq 0. \end{cases} \tag{5.7}$$

for all values of $k = 0, 1, \cdots, N-1$. Here we use $\ominus$ to denote circular subtraction and superscript * denotes complex conjugation. Let $\mathbf{S}$ be a circulant matrix with the first column equal to $[s(0), s(1), \cdots, s(N-1)]^T$. The autocorrelation property of CAZAC sequences can be written in an equivalent matrix form as

$$\mathbf{S}^H\mathbf{S} = N\mathbf{I}_N, \tag{5.8}$$

where $\mathbf{I}_N$ is the identity matrix of size $N \times N$. This means that $\mathbf{S}$ is both a unitary (up to a normalization factor of N) and a circulant matrix.

In [101], we showed that for single-user MIMO-OFDM systems, using CAZAC sequences as training sequences reduces overhead for channel estimation while achieving Cramer Rao Bound (CRB) performance in the CFO estimation.

Here, we extend this approach to the estimation of multiple CFO values in the uplink of multi-user MIMO-OFDM systems. Let the training sequence of the first user be $\mathbf{s}_1$. The training sequence of the m^{th} user is the circularly-shifted version of the first user, i.e. $\mathbf{s}_m(n) = [\mathbf{s}_1(n \ominus \tau_m)]^T$, where τ_m denotes the shift value. It is straightforward to show that the training sequences for different users have the following properties:

- The autocorrelation of the training sequence for the i^{th} user satisfies

$$\mathbf{S}_i^H \mathbf{S}_i = N\mathbf{I}_N \tag{5.9}$$

  for $i = 1, \cdots, n_t$.

- The cross correlation between training sequences of the i^{th} and j^{th} users satisfies

$$\mathbf{S}_i^H \mathbf{S}_j = N\mathfrak{I}^{\tau_j - \tau_i} \tag{5.10}$$

  where $\mathfrak{I}^{\tau_j - \tau_i}$ denotes a matrix which results from circularly shifting the one elements of the identify matrix to the right by $\tau_j - \tau_i$ positions.

For SISO-OFDM systems, an efficient CFO estimation technique is to use periodic training sequences [38] [39]. In this chapter, we extend this approach to multi-user MIMO-OFDM systems. In this case, each user transmits two periods of the same training sequences and the received signal over two periods can be written as[1]

$$\boldsymbol{\mathcal{R}} = \begin{bmatrix} \mathbf{E}(\phi_1)\mathbf{S}_1 & \cdots & \mathbf{E}(\phi_{n_t})\mathbf{S}_{n_t} \\ e^{jN\phi_1}\mathbf{E}(\phi_1)\mathbf{S}_1 & \cdots & e^{jN\phi_{n_t}}\mathbf{E}(\phi_{n_t})\mathbf{S}_{n_t} \end{bmatrix} \boldsymbol{\mathcal{H}} + \boldsymbol{\mathcal{N}}. \tag{5.11}$$

Without loss of generality, we show how to estimate the CFO of the first user. The same procedure is applied to all the other users to estimate the other CFO values. Since same procedure is applied to all the users, the complexity of this CFO estimation method increases linearly with the number of users.

We first consider a special case when there are no CFO's for all the other users except user one, i.e. $\phi_m = 0$ for $m = 2, \cdots, n_t$. In this case, we cross correlate the training sequence of the first user with the received signal as shown below

$$\begin{aligned} \boldsymbol{\mathcal{Y}}_1' &= \mathbf{W}_1 \boldsymbol{\mathcal{R}} \\ &= \begin{bmatrix} \mathbf{S}_1^H & \mathbf{0} \\ \mathbf{0} & \mathbf{S}_1^H \end{bmatrix} \begin{bmatrix} \mathbf{E}(\phi_1)\mathbf{S}_1 & \cdots & \mathbf{S}_{n_t} \\ e^{jN\phi_1}\mathbf{E}(\phi_1)\mathbf{S}_1 & \cdots & \mathbf{S}_{n_t} \end{bmatrix} \boldsymbol{\mathcal{H}} + \boldsymbol{\mathcal{N}}' \\ &= \begin{bmatrix} \mathbf{S}_1^H\mathbf{E}(\phi_1)\mathbf{S}_1\boldsymbol{\mathcal{H}}_1 + \sum_{m=2}^{n_t} \mathbf{S}_1^H \mathbf{S}_m \boldsymbol{\mathcal{H}}_m \\ e^{jN\phi_1}\mathbf{S}_1^H\mathbf{E}(\phi_1)\mathbf{S}_1\boldsymbol{\mathcal{H}}_1 + \sum_{m=2}^{n_t} \mathbf{S}_1^H \mathbf{S}_m \boldsymbol{\mathcal{H}}_m \end{bmatrix} + \boldsymbol{\mathcal{N}}' \\ &= \begin{bmatrix} \mathbf{S}_1^H\mathbf{E}(\phi_1)\mathbf{S}_1\boldsymbol{\mathcal{H}}_1 + \sum_{m=2}^{n_t} \mathfrak{I}^{\tau_m} \boldsymbol{\mathcal{H}}_m \\ e^{jN\phi_1}\mathbf{S}_1^H\mathbf{E}(\phi_1)\mathbf{S}_1\boldsymbol{\mathcal{H}}_1 + \sum_{m=2}^{n_t} \mathfrak{I}^{\tau_m} \boldsymbol{\mathcal{H}}_m \end{bmatrix} + \boldsymbol{\mathcal{N}}', \end{aligned} \tag{5.12}$$

Because $\mathfrak{I}^{\tau_m}$ is an matrix resulting from circularly shifting the identity matrix to the right by τ_m elements, $\mathfrak{I}^{\tau_m}\boldsymbol{\mathcal{H}}_m$ produces a matrix resulting from

[1] We assume here that timing synchronization is perfect. We also assume that a cyclic prefix with length L is appended to the training sequence during transmission and removed at the receiver.

circularly shifting the rows of $\boldsymbol{\mathcal{H}}_m$ by τ_m elements downwards.

We make sure that the circular shift between the $(m-1)^{\text{th}}$ and m^{th} users is no smaller than the length of the channel impulse response, i.e. $\tau_m - \tau_{m-1} \geq L$. Since the channel has only L multi-path components, only the first L rows in the $N \times n_r$ matrix $\boldsymbol{\mathcal{H}}_m$ are nonzero. Therefore, $\mathfrak{J}^{\tau_m}\boldsymbol{\mathcal{H}}_m$ has all zero elements in the first L rows when $\tau_m - \tau_{m-1} \geq L$ for $m = 2, \cdots, n_t$ and $N - \tau_{n_t} \geq L$. Notice that to ensure these conditions hold, we need to have the training sequence length $N \geq n_t L$. Hence, the first L rows of $\boldsymbol{\mathcal{Y}}_1'$ will be free of the interference from all the other users. Let us define $\boldsymbol{\mathcal{I}}_L$ as the first L rows of the $N \times N$ identity matrix, we have

$$\boldsymbol{\mathcal{Y}}_1 = \begin{bmatrix} \boldsymbol{\mathcal{I}}_L & \mathbf{0} \\ \mathbf{0} & \boldsymbol{\mathcal{I}}_L \end{bmatrix} \boldsymbol{\mathcal{Y}}_1' = \begin{bmatrix} \boldsymbol{\mathcal{I}}_L \mathbf{S}_1^H \mathbf{E}(\phi_1) \mathbf{S}_1 \boldsymbol{\mathcal{H}}_1 \\ e^{jN\phi_1} \boldsymbol{\mathcal{I}}_L \mathbf{S}_1^H \mathbf{E}(\phi_1) \mathbf{S}_1 \boldsymbol{\mathcal{H}}_1 \end{bmatrix} + \boldsymbol{\mathcal{N}}''. \tag{5.13}$$

The multiplication of $\boldsymbol{\mathcal{I}}_L$ serves to select the first L rows from the matrix $\mathbf{S}_1^H \mathbf{E}(\phi_1) \mathbf{S}_1 \boldsymbol{\mathcal{H}}_1$. Because the CFO's of all the other users are 0, the shift orthogonality between their training sequences and user 1's training sequence is maintained. In this case, $\boldsymbol{\mathcal{Y}}_1$ is free of interferences from the other users. Following a similar approach as in [101], we can show that the ML estimate of user 1's CFO given $\boldsymbol{\mathcal{Y}}_1$ can be obtained as

$$\hat{\phi}_1 = \frac{1}{N} \angle \left\{ \sum_{k=1}^{L} \sum_{m=1}^{n_r} \mathcal{Y}_1^*(k,m) \mathcal{Y}_1(k+N,m) \right\}, \tag{5.14}$$

where $\angle(\bullet)$ denotes the angle of a complex number. The computational complexity of this estimator is low.

When the other users' CFO values are not zero, $\boldsymbol{\mathcal{Y}}_1$ is given by

$$\begin{aligned}\boldsymbol{\mathcal{Y}}_1 &= \begin{bmatrix} \boldsymbol{\mathcal{I}}_L \mathbf{S}_1^H \mathbf{E}(\phi_1)\mathbf{S}_1\boldsymbol{\mathcal{H}}_1 \\ e^{jN\phi_1}\boldsymbol{\mathcal{I}}_L \mathbf{S}_1^H \mathbf{E}(\phi_1)\mathbf{S}_1\boldsymbol{\mathcal{H}}_1 \end{bmatrix} + \begin{bmatrix} \boldsymbol{\mathcal{I}}_L \sum_{m=2}^{n_t} \mathbf{S}_1^H \mathbf{E}(\phi_m)\mathbf{S}_m\boldsymbol{\mathcal{H}}_m \\ \boldsymbol{\mathcal{I}}_L \sum_{m=2}^{n_t} e^{jN\phi_m}\mathbf{S}_1^H \mathbf{E}(\phi_m)\mathbf{S}_m\boldsymbol{\mathcal{H}}_m \end{bmatrix} + \boldsymbol{\mathcal{N}}'' \\ &= \begin{bmatrix} \boldsymbol{\mathcal{I}}_L \mathbf{S}_1^H \mathbf{E}(\phi_1)\mathbf{S}_1\boldsymbol{\mathcal{H}}_1 \\ e^{jN\phi_1}\boldsymbol{\mathcal{I}}_L \mathbf{S}_1^H \mathbf{E}(\phi_1)\mathbf{S}_1\boldsymbol{\mathcal{H}}_1 \end{bmatrix} + \boldsymbol{\mathcal{V}} + \boldsymbol{\mathcal{N}}''. \end{aligned} \tag{5.15}$$

From (5.15), we can see that the orthogonality between the training sequences from different users is destroyed by the non-zero CFO values ϕ_m. As a result, there is an extra Multiple Access Interference (MAI) term $\boldsymbol{\mathcal{V}}$ in the correlation output $\boldsymbol{\mathcal{Y}}_1$. This interference is independent of the noise and therefore it will cause an irreducible error floor in MSE of the CFO estimator in (5.14).

The covariance matrix of the MAI can be expressed as

$$\begin{aligned} &\mathrm{E}\left\{\boldsymbol{\mathcal{V}}\boldsymbol{\mathcal{V}}^H\right\} \\ = \; &\mathrm{E}\left\{ \begin{bmatrix} \boldsymbol{\mathcal{I}}_L \sum_{m=2}^{n_t} \mathbf{S}_1^H \mathbf{E}(\phi_m)\mathbf{S}_m\boldsymbol{\mathcal{H}}_m \\ \boldsymbol{\mathcal{I}}_L \sum_{m=2}^{n_t} e^{jN\phi_m}\mathbf{S}_1^H \mathbf{E}(\phi_m)\mathbf{S}_m\boldsymbol{\mathcal{H}}_m \end{bmatrix} \right. \\ &\left. \begin{bmatrix} \sum_{m=2}^{n_t} \boldsymbol{\mathcal{H}}_m^H \mathbf{S}_m^H \mathbf{E}^H(\phi_m)\mathbf{S}_1\boldsymbol{\mathcal{I}}_L^H & \sum_{m=2}^{n_t} e^{-jN\phi_m}\boldsymbol{\mathcal{H}}_m^H \mathbf{S}_m^H \mathbf{E}^H(\phi_m)\mathbf{S}_1\boldsymbol{\mathcal{I}}_L^H \end{bmatrix} \right\} \end{aligned}$$

We assume that the channels between different transmit and receive antennas are uncorrelated in space and that different paths in the multi-path channel are also uncorrelated. We define $\mathbf{p}_{i,m} = [p_{i,m}(0), \cdots, p_{i,m}(L-1), 0, \cdots 0]^T_{(N\times 1)}$ as the power delay profile (PDP) of the channel between the m^{th} user and the

i^{th} receive antenna and we have

$$\mathrm{E}\left\{\boldsymbol{\mathcal{H}}_m\boldsymbol{\mathcal{H}}_n^H\right\} = \begin{cases} \mathbf{0} & m \neq n, \\ \mathrm{diag}(\sum_{i=1}^{n_r}\mathbf{p}_{i,m}) & n = m. \end{cases} \tag{5.16}$$

Defining $\mathbf{P}_m = \mathrm{diag}(\sum_{i=1}^{n_r}\mathbf{p}_{i,m})$, we can re-write the covariance matrix of the interference as

$$\mathrm{E}\left\{\boldsymbol{\mathcal{V}}\boldsymbol{\mathcal{V}}^H\right\} = \begin{bmatrix} \mathbf{C} & \mathbf{D} \\ \mathbf{D}^H & \mathbf{C} \end{bmatrix}, \tag{5.17}$$

where

$$\mathbf{C} = \boldsymbol{\mathcal{I}}_L\left\{\sum_{m=2}^{n_t}\mathbf{S}_1^H\mathbf{E}(\phi_m)\mathbf{S}_m\mathbf{P}_m\mathbf{S}_m^H\mathbf{E}^H(\phi_m)\mathbf{S}_1\right\}\boldsymbol{\mathcal{I}}_L^H \quad \text{and}$$
$$\mathbf{D} = \boldsymbol{\mathcal{I}}_L\left\{\sum_{m=2}^{n_t}e^{-jN2\phi_m}\mathbf{S}_1^H\mathbf{E}(\phi_m)\mathbf{S}_m\mathbf{P}_m\mathbf{S}_m^H\mathbf{E}^H(\phi_m)\mathbf{S}_1\right\}\boldsymbol{\mathcal{I}}_L^H.$$

We see that the interference power is a function of the training sequence $\mathbf{S}_m$, the channel delay power profile matrix $\mathbf{P}_m$ and the CFO matrices $\mathbf{E}(\phi_m)$.

5.4 Training Sequence Optimization

In the previous section, we showed that the multiple CFO values introduce multiple access interference (MAI) in the CFO estimation. In this section, we study how to find the training sequences such that the signal to interference ratio (SIR) is maximized.

5.4.1 Cost Function Based on SIR

From the signal model in (5.15), we can define the SIR for CFO estimation of the first user as

$$\mathrm{SIR}_1 = \frac{\mathbf{tr}\left[\boldsymbol{\mathcal{I}}_L\{\mathbf{S}_1^H\mathbf{E}(\phi_1)\mathbf{S}_1\mathbf{P}_1\mathbf{S}_1^H\mathbf{E}^H(\phi_1)\mathbf{S}_1\}\boldsymbol{\mathcal{I}}_L^H\right]}{\mathbf{tr}\left[\boldsymbol{\mathcal{I}}_L\{\sum_{m=2}^{n_t}\mathbf{S}_1^H\mathbf{E}(\phi_m)\mathbf{S}_m\mathbf{P}_m\mathbf{S}_m^H\mathbf{E}^H(\phi_m)\mathbf{S}_1\}\boldsymbol{\mathcal{I}}_L^H\right]}. \tag{5.18}$$

From the denominator of (5.18), we can see that the total interference power depends on the CFO values ϕ_m of all the other users. As a result, the optimal training sequence that maximizes the SIR is also dependent on ϕ_m for $m = 1, \cdots, n_t$. In this case, even if we can find the optimal training sequences for different values of ϕ_m, we still do not know which one to choose during the actual transmission as the values ϕ_m are not available before transmission. This makes (5.18) an unpractical cost function.

To solve this problem, let us look at user 1 again. In the absence of the CFO, all the signal from user 1 is contained in the first L rows of the correlation output $\boldsymbol{\mathcal{Y}}_1'$. When the CFO is present, this orthogonality is destroyed and some information from user 1 will be "spilled" to the other rows of $\boldsymbol{\mathcal{Y}}_1'$, thus causing interference to the other users. For user 1, therefore, to keep the interference to the other users small, such "spilled" signal power should be minimized. On the other hand, the useful signal we used to estimate the CFO of user 1 is contained in the first L rows of $\boldsymbol{\mathcal{Y}}_1'$ and this signal power should be maximized. Therefore, considering user 1 alone, we can define the signal to "spilled" interference (to other users) ratio for user 1 as

$$\mathrm{SIR}_1' = \frac{\mathbf{tr}\left[\boldsymbol{\mathcal{I}}_L\{\mathbf{S}_1^H\mathbf{E}(\phi_1)\mathbf{S}_1\mathbf{P}_1\mathbf{S}_1^H\mathbf{E}^H(\phi_1)\mathbf{S}_1\}\boldsymbol{\mathcal{I}}_L^H\right]}{\mathbf{tr}\left[\overline{\boldsymbol{\mathcal{I}}_L}\{\mathbf{S}_1^H\mathbf{E}(\phi_1)\mathbf{S}_1\mathbf{P}_1\mathbf{S}_1^H\mathbf{E}^H(\phi_1)\mathbf{S}_1\}\overline{\boldsymbol{\mathcal{I}}_L}^H\right]} \tag{5.19}$$

where $\overline{\boldsymbol{\mathcal{I}}_L}$ is the complement of $\boldsymbol{\mathcal{I}}_L$, i.e. $\overline{\boldsymbol{\mathcal{I}}_L}$ is the last $N-L$ rows of the $N\times N$ identity matrix.

The denominator in (5.19) can be expressed as

$$\begin{aligned}
&\mathbf{tr}\left[\overline{\boldsymbol{\mathcal{I}}_L}\{\mathbf{S}_1^H\mathbf{E}(\phi_1)\mathbf{S}_1\mathbf{P}_1\mathbf{S}_1^H\mathbf{E}^H(\phi_1)\mathbf{S}_1\}\overline{\boldsymbol{\mathcal{I}}_L}^H\right]\\
&= N\mathbf{tr}\left[\mathbf{S}_1\mathbf{P}_1\mathbf{S}_1^H\right] - \mathbf{tr}\left[\boldsymbol{\mathcal{I}}_L\{\mathbf{S}_1^H\mathbf{E}(\phi_1)\mathbf{S}_1\mathbf{P}_1\mathbf{S}_1^H\mathbf{E}^H(\phi_1)\mathbf{S}_1\}\boldsymbol{\mathcal{I}}_L{}^H\right]\\
&= N^2\mathbf{tr}\left[\mathbf{P}_1\right] - \mathbf{tr}\left[\boldsymbol{\mathcal{I}}_L\{\mathbf{S}_1^H\mathbf{E}(\phi_1)\mathbf{S}_1\mathbf{P}_1\mathbf{S}_1^H\mathbf{E}^H(\phi_1)\mathbf{S}_1\}\boldsymbol{\mathcal{I}}_L{}^H\right].
\end{aligned}$$

Substituting this into (5.19), we have

$$\mathrm{SIR}_1' = \frac{\mathbf{tr}\left[\boldsymbol{\mathcal{I}}_L\{\mathbf{S}_1^H\mathbf{E}(\phi_1)\mathbf{S}_1\mathbf{P}_1\mathbf{S}_1^H\mathbf{E}^H(\phi_1)\mathbf{S}_1\}\boldsymbol{\mathcal{I}}_L^H\right]}{N^2\mathbf{tr}[\mathbf{P}_1] - \mathbf{tr}\left[\boldsymbol{\mathcal{I}}_L\{\mathbf{S}_1^H\mathbf{E}(\phi_1)\mathbf{S}_1\mathbf{P}_1\mathbf{S}_1^H\mathbf{E}^H(\phi_1)\mathbf{S}_1\}\boldsymbol{\mathcal{I}}_L^H\right]}. \tag{5.20}$$

Now we can define the training sequence optimization problem as

$$
\begin{aligned}
\mathbf{S}_{\text{opt}} &= \arg\max_{\tilde{\mathbf{S}}_1} \mathrm{SIR}_1' \\
&= \arg\max_{\tilde{\mathbf{S}}_1} \frac{\mathbf{tr}\left[\boldsymbol{\mathcal{I}}_L\{\tilde{\mathbf{S}}_1^H\mathbf{E}(\phi_1)\tilde{\mathbf{S}}_1\mathbf{P}_1\tilde{\mathbf{S}}_1^H\mathbf{E}^H(\phi_1)\tilde{\mathbf{S}}_1\}\boldsymbol{\mathcal{I}}_L^H\right]}{N^2\mathbf{tr}[\mathbf{P}_1] - \mathbf{tr}\left[\boldsymbol{\mathcal{I}}_L\{\tilde{\mathbf{S}}_1^H\mathbf{E}(\phi_1)\tilde{\mathbf{S}}_1\mathbf{P}_1\tilde{\mathbf{S}}_1^H\mathbf{E}^H(\phi_1)\tilde{\mathbf{S}}_1\}\boldsymbol{\mathcal{I}}_L^H\right]} \\
&= \arg\min_{\tilde{\mathbf{S}}_1} \frac{N^2\mathbf{tr}[\mathbf{P}_1] - \mathbf{tr}\left[\boldsymbol{\mathcal{I}}_L\{\tilde{\mathbf{S}}_1^H\mathbf{E}(\phi_1)\tilde{\mathbf{S}}_1\mathbf{P}_1\tilde{\mathbf{S}}_1^H\mathbf{E}^H(\phi_1)\tilde{\mathbf{S}}_1\}\boldsymbol{\mathcal{I}}_L^H\right]}{\mathbf{tr}\left[\boldsymbol{\mathcal{I}}_L\{\tilde{\mathbf{S}}_1^H\mathbf{E}(\phi_1)\tilde{\mathbf{S}}_1\mathbf{P}_1\tilde{\mathbf{S}}_1^H\mathbf{E}^H(\phi_1)\tilde{\mathbf{S}}_1\}\boldsymbol{\mathcal{I}}_L^H\right]} \\
&= \arg\min_{\tilde{\mathbf{S}}_1} \left\{ \frac{N^2\mathbf{tr}[\mathbf{P}_1]}{\mathbf{tr}\left[\boldsymbol{\mathcal{I}}_L\{\tilde{\mathbf{S}}_1^H\mathbf{E}(\phi_1)\tilde{\mathbf{S}}_1\mathbf{P}_1\tilde{\mathbf{S}}_1^H\mathbf{E}^H(\phi_1)\tilde{\mathbf{S}}_1\}\boldsymbol{\mathcal{I}}_L^H\right]} - 1 \right\} \\
&= \arg\max_{\tilde{\mathbf{S}}_1} \left\{ \mathbf{tr}\left[\boldsymbol{\mathcal{I}}_L\{\tilde{\mathbf{S}}_1^H\mathbf{E}(\phi_1)\tilde{\mathbf{S}}_1\mathbf{P}_1\tilde{\mathbf{S}}_1^H\mathbf{E}^H(\phi_1)\tilde{\mathbf{S}}_1\}\boldsymbol{\mathcal{I}}_L^H\right] \right\}. \qquad (5.21)
\end{aligned}
$$

From (5.21), we can see that the optimal training sequence depends on the power delay profile $\mathbf{P}_1$ and the actual CFO value ϕ_1. The channel delay profile is an environment-dependent statistical property that does not change very frequently. Therefore, in practice, we can store a few training sequences for different typical power delay profiles at the transmitter and select the one that matches the actual channel delay profile. On the other hand, it is impossible to know the actual CFO ϕ in advance to select the optimal training sequence. Next, we will propose a new cost function based on SIR approximation which can remove the dependency on the actual CFO ϕ_1 in the optimization.

Table 5.1: Number of possible Frank-Zadoff and Chu sequences for different sequence lengths.

N	Frank-Zadoff Seq	Chu Seq
16	2	8
36	2	12
64	4	32

5.4.2 CFO-Independent Cost Function

Let us assume that the CFO value ϕ is small. In this case, we can approximate the exponential function in the original cost function by its first-order Taylor series expansion, i.e. $\exp(j\phi) \approx 1 + j\phi$. Therefore, we have

$$\mathbf{E}(\phi_1) \approx \mathbf{I}_N + j\phi_1\mathbf{N}, \tag{5.22}$$

where $\mathbf{N}$ is a diagonal matrix given by $\mathbf{N} = \text{diag}[0, 1, 2, \cdots, N-1]$. Using this approximation, we get

$$\begin{aligned} \mathbf{S}^H\mathbf{E}(\phi)\mathbf{SPS}^H\mathbf{E}^H(\phi)\mathbf{S} &\approx \mathbf{S}^H(\mathbf{I}+j\phi\mathbf{N})\mathbf{SPS}^H(\mathbf{I}-j\phi\mathbf{N})\mathbf{S} \\ &= \mathbf{P} + j\phi\mathbf{S}^H\mathbf{NSP} - j\phi\mathbf{PS}^H\mathbf{NS} + \phi^2\mathbf{S}^H\mathbf{NSPS}^H\mathbf{NS}. \end{aligned} \tag{5.23}$$

Here we omitted the subscript 1 for clearness of presentation. Therefore, the optimization problem can be approximated as

$$\mathbf{S}_{\text{opt}} = \arg\max_{\tilde{\mathbf{S}}} \left\{ \mathbf{tr}\left[\boldsymbol{\mathcal{I}}_L \left(\mathbf{P} + j\phi\tilde{\mathbf{S}}^H\mathbf{N}\tilde{\mathbf{S}}\mathbf{P} - j\phi\mathbf{P}\tilde{\mathbf{S}}^H\mathbf{N}\tilde{\mathbf{S}} + \phi^2\tilde{\mathbf{S}}^H\mathbf{N}\tilde{\mathbf{S}}\mathbf{P}\tilde{\mathbf{S}}^H\mathbf{N}\tilde{\mathbf{S}} \right) \boldsymbol{\mathcal{I}}_L^H \right] \right\}. \tag{5.24}$$

Notice that the first term $\mathbf{P}$ in the summation is independent of $\tilde{\mathbf{S}}$ and hence can be dropped. It can be shown that the diagonal elements of the second term $j\phi\tilde{\mathbf{S}}^H\mathbf{N}\tilde{\mathbf{S}}\mathbf{P}$ are constant and independent of $\tilde{\mathbf{S}}$. Therefore $\mathbf{tr}\left[\boldsymbol{\mathcal{I}}_L(j\phi\tilde{\mathbf{S}}^H\mathbf{N}\tilde{\mathbf{S}}\mathbf{P})\boldsymbol{\mathcal{I}}_L^H\right]$ is also independent of $\tilde{\mathbf{S}}$ and hence can be dropped from the cost function. The same applies to the third term $-j\phi\mathbf{P}\tilde{\mathbf{S}}^H\mathbf{N}\tilde{\mathbf{S}}$, which is the conjugate of the second term. Therefore, the final form of the optimization using Taylor's series approximation can be written as

$$\mathbf{S}_{\text{opt}} = \arg\max_{\tilde{\mathbf{S}}} \left\{ \mathbf{tr}\left[\boldsymbol{\mathcal{I}}_L\left(\tilde{\mathbf{S}}^H\mathbf{N}\tilde{\mathbf{S}}\mathbf{P}\tilde{\mathbf{S}}^H\mathbf{N}\tilde{\mathbf{S}}\right)\boldsymbol{\mathcal{I}}_L^H\right]\right\}. \tag{5.25}$$

The advantage of (5.25) is that the optimization problem is independent of the actual CFO value ϕ as long as the value of ϕ is small enough to ensure the accuracy of the Taylor's series approximation in (5.22).

Now we look at how we can obtain the optimal CAZAC training sequences for the cost function in (5.25). In particular, we look at three classes of CAZAC sequences, namely the Frank-Zadoff sequences [85], the Chu sequences [86] and the S&H sequences [87]. The Frank-Zadoff sequences exist for sequence length $N = K^2$ where K is any positive integer greater than 1. For $N = 16$, all elements of the Frank-Zadoff sequences are BPSK symbols while for $N = 64$, all elements are BPSK and QPSK symbols. Therefore the advantage of the Frank-Zadoff sequences is that they are simple for practical implementation. The disadvantage is that there are limited numbers of sequences available for each sequence length as shown in Table 5.1. The advantage of the Chu sequences is that the length of the sequence can be an arbitrary positive integer $N > 1$. Compared to the Frank-Zadoff sequences, there are more sequences available for the same sequence length as shown in Table 5.1. For both the Frank-Zadoff and the Chu sequences, there is a finite number of possible sequences for each N. The optimal sequence can be found by using a computer search using the cost function in (5.25). The S&H sequences only exists for sequence length $N = K^2$. The sequences are constructed using a size K phase vector $\exp(j\boldsymbol{\theta}) = [e^{j\theta_1}, \cdots, e^{j\theta_K}]^T$. Therefore the optimization of training sequence $\mathbf{S}$ is equivalent to the optimization on the phase vector $\boldsymbol{\theta}$ given by

$$\begin{aligned} \boldsymbol{\theta} &= \arg\max_{\tilde{\boldsymbol{\theta}}} \left\{ \mathcal{J}(\tilde{\boldsymbol{\theta}}) \right\} \quad \text{with} \\ \mathcal{J}(\tilde{\boldsymbol{\theta}}) &= \mathbf{tr}\left[\boldsymbol{\mathcal{I}}_L \left(\mathbf{S}^H(\tilde{\boldsymbol{\theta}}) \mathbf{N} \mathbf{S}(\tilde{\boldsymbol{\theta}}) \mathbf{P} \mathbf{S}^{H}(\tilde{\boldsymbol{\theta}}) \mathbf{N} \mathbf{S}(\tilde{\boldsymbol{\theta}}) \right) \boldsymbol{\mathcal{I}}_L^H \right]. \end{aligned} \tag{5.26}$$

Notice that each element of the phase vector can take any values in the interval $[0, 2\pi)$. From the construction of the S&H sequence [87], it can be easily show that $\mathbf{S}(\boldsymbol{\theta} + \psi) = e^{j\psi}\mathbf{S}(\boldsymbol{\theta})$, where $\boldsymbol{\theta} + \psi = [\theta_1 + \psi, \cdots, \theta_K + \psi]^T$. Hence, from (5.26), we can get $\mathcal{J}(\boldsymbol{\theta}) = \mathcal{J}(\boldsymbol{\theta} + \psi)$. By letting $\psi = -\theta_1$, the original optimization problem over the K-dimension phase vector $\boldsymbol{\theta} = [\theta_1, \theta_2, \cdots, \theta_K]^T$ can be simplified to the optimization over a $(K-1)$-dimension phase vector $\boldsymbol{\theta}' = [0, \theta'_1, \cdots, \theta'_{K-1}]^T$ where $\theta'_k = \theta_{k+1} - \theta_1$.

Since there is an infinite number of possible S&H sequences for each sequence length, it is impossible to use exhaustive computer search to obtain the optimal sequence for the cost function in (5.26). Instead, we resort to numerical methods and use the adaptive simulated annealing (ASA) method [99] to find a near-optimal sequence. To test the near-optimality of the sequence obtained using the ASA, for smaller sequence lengths of $N = 16$ and $N = 36$, we use exhaustive computer search to obtain the globally optimal S&H sequence [2]. The obtained sequence through computer search is consistent with the sequence obtained using ASA and this suggests the effectiveness of the ASA in approaching the globally optimal sequence.

5.5 Simulation Results

In this section, we use computer simulations to study the performance of the CFO estimation using CAZAC sequences and demonstrate the performance gain achieved by using optimal training sequences. In the simulations, we assume a multi-user MIMO-OFDM systems with two users. Each user has one transmit antenna and the base station has two receive antennas. We simulate an OFDM system with 128 subcarriers. The CFO is normalized with respect to the subcarrier spacing. Unless otherwise stated, the actual CFO values for the two users are modeled as random variables uniformly distributed between [-0.5, 0.5]. The mean square error (MSE) of the CFO estimation is defined as

$$\mathrm{MSE} = \frac{1}{N_s}\sum_{i=1}^{N_s}\sum_{m=1}^{n_t}\left(\frac{\hat{\phi}_m - \phi_m}{2\pi/M}\right)^2, \tag{5.27}$$

where $\hat{\phi}_m$ and ϕ_m represent the estimated and true CFO's of the m^{th} user respectively, n_t is the number of users, M is the number of subcarriers, and

[2]Because CFO values are continuous variables, strictly speaking, it is not possible to obtain the exact optimum using exhaustive computer search, because the search works with discrete variables. If we keep the step size in the search small enough, we can be sure that the obtained "optimum" is very close to the actual optimum and can be practically assumed to be the actual optimum.

N_s denotes the total number of Monte Carlo trials.

First we compare the performance of CFO estimation using CAZAC sequences with the following two sequences which also have good autocorrelation properties

1. IEEE 802.11n short training field (STF) [5];
2. m sequences [100].

In the simulations, we use the 802.11n STF for 40MHz operations which has a length of 32. For the m sequence, we use a sequence length of 31. To provide a fair comparison, we compare the performance using the 802.11n STF with a length-32 Chu (CAZAC) sequence generated by [86]

$$s(n) = \exp\left[j\pi\frac{(n-1)^2}{N}\right], \tag{5.28}$$

and we compare the performance with the m sequence using a length-31 Chu sequence generated by [86]

$$s(n) = \exp\left[j\pi\frac{(n-1)n}{N}\right]. \tag{5.29}$$

The performance of CFO estimation using the 802.11n STF and $N = 32$ Chu sequence is shown in Figure 5.2. Here we use 16-tap multipath channels with uniform power delay profile and the circular shift between the training sequences of the two users $\tau_2 = 16$. The SNR on the x-axis is the average SNR per user per receive antenna defined as

$$\gamma = \frac{\mathrm{E}\left(\|\sum_{m=1}^{n_t}\sum_{k=1}^{n_r}\mathbf{S}_m\mathbf{h}_{k,m}\|^2\right)}{Nn_tn_r\sigma_n^2}, \tag{5.30}$$

where $\mathrm{E}(\bullet)$ denotes statistical expectation, $\mathbf{S}_m$ is the transmitted signal from the m^{th} user and $\mathbf{h}_{k,m}$ is the channel impulse response between the m^{th} user to the k^{th} receiver antenna. We use n_t to denote the number of users and n_r to denote the number of receive antennas and σ_n^2 is the variance of the receiver AWGN noise. To gauge the performance of the CFO estimation, we also included the single-user CRB in the comparison. The single-user CRB is obtained by assuming no MAI and can be shown to be [50]

$$\mathrm{CRB} = \frac{M^2}{4\pi^2 n_r N^3\gamma}, \tag{5.31}$$

where M is the number of subcarriers and γ is the SNR per user per receive antenna. From the results, we can see that the CFO estimation using the 802.11n STF has a very high error floor above MSE of 10^{-3}. The performance using CAZAC sequences is much better. In low to medium SNR regions, the performance is very close to the single-user CRB. An error floor starts to appear at SNR of about 25 dB. The error floor is around 100 times smaller compared to the error floor using the 802.11n STF.

The performance of the CFO estimation using the $N = 31$ m sequence and Chu sequence is shown in Figure 5.3. Here to satisfy the condition of $N \geq n_tL$, we use 15-tap multipath fading channels with uniform power delay profile and

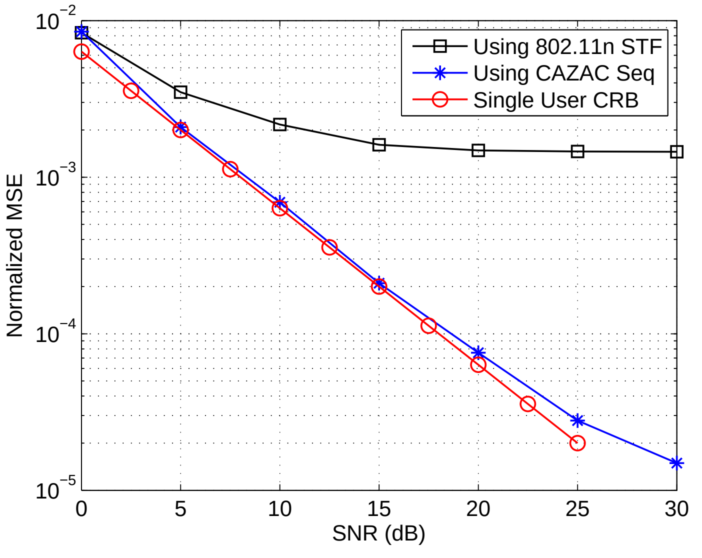

Fig. 5.2: MSE of CFO estimation using $N = 32$ Chu sequences and IEEE 802.11n STF for uniform power delay profile.

the circular shift between user 1 and 2's training sequence is also set to 15. Again, using CAZAC sequences leads to a much better performance. We can see that in low to medium SNR regions, the performance is very close to the single-user CRB. The error floor using CAZAC sequences is more than 10 times smaller than that using the m sequence.

Figure 5.4 shows the symbol error rate (SER) performance of the uplink of a 2-user MIMO-OFDM systems with QPSK modulation using four different training sequences for CFO estimation, namely, the $N = 32$ IEEE 802.11n STF, the $N = 31$ m sequence, the $N = 32$ and $N = 31$ Chu sequences. As in [102] [103], we assume that the CFO's from different users are first estimated at the base station using the proposed algorithm and transmitted back to different users using a downlink control channel. These CFO's are

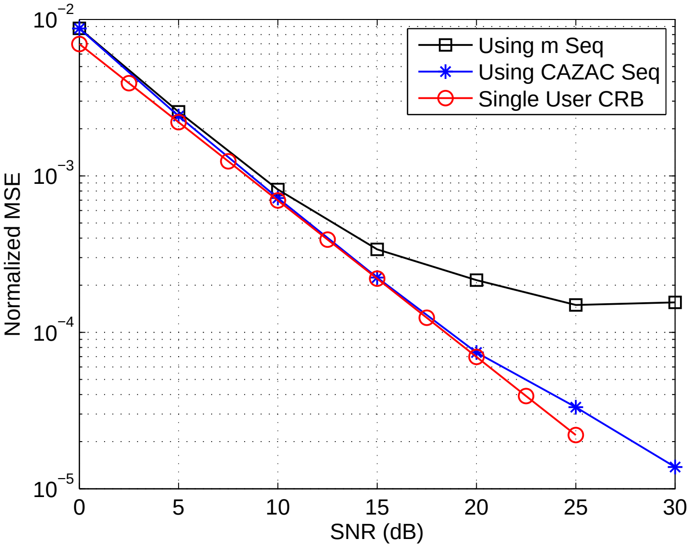

Fig. 5.3: Comparison of CFO estimation using $N = 31$ Chu sequences and m sequence for uniform power delay profile.

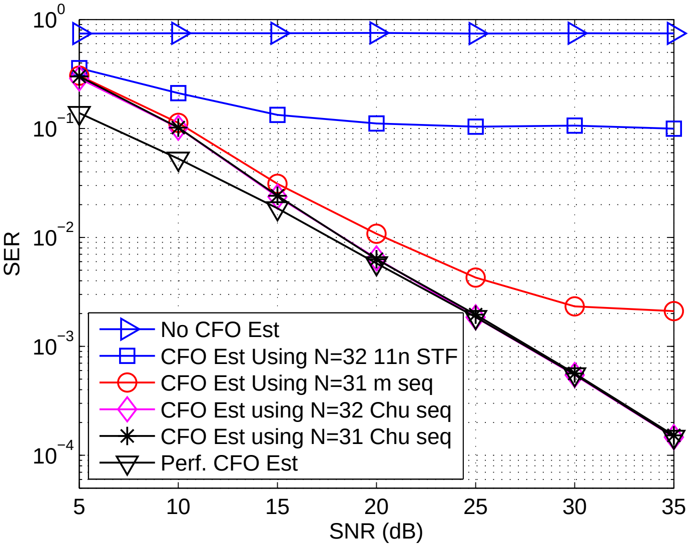

Fig. 5.4: Comparison of SER using QPSK modulation for CFO estimation using different sequences for uniform power delay profile.

pre-compensated at each user's transmitter and the SER is measured at the receiver for this transmission. We assume perfect channel knowledge at the receiver and linear minimum mean square error (LMMSE) detection is used. We can see that the system fails if there is no CFO estimation. Due to the high error floor in the CFO estimation using the IEEE 802.11n STF, the SER performance is very poor. The performance using m sequence is better and has an error floor at SER of 0.002. The performance using the two Chu sequences does not have any error floor and is very close to the performance of perfect CFO estimation for SNR above 15 dB.

The performance of CFO estimation using different CAZAC sequences is compared in Figure 5.5. Here we fix the sequence length to 36 and the multi-path channel has $L = 18$ taps with uniform power delay profile. Comparing the performances of the optimal Chu sequence and the optimal Frank-Zadoff sequence, we can see that the error floor of the Chu sequence is smaller. This is because there are more possible Chu sequences compared to Frank-Zadoff sequences and hence more degrees of freedom in the optimization. However, comparing the performance of the optimal Chu sequence with that of the optimal S&H sequences, we can see that the additional degrees of freedom in the S& H sequence do not lead to significant performance gain. Compared to the performance using a randomly selected CAZAC sequence, we can see that the error floor using an optimized sequence is significantly smaller.

From Figure 5.5, we can see that the gain of using S& H sequences compared to Chu sequences is really small. Therefore, in practical implementation, it is better to use the Chu sequence because it is simple to generate and it is

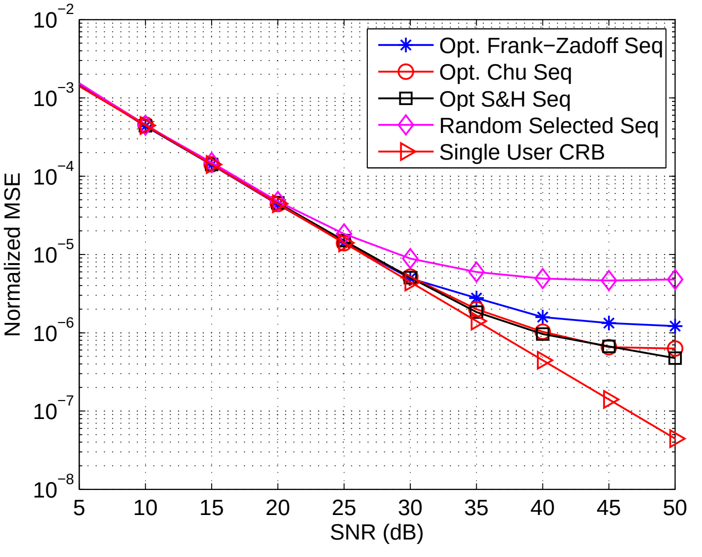

Fig. 5.5: Comparison of CFO estimation using different $N = 36$ CAZAC sequences for $L = 18$ channel for uniform power delay profile.

available for all sequence lengths. Another advantage of the Chu sequence is that the optimal Chu sequence obtained using cost function (5.25) is the same for the uniform power delay profile and some exponential power delay profiles we tested. Hence, a common optimal Chu sequence can be used for both the uniform and exponential PDP's. This is not the case for the S & H sequences.

Figure 5.6 shows the performance of CFO estimation for different lengths of optimal Chu sequences. Here we fix the channel length to $L = 18$. From the previous sections, to accommodate two users, the minimum sequence length is $n_t L$. Therefore, we need Chu sequences of length at least 36. We compare the performance of the optimal length-36 sequence with that of optimal length-49 and length-64 sequences. For the length-49 sequence, the circular shift between training sequence of two users is 24, while for length-64 sequence, the circular

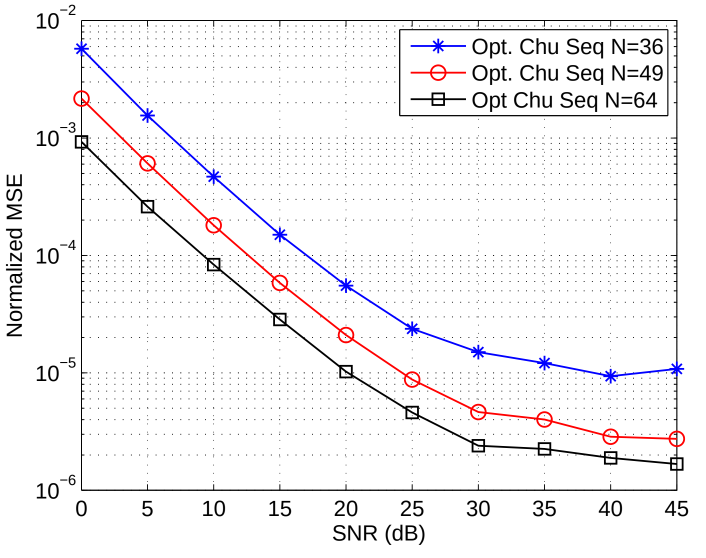

Fig. 5.6: Comparison of CFO estimation using different length of optimal Chu sequences for $L = 18$ channel for uniform power delay profile.

shift is 32. From the comparison, we can see that there are two advantages using a longer sequence. Firstly, in the low to medium SNR regions, there is SNR gain in the CFO estimation due to the longer sequence length. Secondly, in the high SNR region, the error floor using longer sequences is much smaller. This can be explained using Figure 5.7. In Figure 5.7, we plotted the signal power for user 1 and user 2 after the correlation operation in (5.12) for sequence length of 36 and 64 using Chu sequences. In the absence of the CFO, the signal of user 1 should be contained in the first 18 samples ($L = 18$). However, due to CFO, some signal components are leaked into the other samples, and become interference to user 2. For the case of $L = 18$ and $N = 36$, all the leaked signals from user 1 become interference to user 2 and vice versa. If we use a longer training sequence, there is some "guard time" between the useful signals of the two users as shown in Figure 5.7 for the $N = 64$ case. As

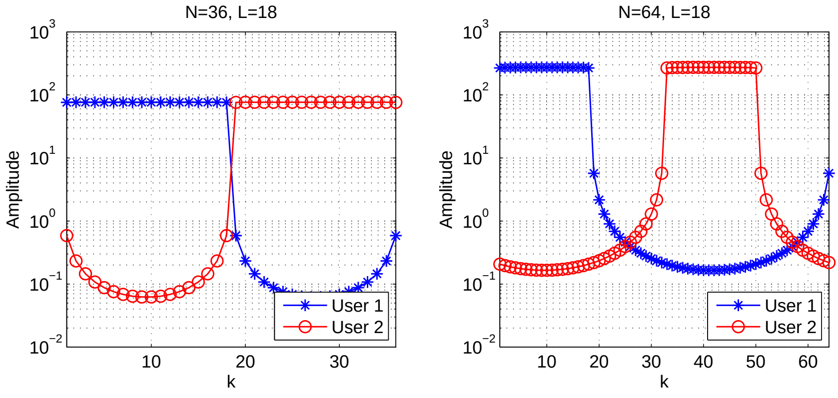

Fig. 5.7: Comparison of useful signal and interference power for different sequence lengths using Chu sequences (uniform power delay profile).

we only take the useful L samples for CFO estimation (5.13), only part of the leaked signal becomes interference. Hence, the overall SIR is improved. The cost of using longer sequences is the additional training overhead that is required. Therefore, based on the requirement on the precision of CFO estimation, the system designer should choose the best sequence length that achieves the best compromise between performance and overhead.

5.6 Conclusions

In this chapter, we studied the CFO estimation algorithm in the uplink of the multi-user MIMO-OFDM systems. We proposed a low-complexity sub-optimal CFO estimation algorithm using CAZAC sequences. The complexity of the proposed algorithm grows only linearly with the number of users. We showed that in this algorithm, multiple CFO values from multiple users cause multiple access interference in the CFO estimation. To reduce this detrimental effect, we formulated an optimization problem based on the maximization of the signal to interference ratio (SIR) in the CFO estimation. However, the optimization problem is dependent on the actual CFO values which are not known in advance. To remove this dependency, we proposed a new cost function which closely approximates the SIR for small CFO values. Using the new cost function, we can obtain optimal training sequences for different classes of CAZAC sequences. Computer simulations showed that the performance of the CFO estimation using CAZAC sequences is very close to the single user CRB for low to medium SNR values. For high SNR values, there is an error floor due to the multiple access interference. By using the obtained optimal CAZAC sequences, this floor can be significantly reduced compared to using a randomly chosen CAZAC sequence.

Chapter 6

Conclusions and Future Work

6.1 Conclusions

Sensitivity to carrier frequency offset (CFO) is a major drawback of orthogonal frequency division multiplexing (OFDM) systems. In this thesis, we study low-complexity frequency synchronization techniques that can accurately estimate the CFO for wireless OFDM systems. The focus is on finding frequency synchronization techniques that achieve a good balance between performance and computational complexity. We developed CFO estimation algorithms for various wireless OFDM systems that can be implemented with low complexity, and at the same time achieve close to maximum-likelihood (ML) or Cramer-Rao Bound (CRB) performance for practical CFO values.

In Chapters 2 and 3 of the thesis, we studied low-complexity blind CFO estimation algorithms that exploit frequency-domain null subcarriers, which are subcarriers that are left empty. Existing algorithms of this type have a high computational complexity because the cost function of CFO estimation is a high-order polynomial and a search method is needed to find the CFO estimate. By using a low-order Taylor series approximation of the cost function, we derived a closed-form solution for the CFO estimate. We also developed a new factorization of the cost function such that the error between the original cost function and the low-order Taylor series approximation is reduced. We noticed that when the CFO is large, the approximation error still causes some performance degradation in CFO estimation especially in the high SNR region. To reduce this degradation, we further developed a successive algorithm, in which the CFO is estimated and compensated successively in several iterations. A convergence monitoring method was implemented to ensure that the CFO obtained using the successive algorithm converges to the same CFO obtained using the high-complexity search method. We showed using computer simulations that the proposed successive algorithm achieves the same performance as the search method in 2 to 3 iterations. The computational complexity of the developed algorithm is significantly lower than that using the search method. In the literature, it was shown that the CRB of the CFO estimation is minimized if the null subcarriers are placed with equal spacing in an OFDM symbol. In our study in Chapter 3, we found that the signal to noise ratio (SNR) of the CFO estimation is related to the null subcarrier placement. To gain additional insight on the best null subcarrier placement, we studied the null subcarrier placement that maximizes this SNR. For small CFO values, we showed that this optimization problem is convex and the SNR of the CFO estimation is maximized when the null subcarriers are evenly spaced.

This is consistent with the null subcarrier placement that minimizes the CRB. However, when the number of subcarriers is not divisible by the number of null subcarriers, it is not possible to place null subcarriers with even spacing. To solve this practical problem, we proposed a heuristic null subcarrier placement, which still leads to good performance in the CFO estimation. For practical OFDM systems where two guard bands are required at both ends of the spectrum, we showed that by placing a few null subcarriers optimally inside the data band, the performance of the CFO estimation can be significantly improved.

In Chapter 4, we studied frequency synchronization for multiple input multiple output (MIMO) OFDM systems. We proposed an efficient training sequence design for joint CFO and channel estimation in MIMO-OFDM systems. We showed that using the proposed training sequence, the ML CFO and channel estimates can be obtained with low computational complexity. The training overhead is also significantly lower than for the conventional frequency-domain training sequence. Moreover, we derived an accurate closed-form approximation of the performance of channel estimation in the presence of residual CFO. In Chapter 4, we also studied the effects of spatial correlation and antenna mutual coupling on the performance of CFO estimation in MIMO systems. We showed that spatial correlation degrades the performance of CFO estimation. Antenna mutual coupling has two effects. Firstly, it reduces spatial correlation, which is beneficial. Secondly it also reduces the power of the received signal, which is detrimental. Computer simulations showed that the combined effect of mutual coupling adds additional degradation to the CFO estimation performance.

In Chapter 5, we studied the frequency synchronization in the uplink of multi-user MIMO-OFDM systems. We proposed a low-complexity CFO estimation algorithm using constant amplitude zero autocorrelation (CAZAC) training sequences. We showed that using the proposed algorithm, the CFO estimates of different users can be obtained using simple correlation operations. The computational complexity of the proposed algorithm is much lower than existing algorithms in the literature, while the performance is close to optimum. Moreover, the computational complexity of the proposed algorithm only grows linearly with the number of users. However, we showed that multiple CFO's cause multiple access interference (MAI) in the CFO estimation of different users using the proposed low-complexity algorithm. This leads to an error floor in the mean square error (MSE) of the CFO estimates. To reduce this degradation, we formulated an optimization problem to find the training sequences that maximize the signal to multiple access interference ratio (SIR). However, the optimal training sequences depend on the actual CFO values, which are not known in advance. To solve this problem, we developed a new cost function that closely approximates the SIR for small CFO values and is independent of the actual CFO values. We showed using computer simulations that the performance of CFO estimation using the proposed CAZAC sequences reaches the single user CRB for low to medium SNR regions. By using the proposed optimal CAZAC sequence, the error floor in the high SNR region is much lower than for a randomly selected CAZAC sequence.

6.2 Future Work

In this section, we would like to make the following recommendations on the possible future work based on the research carried out in this thesis.

- In practical wireless OFDM systems, it is usually required by industrial standards to have guard bands at both ends of the spectrum to avoid aliasing to the adjacent bands and also to avoid interference from the adjacent bands. In this case, the frequency responses of training sequences on the subcarriers in the guard bands are required to be zero. We did not consider this constraint, which must be satisfied in a practical OFDM system, in the design of CAZAC training sequences in MIMO-OFDM systems. Therefore, it is of practical importance to investigate whether there are CAZAC sequences that satisfy this constraint. If not, then it would be interesting to see what other sequences we should use and how to construct and optimize them. In designing a good training sequence with the guard band constraint, we believe there is a trade-off between small guard band response and small auto-correlation of the sequence. Therefore, it is interesting to investigate how we can formulate this trade-off and find a good practical training sequence. Moreover, the constant amplitude requirement on the CAZAC training sequence is not essential as long as the peak to average power ratio (PAPR) of the training sequence is reasonably small. Thus, we can relax the constant amplitude constraint in the training sequence design, which gives us additional degrees of freedom.
- Due to time constraints, in this thesis, we did not consider channel estimation for different users in the uplink of multi-user MIMO-OFDM systems

using CAZAC sequences. It is worthwhile to study the joint CFO and channel estimation and the effect of residual CFO on the channel estimation in the multi-user systems. This study will aid us in the design of a single training sequence for joint CFO and channel estimation in the uplink of multi-user MIMO-OFDM systems. Moreover, a comparison with the results obtained in Chapter 4 for single-user MIMO-OFDM systems can provide us with additional insights on the training sequence design for multi-user systems.

- In Chapter 5, when we studied the symbol error rate (SER) performance in the uplink of multi-user MIMO-OFDM systems, we assumed there is a downlink control link, using which the CFO values for different users are sent back to the transmitter and pre-compensated. It is an interesting problem to study how CFO compensation can be performed at the receiver. In this case, the communication of the CFO values back to the transmitter is not necessary and the system design can be simplified significantly. However, the CFO compensation in a multi-user receiver is not trivial, as compensating one user's CFO might worsen the CFO of another user. If CFO's can be successfully compensated with low complexity, we can re-estimate the residual CFO's using the compensated received signal and obtain a better CFO estimates. This is because the multiple access interference (MAI) for the CFO estimation in multi-user MIMO-OFDM systems is directly related to the amplitude of the CFO. If the initial CFO's are estimated with sufficient accuracy, after CFO compensation, the residual CFO's are smaller than the initial CFO and hence introduce less MAI. Therefore, the residual CFO's can be estimated with better accuracy. In this way, we can re-use the successive CFO estimation and compensation algorithm developed in Chapter 2 in the uplink multi-user MIMO-OFDM systems to improve the performance of the CFO estimation.

- Recently, cooperative wireless communication has become a hot research topic. In a cooperative wireless communication system, different wireless nodes in a communication network cooperate to enhance the quality of the communication link between any two nodes. There are many papers in the literature focusing on transmission strategies to maximize the link throughput or minimize the bit error rate of the transmission. Most of these papers assume perfect timing and frequency synchronization. In practice, both timing and frequency synchronization in cooperative communication systems are difficult due to the distributed nature of the wireless nodes and also the potentially large number of nodes in the network. Due to this difficulty, many transmission strategies have been designed considering only asynchronous communication, which has inferior performance compared to a fully synchronized system. Since the algorithms we proposed in Chapter 5 are targeted to multi-user communication systems, it is interesting to investigate their applicability in and possible extensions to cooperative communication systems.

Bibliography

[1] T. S. Rappaport, *Wireless communications principles & practice.* Prentice Hall Inc., 1996.

[2] W. Jakes, *Microwave mobile communications.* IEEE Press, 1994.

[3] J. G. Proakis, *Digital communications*, 4th ed. McGraw-Hill, 2001.

[4] *IEEE 802.11b-1999 Higher Speed Physical Layer Extension in the 2.4 GHz band*, IEEE Std., Feb. 1999.

[5] *IEEE P802.11n/D1.10 Wireless LAN Medium Access Control (MAC) and Physical Layer (PHY) specifications: Enhancements for Higher Throughput*, IEEE Std., Feb 2007.

[6] E. Perahia, "IEEE P802.11 Wireless LANs VHT 60 GHz PAR plus 5C's," *IEEE 802.11 document IEEE 802.11-08/0806r7*, Oct. 2008.

[7] S. Cherry, "Edholm's law of bandwidth," *IEEE Spectr.*, vol. 41, no. 7, pp. 58–60, July 2004.

[8] G. Moore, "Cramming more components onto integrated circuits," *Electronics*, vol. 38, no. 8, April 1965.

[9] E. A. Lee and D. G. Messerschnitt, *Digital communication*, 2nd ed. Kluwer Academic Publishers, 1999.

[10] S. Haykin, *Adaptive filter theory*, 4th ed. Prentice Hall Inc., 2002.

[11] R. Prasad, *OFDM for wireless communications systems.* Artech House Inc., 2004.

[12] R. Chang, "Synthesis of band-limited orthogonal signals for multichannel data transmission," *Bell Syst. Tech. Journal*, vol. 45, pp. 1775–1796, Dec 1966.

[13] B. Saltzberg, "Performance of an efficient parallel data transmission system," *IEEE Trans. Commun. Technol.*, vol. 15, no. 6, pp. 805–811, December 1967.

[14] J. A. C. Bingham, "Multicarrier modulation for data transmission: an idea whose time has come," *IEEE Commun. Mag.*, vol. 28, no. 5, pp. 5–14, May 1990.

[15] J. M. Cioffi, "A multicarrier primer," *ANSI TlEl.4 Committee Contribution*, pp. 91–157, Nov. 1991.

[16] W. Y. Zou and Y. Wu, "COFDM: an overview," *IEEE Trans. Broadcast.*, vol. 41, no. 1, pp. 1–8, March 1995.

[17] *IEEE 802.11a: Wireless LAN Medium Access Control (MAC) and Physical Layer (PHY) Specifications: High-speed Physical Layer in the 5GHz*

Band, IEEE Std., Sep 1999.

[18] *IEEE 802.11g: Wireless LAN Medium Access Control (MAC) and Physical Layer (PHY) Specifications: Amendment 4: Further Higher Data Rate Extension in the 2.4 GHz Band*, IEEE Std., June 2003.

[19] *IEEE 802.16e: Air Interface for Fixed and Mobile Broadband Wireless Access Systems Amendment 2: Physical and Medium Access Control Layers for Combined Fixed and Mobile Operation in Licensed Bands*, IEEE Std., 2006.

[20] *ETS 300 401: Radio broadcasting systems;digital audio broadcasting (DAB) to mobile, portable and fixed receivers*, ETSI Std., May 1997.

[21] *ETS 300 744: Digital video broadcasting (DVB); framing structure channel coding and modulation for digital terrestrial television (DVB-T)*, ETSI Std., Nov. 1996.

[22] J. Tellado, *Multicarrier modulation with low PAR: applications to DSL and wireless.* Kluwer Academic Publishers, 2000.

[23] Y. Wu, "Peak power reduction schemes for ADSL applications," Master's thesis, National University of Singapore, 2001.

[24] G. Foschini and M.J.Gans, "On limits of wireless communications in a fading environment when using multiple antennas," *Wireless personal communications*, vol. 6, no. 3, pp. 331–335, March 1998.

[25] I. Telatar, "Capacity of multi-antenna gaussian channels," *European Trans. Telecommun. Related Technol.*, vol. 10, pp. 585–595, Nov-Dec

1999.

[26] *3GPP TS 36.201: Evolved Universal Terrestrial Radio Access (E-UTRA): Long Term Evolution (LTE) physical layer: General description*, 3GPP Std., 2008.

[27] A. Paulraj, R. Nabar, and D. Gore, *Introduction to space-time wireless communications.* Cambridge University Press, 2003.

[28] E. Biglieri, R. Calderbank, A. Constantinides, A. Goldsmith, A. Paulraj, and H. V. Poor, *MIMO wireless communications.* Cambridge Univeristy Press, 2007.

[29] V. Tarokh, N. Seshadri, and A. Calderbank, "Space-time codes for high data rate wireless communication: performance criterion and code construction," *IEEE Trans. Inf. Theory*, vol. 44, no. 2, pp. 744–765, March 1998.

[30] S. Alamouti, "A simple transmit diversity technique for wireless communications," *IEEE J. Sel. Areas Commun.*, vol. 16, no. 8, pp. 1451–1458, Oct 1998.

[31] G. Stuber, *Principles of mobile communication.* Kluwer Academic Publishers, 2001.

[32] D. Agrawal, V. Tarokh, A. Naguib, and N. Seshadri, "Space-time coded OFDM for high data-rate wireless communication over wideband channels," in *Proc. 48th IEEE Vehicular Technology Conference VTC 98*, vol. 3, 18–21 May 1998, pp. 2232–2236.

[33] H. Sampath, S. Talwar, J. Tellado, V. Erceg, and A. Paulraj, "A fourth-generation MIMO-OFDM broadband wireless system: design, performance, and field trial results," *IEEE Commun. Mag.*, vol. 40, no. 9, pp. 143–149, Sep 2002.

[34] G. Stuber, J. Barry, S. McLaughlin, Y. Li, M. Ingram, and T. Pratt, "Broadband MIMO-OFDM wireless communications," *Proc. IEEE*, vol. 92, no. 2, pp. 271–294, 2004.

[35] M. Dohler, E. Lefranc, and H. Aghvami, "Virtual antenna arrays for future mobile communication systems," in *IEEE ICT*, Beijing, China, 2002.

[36] K. Fazel and S. Kaiser, *Multi-carrier and spread spectrum systems.* John Wiley & Sons Ltd, 2003.

[37] H. Liu and U. Tureli, "A high efficiency carrier estimator for OFDM communications," *IEEE Commun. Lett.*, vol. 2, pp. 104–106, Apr 1998.

[38] P. Moose, "A technique for orthogonal frequency division multiplexing frequency offset correction," *IEEE Trans. Commun.*, vol. 42, no. 10, pp. 2908–2914, Oct 1994.

[39] T. Schmidl and D. Cox, "Robust frequency and timing synchronization for OFDM," *IEEE Trans. Commun.*, vol. 45, no. 12, pp. 1613–1621, Dec 1997.

[40] M. Morelli and U. Mengali, "An improved frequency offset estimator for OFDM applications," *IEEE Commun. Lett.*, vol. 3, no. 3, pp. 75–77, March 1999.

[41] M. Speth, S. A. Fechtel, G. Fock, and H. Meyr, "Optimum receiver design for wireless broad-band systems using OFDM. I," *IEEE Trans. Commun.*, vol. 47, no. 11, pp. 1668–1677, Nov. 1999.

[42] M. Morelli, A. N. D'Andrea, and U. Mengali, "Frequency ambiguity resolution in OFDM systems," *IEEE Commun. Lett.*, vol. 4, no. 4, pp. 134–136, April 2000.

[43] J. Li, G. Liu, and G. B. Giannakis, "Carrier frequency offset estimation for OFDM-based WLANs," *IEEE Signal Process. Lett.*, vol. 8, no. 3, pp. 80–82, March 2001.

[44] E. G. Larsson, G. Liu, J. Li, and G. B. Giannakis, "Joint symbol timing and channel estimation for OFDM based WLANs," *IEEE Commun. Lett.*, vol. 5, no. 8, pp. 325–327, Aug. 2001.

[45] M. Morelli and U. Mengali, "Carrier-frequency estimation for transmissions over selective channles," *IEEE Trans. Commun.*, vol. 48, no. 9, pp. 1580–1589, Sept. 2000.

[46] Y. Yu, A. P. Petropulu, H. V. Poor, and V. Koivunen, "Blind estimation of multiple carrier frequency offsets," in *Proc. IEEE 18th International Symposium on Personal, Indoor and Mobile Radio Communications PIMRC 2007*, 3–7 Sept. 2007, pp. 1–5.

[47] J. van de Beek, M. Sandell, and P. O. Börjesson, "Ml estimation of time and frequency offset in OFDM systems," *IEEE Trans. Signal Process.*, vol. 45, no. 7, pp. 1800–1805, Jul 1997.

[48] M. Ghogho, A. Swami, and G. Giannakis, “Optimized null-subcarrier selection for CFO estimation in OFDM over frequency-selective fading channels,” in *Proc. IEEE Globecom 2001*, vol. 1, Nov 2001, pp. 202–206.

[49] A. Mody and G. Stüber, “Synchronization for MIMO OFDM systems,” in *Proc. IEEE Global Telecommuncations Conference 2001*, vol. 1, Nov 2001, pp. 509 – 513.

[50] T. Schenk and A. van Zelst, “Frequency synchronization for MIMO OFDM wireless LAN systems,” in *Proceedings IEEE Vehicular Technology Conference (VTC) 2003 Fall*, vol. 2, Oct 2003, pp. 781–785.

[51] Y. Jiang, H. Minn, X. Gao, X. You, and Y. Li, “Frequency offset estimation and training sequence design for MIMO OFDM,” *IEEE Trans. Wireless Commun.*, vol. 7, no. 4, pp. 1244–1254, April 2008.

[52] S. A. Mujtaba and et. al., “IEEE 802.11-04/0889r7 TGn Sync proposal technical specification,” July 2005.

[53] D. Shiu, G. Foschini, M. Gans, and J. Kahn, “Fading correlation and its effect on the capacity of multielement antenna sysetms,” *IEEE Trans. Commun.*, vol. 48, no. 3, pp. 502–513, Mar. 2000.

[54] X. Mestre, J. R. Fonollosa, and A. Pages-Zamora, “Capacity of MIMO channels: asymptotic evaluation under correlated fading,” *IEEE J. Sel. Areas Commun.*, vol. 21, no. 5, pp. 829–838, June 2003.

[55] H. Shin and J. H. Lee, “Capacity of multiple-antenna fading channels: spatial fading correlation, double scattering, and keyhole,” *IEEE Trans. Inf. Theory*, vol. 49, no. 10, pp. 2636–2647, Oct. 2003.

[56] I. Gupta and A. A. Ksienski, “Effect of mutual coupling on the performance of adaptive arrays,” *IEEE Trans. Antennas Propag.*, vol. AP-31, no. 5, pp. 785–791, Sept. 1983.

[57] R. Vaughan and J. Andersen, “Antenna diversity in mobile communications,” *IEEE Trans. Veh. Technol.*, vol. VT-36, no. 4, pp. 149–172, Nov. 1987.

[58] T.Svantesson, “The effects of mutual coupling using a linear array of thin dipoles of finite length,” in *IEEE SP Workshop on Statistical Signal and Array Processing*, Sept. 1998, pp. 232–235.

[59] R. R. Ramirez and F. De Flaviis, “A mutual coupling study of linear polarized microstrip antennas for use in BLAST wireless communications architecture,” in *Proc. IEEE Antennas and Propagation Society International Symposium*, vol. 2, 16–21 July 2000, pp. 490–493.

[60] O. Besson and P. Stoica, “On parameter estimation of MIMO flat-fading channels with frequency offsets,” *IEEE Trans. Signal Process.*, vol. 51, no. 3, pp. 602–613, Mar. 2003.

[61] Y. Yao and T.-S. Ng, “Correlation-based frequency offset estimation in MIMO system,” in *Proc. VTC 2003-Fall Vehicular Technology Conference 2003 IEEE 58th*, vol. 1, 2003, pp. 438–442 Vol.1.

[62] Y. Zeng, A. Leyman, and T.-S. Ng, “Joint semiblind frequency offset and channel estimation for multiuser MIMO-OFDM uplink,” *IEEE Trans. Commun.*, vol. 55, no. 12, pp. 2270–2278, 2007.

[63] J. Chen, Y. C. Wu, S. Ma, and T. S. Ng, "Joint CFO and channel estimation for multiuser MIMO-OFDM systems with optimal training sequences," *IEEE Trans. Signal Process.*, vol. 56, no. 8, pp. 4008–4019, Aug. 2008.

[64] S. Attallah, "Blind estimation of residual carrier offset in OFDM systems," *IEEE Signal Process. Lett.*, vol. 11, no. 2, pp. 216–219, Feb 2004.

[65] F. Gao and A. Nallanathan, "Blind maximum likelihood CFO estimation for OFDM systems via polynomial rooting," *IEEE Signal Process. Lett.*, vol. 13, no. 2, pp. 73–76, 2006.

[66] U. Tureli, D. Kivanc, and H. Liu, "Experimental and analytical studies on a high-resolution OFDM carrier fequency offset estimator," *IEEE Trans. Veh. Technol.*, vol. 50, no. 2, pp. 629–643, Mar 2001.

[67] X. Ma, C. Tepedelenlioğlu, G. Giannakis, and S. Barbarossa, "Non-data-aided carrier offset estimators for OFDM with null subcarriers: dentifiability, algorithms, and performance," *IEEE J. Sel. Areas Commun.*, vol. 9, no. 12, pp. 2504–2515, Dec 2001.

[68] U. Tureli, H. Liu, and M. Zoltowski, "OFDM blind carrier offset estimation:ESPRIT," vol. 48, pp. 1459–1461, Sep 2000.

[69] H. Meyr, M. Moeneclaey, and S. A. Fechtel, *Digital communication receivers.* John Wiley & Sons, Inc., 1998.

[70] D. M. Pozar, *Microwave and RF design of wireless systems.* John Wiley & Sons, Inc., 2001.

[71] A. Stephens, "IEEE 802.11 TGn comparison criteria," *IEEE 802.11 document 802.11-03/814r31*, July 2004.

[72] E. W. Weisstein, *CRC concise encyclopedia of mathematics*, 2nd ed. Chapman & Hall / CRC, 2003.

[73] C. Lanczos, *Applied analysis.* New York: Dover Publications Inc, 1988.

[74] C. Li and S. Roy, "Subspace-based blind channel estimation for OFDM by exploiting virtual carriers," *IEEE Trans. Wireless Commun.*, vol. 2, no. 1, pp. 141–150, Jan 2003.

[75] J. Medbo, H. Hallenberg, and J.-E. Berg, "Propagation characteristics at 5 GHz in typical radio-LAN scenarios," in *Proc. IEEE Vehicular Technology Conference Spring 1999*, vol. 1, May 1999, pp. 185–189.

[76] K. Sathananthan and C. Tellambura, "Probability of error calculation of OFDM systems with frequency offset," *IEEE Trans. Commun.*, vol. 49, no. 11, pp. 1884–1888, Nov 2001.

[77] C. Y. Wong, R. Cheng, K. Lataief, and R. Murch, "Multiuser OFDM with adaptive subcarrier, bit, and power allocation," *IEEE J. Sel. Areas Commun.*, vol. 17, no. 10, pp. 1747–1758, 1999.

[78] S. Boyd and L. Vandenberghe, *Convex optimization.* Cambridge Univeristy Press, 2004.

[79] Y. Wu, S. Attallah, and J. W. M. Bergmans, "Blind iterative carrier offset estimation for OFDM systems," in *Proc. Eighth International Sym-*

posium on Signal Processing and Its Applications, vol. 1, August 28–31, 2005, pp. 123–126.

[80] S. Attallah, Y. Wu, and J. W. M. Bergmans, "Low complexity blind estimation of residual carrier offset in orthogonal frequency division multiplexing based," *IET Communications*, vol. 1, no. 4, pp. 604–611, August 2007.

[81] G. Foschini, G. Golden, R. Valenzuela, and P. Wolniansky, "Simplified processing for high spectral efficiency wireless communication employing multi-element arrays," *IEEE J. Sel. Areas Commun.*, vol. 17, no. 11, pp. 1841–1852, 1999.

[82] Y. Li, "Optimum training sequences for OFDM systems with multiple transmit antennas," in *IEEE Global Telecommunications Conference*, vol. 3, Dec 2000, pp. 1478–1482.

[83] S. Sun, I. Wiemer, C. Ho, and T. T. Tjhung, "Training sequence assisted channel estimation for MIMO OFDM," in *Proceedings IEEE Wireless Communications and Networking Conference*, vol. 1, 2003, pp. 38–43.

[84] D. Tse and P. Viswanath, *Fundamentals of wireless communication.* Cambridge Univeristy Press, 2005.

[85] R. Frank, S. Zadoff, and R. Heimiller, "Phase shift pulse codes with good periodic correlation properties (corresp.)," *IRE Transactions on Information Theory*, vol. 8, no. 6, pp. 381–382, 1962.

[86] D. Chu, "Polyphase codes with good periodic correlation properties (corresp.)," *IEEE Trans. Inf. Theory*, vol. 18, no. 4, pp. 531–532, 1972.

[87] N. Sueshiro and M. Hatori, “Modulatable orthogonal seqeuences and their application to SSMA systems,” *IEEE Trans. Inf. Theory*, vol. 34, no. 1, pp. 93–100, Jan 1988.

[88] Q. Spencer, B. Jeffs, M. Jensen, and A. Swindlehurst, “Modeling the statistical time and angle of arrival characteristics of an indoor multipath channel,” *IEEE J. Sel. Areas Commun.*, vol. 18, no. 3, pp. 347–360, 2000.

[89] C. C. Chong, D. I. Laurenson, and S. McLaughlin, “Statistical characterization of the 5.2 GHz wideband directional indoor propagation channels with clustering and correlation properties,” in *Proc. VTC 2002-Fall Vehicular Technology Conference 2002 IEEE 56th*, vol. 1, 24–28 Sept. 2002, pp. 629–633.

[90] V. Erceg and et.al., “TGn channel models,” *IEEE 802.11 document 802.11-03/940r4*, May 2004.

[91] L. Schumacher and B. Raghothaman, “Closed-form expressions for the correlation coefficient of directive antennas impinged by a multimodal truncated Laplacian PAS,” *IEEE Trans. Wireless Commun.*, vol. 4, no. 4, pp. 1351–1359, 2005.

[92] A. Papoulis and S. U. Pillai, *Probability, random variables and stochastic processes*, 4th ed. McGraw-Hill, 2002.

[93] C. Waldschmidt, J. v. Hagen, and W. Wiesbeck, “Influence and modelling of mutual coupling in MIMO and diversity systems,” in *Proc. IEEE Antennas and Propagation Society International Symposium*, vol. 3, 16–21 June 2002, p. 190.

[94] B. Clerckx, C. Craeye, D. Vanhoenacker-Janvier, and C. Oestges, "Impact of antenna coupling on 2×2 MIMO communications," *IEEE Trans. Veh. Technol.*, vol. 56, no. 3, pp. 1009–1018, May 2007.

[95] C. A. Balanis, *Antenna theory : analysis and design*, 2nd ed. John Wiley & Sons, Inc., 1997.

[96] A. van Zelst and T. Schenk, "Implementation of a MIMO OFDM-based wireless LAN system," *IEEE Trans. Signal Process.*, vol. 52, no. 2, pp. 483–494, Feb 2004.

[97] S. Sezginer, P. Bianchi, and W. Hachem, "Asymptotic Cramer-Rao bounds and training design for uplink MIMO-OFDMA systems with frequency offsets," *IEEE Trans. Signal Process.*, vol. 55, no. 7, pp. 3606–3622, July 2007.

[98] S. Sezginer and P. Bianchi, "Asymptotically efficient reduced complexity frequency offset and channel estimators for uplink MIMO-OFDMA systems," *IEEE Trans. Signal Process.*, vol. 56, no. 3, pp. 964–979, March 2008.

[99] L. Ingber, "Adaptive simulated annealing (ASA)," *Global optimization C-code, Caltech Alumni Association, Pasadena, CA (1993). URL http://www.ingber.com.*

[100] S. Solomon and G. Gong, *Signal design for good correlation: for wireless communication, cryptography, and radar.* Cambridge Univeristy Press, 2005.

[101] Y. Wu, S. Attallah, and J. W. M. Bergmans, "Efficient training sequence for joint carrier fequency offset and channel estimation for MIMO-OFDM systems," in *Proc. IEEE International Conference on Communications ICC '07*, 2007, pp. 2604–2609.

[102] J. J. van de Beek, P. O. Borjesson, M. L. Boucheret, D. Landstrom, J. M. Arenas, P. Odling, C. Ostberg, M. Wahlqvist, and S. K. Wilson, "A time and frequency synchronization scheme for multiuser OFDM," *IEEE J. Sel. Areas Commun.*, vol. 17, no. 11, pp. 1900–1914, Nov. 1999.

[103] M. Morelli, "Timing and frequency synchronization for the uplink of an OFDMA system," *IEEE Trans. Commun.*, vol. 52, no. 2, pp. 296–306, Feb. 2004.

Curriculum vitae

Wu Yan was born in Qingdao, China in 1975. He received the B. Eng. (first-class Honours) and the M. Eng degrees from the department of Electrical Engineering, National University of Singapore (NUS) in 1999 and 2001 respectively. He was with the Institute for Infocomm Research (I^2R), A^*STAR, Singapore from March 2001 to January 2008. In August 2004, he was enrolled into the joint-PhD program between NUS and Technische Universiteit Eindhoven (TU/e). Since January 2008, he has been working full-time in the Signal Processing Systems (SPS) group in the department of Electrical Engineering, TU/e as a PhD candidate. His research interest mainly lies in signal processing, including timing and frequency synchronizations, detection, space-time processing, for multicarrier communication systems.